EPIGENETIC COMPONENT FVE ORCHESTRATES CYTOPLASMIC SGS3-DRB4-DCL4 ACTIVITIES TO PROMOTE RNA SILENCING IN *ARABIDOPSIS*

A Dissertation

by

DI SUN

Submitted to the Office of Graduate and Professional Studies of
Texas A&M University
in partial fulfillment of the requirements for the degree of

DOCTOR OF PHILOSOPHY

Chair of Committee,	Xiuren Zhang
Committee Members,	Hisashi Koiwa
	Pingwei Li
	Matthew S. Sachs
Head of Department,	Dirk Hays

May 2021

Major Subject: Molecular and Environmental Plant Sciences

ABSTRACT

Posttranscriptional gene silencing (PTGS) involves two kinds of small non-coding regulatory RNAs, miRNA and small interfering RNA (siRNA) that regulate gene expression in diverse biological processes in eukaryotic organisms. miRNAs originate from primary transcripts (pri-miRNAs) through sequential cleavage by Microprocessor that comprises DCL1 and DRB1/HYL1. The mode of action of siRNAs is similar to that of miRNAs. However, the prerequisite step for initiating siRNA-mediated RNA silencing in plants is the conversion of single-stranded (ss) RNA substrates to double-stranded (ds) RNAs, which is fulfilled by RNA-dependent RNA polymerase 6 (RDR6) and Suppressor of Gene Silencing 3 (SGS3). In turn, dsRNAs are processed by DCL2 or, DCL4 together with its partner DRB4, to 21–22 nt siRNAs, which are eventually loaded into AGO1 to destroy target RNAs. Notwithstanding, the biochemical partners and functional bridges of RDR6/SGS3-DCL4/DRB4 are far less understood compared with microprocessor.

FLOWER LOCUS VE (*FVE*), a plant homolog of mammalian retinoblastoma-associated protein (RbAp48), has been well known as an epigenetic component in nucleus. However, whether and/ how *FVE* is involved in PTGS is unknown.

We generated a dual LUC reporter system for miRNA and siRNA pathways. Through an Ethyl methanesulfonate (EMS) mutagenesis of the reporter line, we screened an allele of *FVE* (*fve-8,* a mutant encodes a truncated FVE protein FVE-8) displaying enhanced LUC expression level at transcription and protein levels. We observed that FVE protein is localized in both nucleus and cytoplasm. Cytoplasmic FVE (FVE_{NES}) could fully

rescue the LUC signal, but not the epigenetic-related later flowering phenotype, in *fve-8*. Through RNA-seq and small RNA-seq, we found that FVE promoted the accumulation of transgene-derived siRNAs in several reporter lines. Through candidate search method, we found that FVE interacts with SGS3, the master regulator of PTGS and promotes SGS3 homodimerization, which is prerequisite for its function in vivo. On the other hand, the truncated FVE-8 protein does not interact with SGS3 as FVE-8 itself forms a homodimer or oligomer.

We then found that FVE is an RNA binding protein. FVE and FVE-8 show similar binding affinity to single-stranded (ss) RNA while SGS3 does not bind to ssRNA. Thus, FVE/SGS3 can form a ribonucleoprotein complex to present ssRNA to RDR6 for generation of dsRNA in vivo. By contrast, FVE-8 gains a new function by binding dsRNA with a significantly increased binding affinity, leading to its hijacking of dsRNA from the SGS3 complex.

Finally, we found that FVE/SGS3 is recruited to DCL4 complexes through interaction with the DCL4 partner, DRB4 protein. In vitro DCL4/DRB4 reconstitution assays showed that FVE directly promotes, while FVE-8 impedes, DCL2/4 activity of siRNA production in vitro.

Based on these results, we concluded that FVE has a novel role in cytoplasmic PTGS pathway. We proposed that FVE can synchronize RDR6/SGS3 and DRB4/DCL4 activity through interaction with the proteins and RNA substrates to promote the synthesis of transgene-derived siRNAs and therefore RNA silencing.

DEDICATION

This dissertation is dedicated to my family.

To my parents, Xianyu Tang and Yuean Sun, for their unconditional support for my every decision in my study, for their encouragement and sunshine-like love protecting me and raising me to go further and higher.

To my sweet boyfriend Wei, for his exceptional example as a scientist, for his love leading me to happiness, and for his magic which turns this challenge into a joyful journey.

ACKNOWLEDGEMENTS

I would like to sincerely thank my advisor and committee chair, Dr. Xiuren Zhang, for training me, guiding me, and supporting me during my research. I would like to thank Drs. Hisashi Koiwa, Pingwei Li and Matthew Sachs for being my committee members and their precious advice and help to my project through these years.

Thanks also go to all my lab colleagues including postdocs, especially to Dr. Zeyang Ma as my mentor, graduate students, visiting scholars, and undergraduate students, for various kinds of help during my graduate career. I also would like to thank my friends Drs. Qiulin Wu, Yingmu Zhang and Xiaomei Hu as my best friends going through this memorable life and sharing joy and sorrows together. In addition, I want to thank Dr. Xu Peng for his help in improving my presentation.

Finally, I would like to thank my friends, colleagues, faculty and staff from the Department of MEPS, BICH, and IPGB for making my time at Texas A&M University a great experience.

CONTRIBUTORS AND FUNDING SOURCES

Contributors

This work was supervised by a dissertation committee consisting of Professors Xiuren Zhang (chair and advisor) and Hisashi Koiwa of the Department of Molecular Environmental Plant Sciences, Professor Pingwei Li of the Department of Biochemistry and Biophysics, and Professor Matthew S. Sachs from the Department of Biology.

The whole genome sequencing data and RNA-seq library in Chapter II were analyzed by Dr. Zeyang Ma at the Department of Biochemistry and Biophysics. The sRNA blot in Chapter II was done by Dr. Xiaomei Hu at the Department of Biochemistry and Biophysics. Partial EMS system verification was done by Niankui Li at the Department of Molecular Environmental Plant Sciences. The protein purification in Chapter III was done by Xingxing Yan at the Department of Molecular Environmental Plant Sciences. Co-IP and part of yeast-2-hybrid in Chapter III was done by Dr. Yanjun Li at the Department of Biochemistry and Biophysics. Confocal assays in Chapter III were helped by Dr. Baoshuan Shang at the Department of Biochemistry and Biophysics.

All other work conducted for the thesis (or) dissertation was completed by the student independently.

Funding Sources

Graduate study was supported by China Scholar Council fellowship awarded to me. The work was supported by grants from US National Institutes of Health

1R01GM132401, and US National Science Foundation (MCB-1716243) awarded to Professor Xiuren Zhang.

NOMENCLATURE

SAM	Shoot apical meristem
DNA	Deoxyribonucleic acid
RNA	Ribonucleic acid
RNAi	RNA interference
AGO	Argonaute
sRNA	Small RNA
RISC	RNA-induced silencing complex
miRNA	MicroRNA
siRNA	Small-interfering RNA
dsRNA	Double-strand RNA
ssRNA	Single-strand RNA
pre-miRNA	precursor miRNA, consists only of the hairpin structure
pri-miRNA	primary miRNA, it is the mRNA from the *MIRNA* gene
PTGS	Post-transcriptional Gene Silencing
TGS	Transcriptional Gene Silencing
S-PTGS	Sense Post-transcriptional Gene Silencing
IR-PTGS	Inverted Repeat Post-transcriptional Gene Silencing
RdDM	RNA directed DNA Methylation
RDR	RNA-dependent RNA Polymerase
tasiRNA	trans-acting small-interfering RNA

RQC	RNA quality control
HDAC	histone deacetylase complex
FVE	FLOWERAL LOCUS VE
EMS	Ethyl methanesulfonate

TABLE OF CONTENTS

Page

LIST OF FIGURES

Page

LIST OF TABLES

Page

CHAPTER I

INTRODUCTION

1.1 RNA silencing

RNA silencing, also named RNA interference, plays a central role in regulating growth and development, plant defense to viral infections, heterochromatin maintenance and other biological processes (Liu and Chen, 2016; Cui, et al., 2017; Golden, et al., 2017; Song, et al., 2019). In 1990, Napoli et al. unexpectedly found a co-suppression of both endogenous and foreign genes when a chimeric *Chalcone Synthase* (*CHS*) gene was transformed into petunia (Napoli, et al., 1990). Since then, sense, antisense and especially double-strand RNA (dsRNA) have been all reported to cause interference (Fire, et al., 1991; Guo and Kemphues, 1995; Fire, et al., 1998). In 1999, small RNAs (sRNAs) were discovered to accompany RNAi in plants (Hamilton and Baulcombe, 1999). RNA silencing is triggered by non-coding sRNA and leads to a sequence-specific repression of the expression of target genes with complementary sequences. In plants, RNA silencing occurs at transcriptional and posttranscriptional levels. At the posttranscriptional levels, RNA silencing mainly includes mRNA cleavage or translational repression, sometimes combined with accelerated RNA decay or RNA splicing (Stepien, et al., 2017); and this process is typically referred to post-transcriptional gene silencing (PTGS). By contrast, RNA silencing can also involve DNA and/or histone epigenetically modification and subsequent turn off the expression of gene transcription and this process is known as

transcriptional gene silencing (TGS) (Wang, et al., 2011; Fang and Qi, 2016; Suzuki, et al., 2017).

1.1.1 miRNA-meditated RNA silencing

RNA silencing is guided through sRNAs, which consist of two kinds of sRNAs: microRNAs (miRNAs) and small interfering RNAs (siRNAs) (Bartel, 2018; Ma and Zhang, 2018). miRNAs are short (usually 21-24 nt) non-coding single-strand RNAs. In Arabidopsis, one *MIR* gene is transcribed by RNA polymerase II into a primary miRNA (pri-miRNA) with one or more imperfect hairpin-loop structure (Bielewicz, et al., 2013). Pri-miRNAs will be processed into precursor-miRNAs (pre-miRNAs) and further into miRNA/miRNA* duplex in a complex named Dicing body (D body) (Park, et al., 2011; Rogers and Chen, 2013; Zhu, et al., 2013; Wang, et al., 2019). The D body mainly contains a nuclear RNase III Dicer-like1 (DCL1), a dsRNA-binding protein HYPONASTIC LEAVES 1 (HYL1), and an arguable C2H2 zinc finger protein SERRATE (SE) (Figure 1) (Ma and Zhang, 2018). The three components are responsible for accurate pri-miRNA processing.

DCL1 contains a DExD/H-box RNA helicase domain, a DUF283 domain, a Piwi Argonaute and Zwille (PAZ) domain, two tandem dsRNA-binding domains and two tandem RNaseIII (RIIIa and RIIIb) domains (Zhu, et al., 2013). Similar to Dicer protein in mammalians, DCL1 performs the core catalytic role of cutting dsRNAs concomitantly. The helicase domain is required for the ATP-dependent miRNA processing (Liu, et al., 2012). Recently the human homolog Drosha was reported that the helix hairpin of PAZ

domain and MB helix of RIIIa are responsible for the recognition of the basal junction of pri-miRNAs to ensure efficient and accurate processing (Jin, et al., 2020; Partin, et al., 2020). For canonical miRNA processing, DCL1 sequentially cuts pri-miRNAs from base to loop; while for the noncanonical miRNA processing from pri-miRNAs harboring branched terminal loops, DCL1 processes pri-miRNAs bidirectionally, either from base to loop, or from loop to base (Zhu, et al., 2013). The binding of DCL1 and *MIR* loci suggests that pri-miRNAs transcription and processing may be coupled (Fang, et al., 2015). Containing two tandem dsRBDs at N-terminal, HYL1 is not only responsible for the accuracy and efficiency of DCL activity (Kurihara, et al., 2006; Liu, et al., 2012), but also guides miRNA/* duplexes strand selection (Eamens, et al., 2009). HYL1 binds to miRNA/* region of precursors as a homodimer mediated by its dsRBD2 (Yang, et al., 2010). It is suggested that SE does not directly contribute to miRNA processing, while SE can serve as a scaffold for protein complexes regulating miRNA biogenesis (Manavella, et al., 2012; Zhu, et al., 2013). Apart from these three key components, there are more than 20 other factors regulating the miRNA biogenesis (Stepien, et al., 2017; Song, et al., 2019). For instance, CELL DIVISION CYCLE 5 (CDC5), a MYB-related transcriptional factor, C-TERMINAL DOMAIN PHOSPHATASE-LIKE 1 (CPL1) and Negative on TATA less2 (NOT2) interact with Pol II and promotes *MIR* genes transcription (Koiwa, et al., 2002; Wang, et al., 2013; Zhang, et al., 2013). These three proteins can also interact with microprocessor through interaction with SE. Two cap-binding proteins, CBP20 and CBP80 can also interact with SE and promote pri-miRNAs to be processed into miRNAs (Gregory, et al., 2008; Kim, et al., 2008; Laubinger, et al., 2008). CHROMATIN

REMODELING FACTOR 2 (CHR2) promotes *MIR* transcription while suppresses miRNA biogenesis through interacting with SE (Wang, et al., 2018). 20S core proteasome α subunit G1 (PAG1) can bind to SE. It degrades the intrinsically disordered portion of SE to protect the functionality of folded SE (Li, et al., 2020). MOS4-ASSOCIATED COMPLEX (MAC) subunits PRL1, PRL2, MAC3, MAC7 can interact with DCL1 complex, correct HYL1 localization and promote miRNA biogenesis (Li, et al., 2018). Karyopherin enabling the transport of the cytoplasmic HYL1 (KETCH1) can facilitate miRNA processing through transporting HYL1 from cytoplasm to nucleus (Zhang, et al., 2017). CPL1 can interact with HYL1 through SE. It dephosphorylates HYL1 to ensure its full function (Manavella, et al., 2012). Transcription-coupled export 2 (TREX-2) subunits THP1 and SAC3A can both promote *MIR* gene transcription and promote Dicing body formation through interacting with SE (Zhang, et al., 2020).

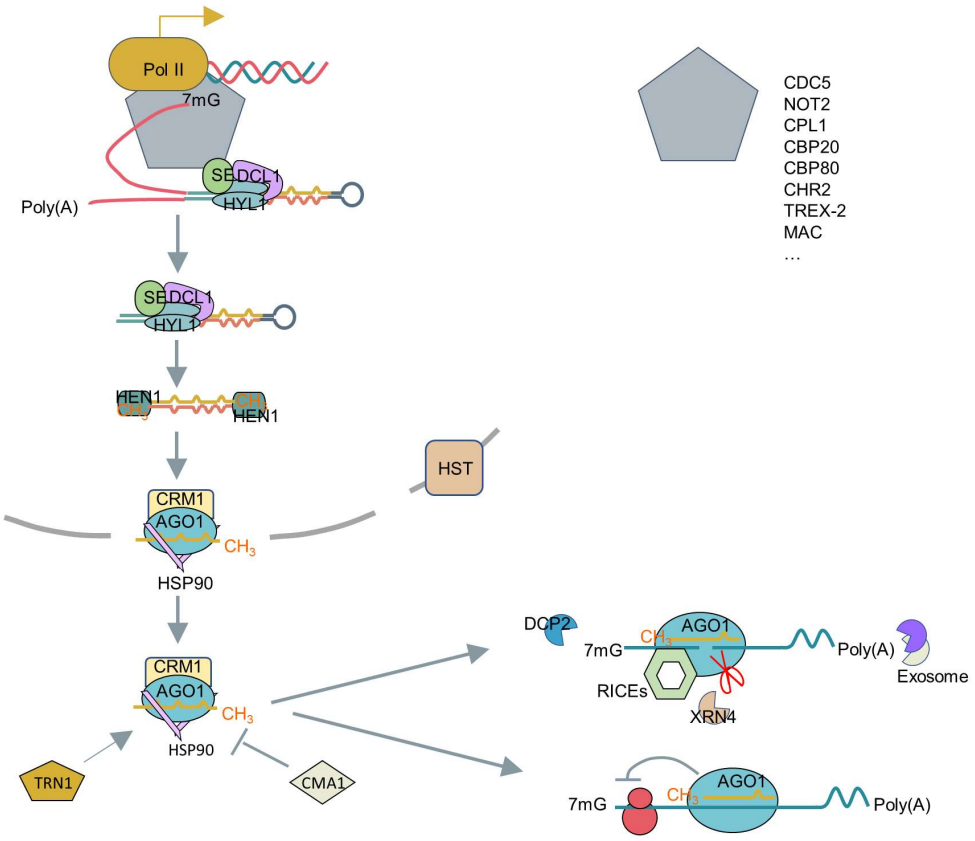

Figure 1 The miRNA pathway in *Arabidopsis*
An MIR gene is transcribed by RNA PolII under the regulation of several transcription factors into a pri-miRNA. This pri-miRNA is processed by Dicing body into pre-miRNA and further into miRNA/* duplexes. Then a 2'-O-methylation of the miRNA/* duplexes at their 3'-ends is deposited by HEN1. The mature miRNA will be loaded into AGO1 in nucleus and be transported into cytoplasm by CRM1 (EXPO1). TRN1 and CMA1 are positive and negative regulators to the loading of miRNA into RISC complex, respectively. RISC complex recruits the corresponding target mRNA and guide its cleavage or translational repression. The cleaved 3' fragment will be degraded by exosome and XRN4, while the 5' fragment will be uridylated and digested by RICEs.

miRNA/miRNAs* will be 2'-O-methylated by HUA ENHANCER 1 (HEN1) at the 3' termini to prevent uridylation and further degradation (Yu, et al., 2005). Some duplexes are competitively loaded into ARGONAUTE1 (AGO1) protein with the

mandatory help of chaperone HSP90 in nucleus and reveal the Nuclear export signal (NES) of AGO1 (Tomari, et al., 2007; Bologna, et al., 2018). The loading of miRNA to AGO1 is positively and negatively regulated by ENHANCED MIRNA ACTIVITY1 (EMA1) and TRANSPORTIN1 (TRN1) belonging to importin-β family proteins, respectively (Wang, et al., 2011; Cui, et al., 2016). The strand with lower 5' thermodynamic stability is usually selected as the mature miRNA while the other strand will be degraded (Tomari, et al., 2004; Eamens, et al., 2009). The complex can form RNA induced silencing complex (RISC). The nucleo-cytosolic transportation of miRNA-AGO1 complex is dependent on CRM1/EXPORTIN1 (EXPO1) (Bologna, et al., 2018). TREX-2 also promotes the nuclear export of miRNA and AGO1 (Zhang, et al., 2020). RISC recognizes target mRNA through complementary base-pairing between miRNA and its complementary sequences in mRNA target and activates RNA silencing through target cleavage and/or translation repression in cytoplasm (Rogers and Chen, 2013). After cleavage, the cleaved mRNA 3' fragment will be degraded by EXORIBONUCLEASE 4 (XRN4), while the 5' fragment will be uridylated by HEN1 suppressor 1 (HESO1) and then digested by RISC-interacting clearing 3'- 5' exoribonucleases 1 (RICE1) and RICE2 (Figure 1) (Souret, et al., 2004; Zhang, et al., 2017).

Arabidopsis has 10 AGO family members. A typical AGO protein contains an N-terminal domain, PAZ domain, MID domain and P-element-induced wimpy testes (PIWI) domain (Song, et al., 2004; Schirle and MacRae, 2012; Ren, et al., 2014). The N-terminal domain is required for sRNA duplex unwinding and miRNA-target RNA binding and cleavage (Kwak and Tomari, 2012). The MID domain recognizes the 5'-terminal

nucleotide and provides a binding pocket for the 5'-phosphate of sRNAs, while the PAZ domain binds to the 3' end of sRNAs (Hutvagner and Simard, 2008; Boland, et al., 2010; Frank, et al., 2010). The PIWI domain resembles RNaseH and is essential for the target cleavage. The endonuclease activity is carried out by the active site, Asp-Asp-His (DDH) motif (Rivas, et al., 2005; Vaucheret, 2008; Cheloufi, et al., 2010). Apart from the pseudogene AGO8, the other nine functional AGOs can be classified into 3 clusters dependent on sequence similarity: AGO1/5/10, AGO2/3/7 and AGO4/6/9 (Zhang, et al., 2015). AGOs bind with different miRNAs based on their 5'-nucletides (Khvorova, et al., 2003). AGO1 associates with most miRNAs (about 95% cargoes under healthy conditions) including miR166/165 and a certain number of siRNAs such as ta-siRNAs (Howell, et al., 2007; Vaucheret, 2008; Bologna, et al., 2018). AGO1 predominantly binds to sRNAs with a 5' uridine (U) (Mi, et al., 2008). AGO2 preferentially associates with 21-nt sRNAs with a 5' adenosine (A) and play a role in DNA repair and innate immunity (Zhang, et al., 2011; Wei, et al., 2012). Even though AGO2 and AGO3 shared 70% sequence identity, AGO3 was found to preferentially bind to 24-nt sRNAs with a bias for a 5'-A and show a redundancy with AGO4 (Zhang, et al., 2016). AGO4/6/9 all bind to 24-nt sRNAs with a 5'-A (Mi, et al., 2008). AGO7 was highly specific to interact with miR390, a 21-nt miRNA with a 5'-A (Montgomery, et al., 2008). AGO5 prefers sRNA with a 5' cytosine (C) (Mi, et al., 2008) and is mainly expressed near reproductive cells during megasporogenesis (Tucker, et al., 2012). AGO1 and AGO10 are well documented as key components for plant shoot apical meristem (SAM) development (Zhu, et al., 2011). SAM cell differentiation is regulated by class III HOMEODOMAIN LEUCINE

ZIPPER (HD-ZIP III) transcriptional factors which contains five members: PHABULOSA (PHB), PHAVOLUTA (PHV), REVOLUTA (REV), and AT HOMEBOX 8 (ATHB-8) and ATHB-15 (also named CORONA (CNA)) (Barton, 2010). AGO10 has a higher affinity to bind with miR166/165 compared to AGO1. Importantly, this protein function enables it to act as a decoy for miR166/165 to prevent miR166/165 binding to the AGO1-cored RISC complex, leading to increased HD-ZIP III gene expression (Figure 2) (Zhu, et al., 2011).

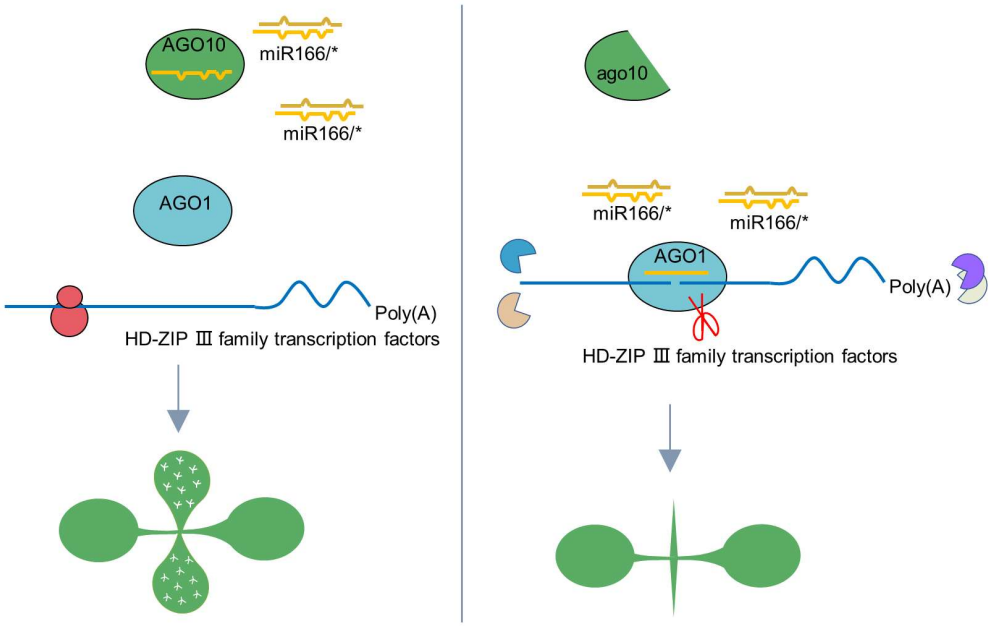

Figure 2 AGO10 sequesters miR166/165 to regulate SAM development
In wildtype condition, miR166/165 is preferentially loaded into AGO10 through its higher binding but not catalytic activity, which prevent itself being loaded into AGO1-RISC complex. Consequently, the target genes of miR166/165, HD-ZIP III family can accumulate and promote SAM differentiation. In ago10 mutant, loss of function AGO10 fails to interact with miR166/165 but AGO1 recruits miR166/165 to perform cleavage to HD-ZIP III family transcripts, resulting in a developmental defect of SAM.

1.1.2 siRNA-mediated RNA silencing

siRNAs are also short (usually 21 nt-25 nt) non-coding RNAs which can be both endogenous and exogenous. Endogenous siRNAs contain *trans*-acting siRNAs (ta-siRNAs) (Vazquez, et al., 2004; Allen, et al., 2005), phasiRNAs (Borsani, et al., 2005), hairpin-derived siRNAs (hp-siRNAs) and heterochromatic siRNAs (hetsiRNAs) (Xie, et al., 2004; Borges and Martienssen, 2015). Exogenous siRNAs can be induced by virus infection (Xie, et al., 2004) and introduction of transgenes (Hamilton and Baulcombe, 1999).

ta-siRNAs are derived from tasiRNA-precursor (*TAS*) mRNAs. In Arabidopsis genome, there are eight TAS genes grouped into four families. The initial step of ta-siRNAs synthesis is that *TAS* transcripts are targeted by miRNAs in a phased manner. *TAS1* and *TAS2* are targeted by miR173 (Yoshikawa, et al., 2013). TAS3 transcripts are targeted by miR390 (Montgomery, et al., 2008; Endo, et al., 2013), and miR828 targets *TAS4* mRNA (Chen, et al., 2010; Fei, et al., 2013). The mode of action of siRNAs is similar to that of miRNAs. However, for ta-siRNAs, after being cleaved by miR173/390-RISC complex containing AGO1/AGO7, the prerequisite step is the conversion of single-stranded (ss) RNA substrates to double-stranded (ds) RNAs, which is fulfilled by RNA-dependent RNA Polymerase 6 (RDR6) and Suppressor of Gene Silencing 3 (SGS3) (Dalmay, et al., 2000; Mourrain, et al., 2000). In Arabidopsis, there are four DCLs. DCL1 is responsible for the process of miRNAs as mentioned above. DCL4 accounts for the process of ta-siRNAs and other 21 nt siRNAs from viral transcripts and transgenes (Bouché, et al., 2006), DCL4 can recognize those dsRNAs as substrates to generate 21 nt

ta-siRNAs. The mature ta-siRNAs will also be methylated by HEN1 (Howell, et al., 2007; Fei, et al., 2013). DCL2 participates in the synthesis of 22 nt siRNAs from endogenous inverted repeats, and also aberrant transcripts from virus and transgenes (Borsani, et al., 2005; Deleris, et al., 2006; Parent, et al., 2015). Among them, DCL2 and DCL4 are phylogenetically more proximate to each other than to other DCLs in plants (Figure 3) (Parent, et al., 2015). When DCL4 is absent, DCL2 can take over redundantly and produce 22 nt siRNAs instead (Gasciolli, et al., 2005; Adenot, et al., 2006). Compared with DCL2, DCL4 exhibits a higher binding affinity with dsRNA (Parent, et al., 2015). However, compared with 21-nt siRNAs, which are less efficient in triggering S-PTGS but play roles as secondary siRNAs, 22-nt siRNAs are more efficient at inducing target RNA degradation and transferring target RNA cleavage products into dsRNA by RDR6 and SGS3, which serves as primary siRNAs (Mlotshwa, et al., 2008; Parent, et al., 2015; Wu, et al., 2017). Recent studies also showed that DCL2 derived 22 nt siRNAs can both trigger amplification of gene silencing and induce translation repression (Wu, et al., 2020). Previously plant DCLs were assigned a nuclear localization (Xie, et al., 2004; Hiraguri, et al., 2005; Kumakura, et al., 2009). However, recent studies indicated that ancestral DCL4 localizes in cytoplasm when *DCL4* gene was driven by its native promoter (Pumplin, et al., 2016; Montavon, et al., 2017).

phasiRNAs are similar to tasiRNAs but can be derived from both coding and non-coding transcripts (Borges and Martienssen, 2015). The loading of siRNAs (ta-siRNAs, phasiRNAs and transgene derived siRNAs which are RDR6 and DCL4-dependent) to

AGO1 occurs in cytosol rather than in nucleus and also is HSP90-required (Bologna, et al., 2018).

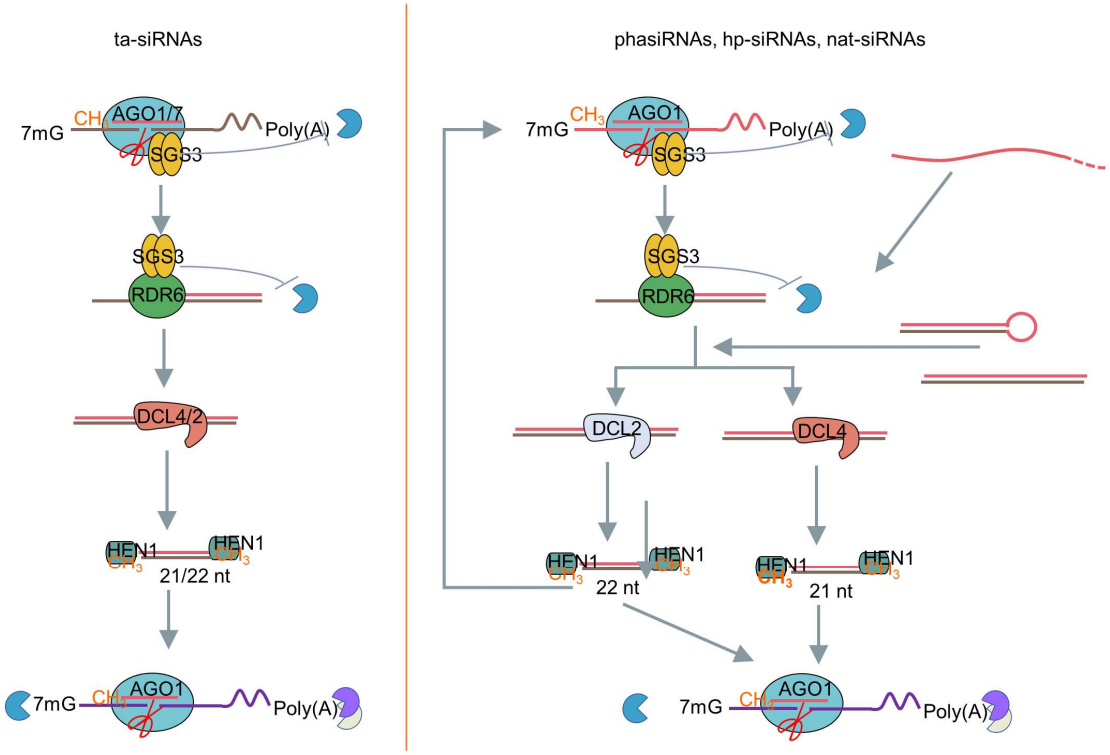

Figure 3 ta-siRNAs, phasiRNAs and hp-siRNAs biogenesis
(Left) ta-siRNAs was processed by DCL4/2 utilizing dsRNA substrates, which was synthesized by RDR6/SGS3 complex from miR173/390/828-cleaved *TAS* mRNA fragments. 21/22 nt ta-siRNAs are loaded into RISC complex and perform cleavage to their targets. (Right) phasiRNAs and hp-siRNAs are similar to ta-siRNAs. DCL2 diced 22-nt siRNAs can also generate next level siRNAs.

1.1.3 S-PTGS and IR-PTGS pathway

The miRNA and siRNA mediated gene silencing mechanisms mentioned above belong to the PTGS pathway. PTGS functions mainly to eliminate invading RNAs, and regulate the expression of stress-regulated genes and genes involved in cell-type

specification (Wang and Chekanova, 2016; Pooggin, 2017). The induction of PTGS takes place when the aberrant RNA accumulation reaches a threshold (Christie, et al., 2011). For transgene induced PTGS, there are two branched pathways according the forms of RNA transcribed from the transgene loci: sense PTGS (S-PTGS) and inverted repeat PTGS (IR-PTGS) (Martinez de Alba, et al., 2013). S-PTGS is usually triggered by external factors, such as virus or pathogen RNA and transgene RNA. Those RNAs serve as the template to form dsRNAs via RDR6 at siRNA-bodies. The dsRNAs are further processed through a DCL2/4-dependent way into 22/21 nt siRNAs (Hamilton and Baulcombe, 1999; Komiya, 2017). IR-PTGS is triggered by double-stranded RNA (dsRNA) that formed from the self-folding of single-stranded RNA (ssRNA) such as hp-siRNAs (Parent, et al., 2015). As a special scenario, IR or hairpin PTGS is triggered by self-folded dsRNA can bypass the RDR6/SGS3 activity. However, the IR/hairpin-derived siRNAs could in turn target beyond the IR region to produce secondary siRNAs; and this process entails RDR6/SGS3 function (Tijsterman, et al., 2002; Harmoko, et al., 2013; Parent, et al., 2015). The recruitment of RDR6 to the sliced transcripts may depend on target cleavage preferably triggered by 22 nt sRNA (Cuperus, et al., 2010). Based on previous studies, RDR6 is a primer-independent RNA polymerase, which can use ssRNA or ssDNA but not dsRNA to synthesize RNA. RDR6 activity is not influenced by cap or poly(A) (Curaba and Chen, 2008). Notwithstanding, biochemical partners and functions of RDR6/SGS3-DCL4/DRB4 are far less understood compared with the knowledge of microprocessor.

1.1.4 sRNA-mediated TGS pathway

PTGS functions mainly to regulate plant development and physiology, eliminate invading RNAs and endogenous aberrant RNAs, and respond to abiotic stress (Wang and Chekanova, 2016; Pooggin, 2017). Apart from mediating PTGS, sRNAs can also mediate TGS pathway. TGS functions in transposon control, biotic and abiotic resistance, reproduction and intercellular and intracellular communication (Matzke and Mosher, 2014). siRNAs involved in TGS mainly contains hetsiRNAs, which is the most abundant siRNAs, and part of phasiRNAs (Pikaard and Scheid, 2014). In this case, partially or fully paired dsRNAs are generated from the paired secondary structure of long inverted repeating transcription, or dsRNAs synthesis from RDRs (Matzke, et al., 2015). RNA-directed DNA methylation (RdDM) is a major siRNA-mediated epigenetic pathway. RdDM can suppress many pericentrometic regions, endogenous transposable elements (TEs) and repeat regions to prevent transposition and transcription (Matzke, et al., 2009; Matzke, et al., 2015). Canonical RdDM involves PolIV-dependent siRNA biogenesis and PolV-mediated de novo DNA methylation and maintenance of epigenetic modifications (Matzke and Mosher, 2014). ssRNAs transcribed by RNA polymerase IV (Pol IV) plays roles as templates for RDR2, which transcribes ssRNAs into dsRNAs. dsRNAs serve as substrates of Dicer-like 3 to be cleaved into 24 nt siRNAs (Holoch and Moazed, 2015; Komiya, 2017). PolIV derived siRNAs (p4-siRNAs) have been grouped into two clusters named type I and type II: type I p4-siRNAs are only present in flowers and young siliques, whereas type II express in all tissues (Mosher, et al., 2009). These siRNAs are loaded into AGO4 (mainly, also AGO3 and AGO6, which is redundant with AGO4 (Havecker, et al.,

2010; Zhang, et al., 2016); and AGO9, which specifically expresses in reproductive tissues(Olmedo-Monfil, et al., 2010)) containing complex and bind with target sites. AGO4 interacts with the GW domain of PolV and recruits PolV and also its transcripts in an siRNA-dependent way. AGO4/PolV recruits the CHH DNA methyltransferase DOMAINS REARRANGED METHYLTRANSFERASE 2 (DRM2). RNA-DIRECTED DNA METHYLATION 1 (RDM1) associates with AGO4/PolV/DRM2 complex and deposits them to methylated DNA loci (Gao, et al., 2010). Some histone modifications including Histone 3 Lysine 9 methylation (H3K9Me) readers (for example, SAWADEE HOMEODOMAIN HOMOLOG 1 (SHH1)) can reinforce the silent status in combination with DNA methylation (Holoch and Moazed, 2015). Several enzymes are identified to be involved, including HISTONE DEACETYLASE 6 (HDA6), which catalyzes deacetylation of multiple lysines on histones (Aufsatz, et al., 2002; Blevins, et al., 2014), and KRYPTONITE (KYP), which can be recruited to methylated DNA and methylates histones nearby, and this H3K9me2 will recruits CHROMOMETHYLASE 3 (CMT3) to catalyze non-CG methylation (Law and Jacobsen, 2010; Du, et al., 2015). Thus, the methylation enzymes, readers, two polymerases and AGO4 coordinate together to develop the self-reinforcing loop RdDM (Figure 4).

Apart from canonical RdDM, there are emerging non-canonical mechanisms which utilize components involved in classic TGS pathway. For instance, cleaved *TAS* transcripts can be transcribed by RDR6/SGS3 into dsRNAs, and the dsRNAs can be either digested by DCL4 with redundant DCL2 to silence target genes in a PTGS manner; or processed by DCL1 or DCL2/3/4 to trigger AGO4/6/PolV-mediated DNA methylation on

TAS loci (Wu, et al., 2012). In actively transcribed TE loci, ssRNA transcribed by PolII can be converted by RDR6 to dsRNA and further processed into 21-22 nt siRNAs by DCL4/2. Some of these siRNAs are loaded into AGO1-RISC complex to mediate PTGS silencing to TE loci, while some siRNAs are loaded into AGO6 recruiting PolV transcripts and DRM2 to trigger and reestablish TE DNA methylation and epigenetic silencing (Nuthikattu, et al., 2013; McCue, et al., 2015). Once the RDR6-derived dsRNAs pass the threshold of DCL2/4, DCL3 may takeover and produce 24-nt siRNAs in a compensatory way (Marí-Ordóñez, et al., 2013) (Figure 5). Besides, a GW repeat- and PHD finger-containing protein NEEDED FOR RDR2INDEPENDENT DNA METHYLATION (NERD) can also mediate RdDM which requires Pol IV and PolV, and also PTGS elements including RDR6, SGS3, AGO2, SILENCING DEFECTIVE PROTEIN 3 (SDE3) and SDE5 (Pontier, et al., 2012).

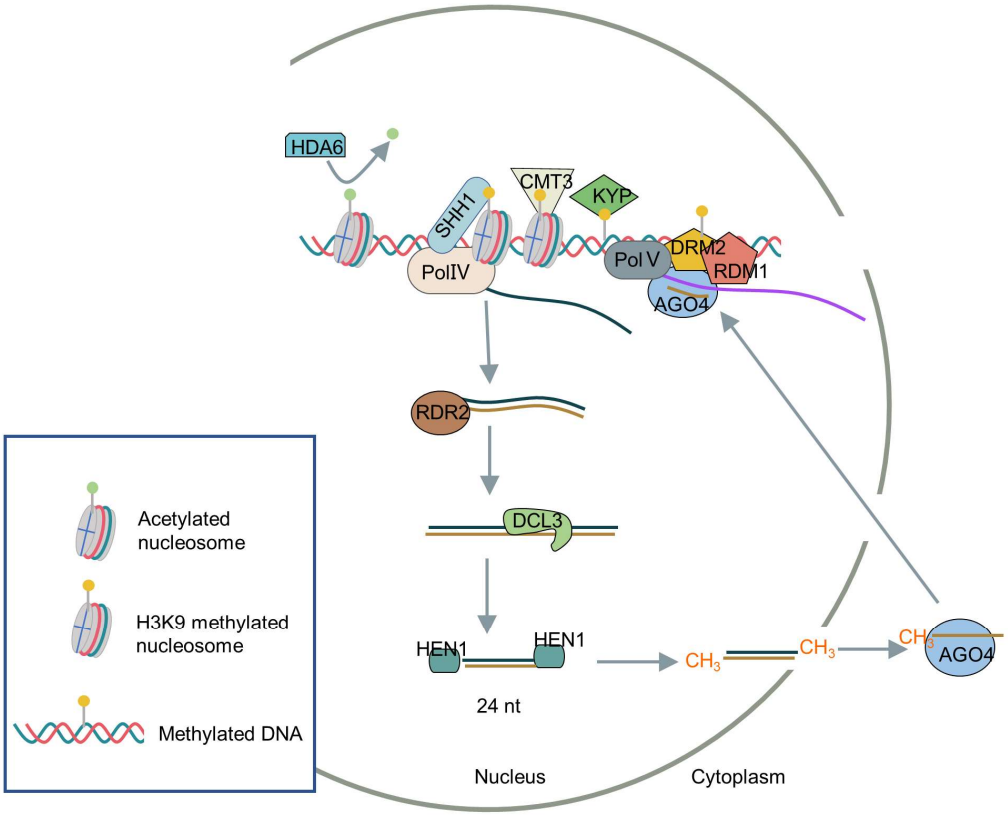

Figure 4 Canonical RdDM pathway in *Arabidopsis*
PolIV transcripts serve as template of RDR2 to synthesis short dsRNAs. After processing of DCL3, 24 nt siRNAs are loaded into AGO4 in cytoplasm and then be co-transported back to nucleus. AGO4/p4-siRNAs interacts with PolV and its transcripts in an RNA-dependent manner. AGO4/p4-siRNA/PolV recruit DRM2 to perform CHH methylation and this methylation will be recognized by RDM1 and reinforce the AGO4/PolV/DRM2 recruitment. Histone methylation readers and methylase also coordinate with those components to create this reinforce feedback loop.

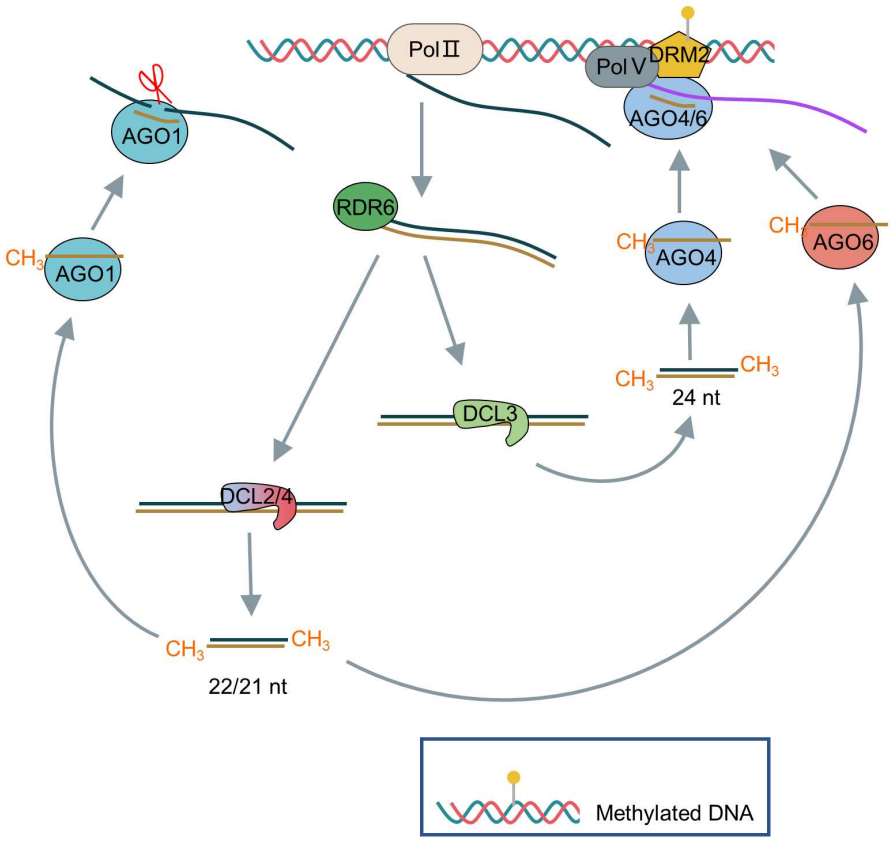

Figure 5 Non-canonical RDR6-RdDM pathway in *Arabidopsis*
In actively transcribed TE loci, RDR6 can copy PolII-transcribed ssRNAs into dsRNAs. The dsRNAs can be be chopped by DCL3 into 24-nt siRNAs to perform canonical RdDM regulation, or be processed by DCL2/4 into 21/22-nt siRNAs. The siRNAs are either loaded to AGO1-RISC complex and execute PTGS silencing to TE transcripts, or be loaded into AGO6 and initial a low-level DNA methylation dependent on PolV and DRM2.

Notably, not only PTGS components have crosstalk with TGS pathway, but also classic TGS proteins such as RDR2/DCL3/AGO4/Pol IV also participate in systemic PTGS and long-distance RNA silencing (Brosnan, et al., 2007; Melnyk, et al., 2011; Gaffar and Koch, 2019). RDR2 partially antagonizes RDR6 in S-PTGS pathway (Jauvion, et al., 2012).

1.1.5 RNA quality control

RNA quality control pathways can serve as RNA-silencing suppressors to supervise inappropriate RNA silencing. Vice versa, when RNA surveillance failed to eliminate aberrant RNAs, RNA silencing can be activated (Liu and Chen, 2016; Zhang and Guo, 2017). These two mechanisms coregulate RNA homeostasis in a tug-of-war manner. In eukaryotes, there are three types of mRNA decay pathways: nonsense-mediated decay (NMD), non-stop decay (NSD) and non-go decay (NGD) pathways. 1) NMD pathway is triggered by a premature termination codon (PTC), or other features like an excessive long 3'UTR, a translated open reading frame (ORF) which is out of the main ORF and alternative splicing in UTRs (Reddy, et al., 2013; Chantarachot and Bailey-Serres, 2018). NMD requires three core elements: UP FRAMESHIFT1 (UPF1), UPF2, and UPF3 which can be recruited by PTC-containing transcripts and direct RNA decay. UPF1 is responsible for the activation of NMD and recruitment of UPF2 and UPF3 (Dai, et al., 2016). UPF1 and UPF3 are PTGS suppressors given that defects in UPF1 and UPF3 can positively affect PTGS (Moreno, et al., 2013). 2) NSD pathway targets mRNAs lack of stop codons composed of nonstop mRNAs, which contains poly (A) tail at 3' end generated by premature polyadenylation, and stop codon-less mRNAs, which lack poly (A) tail because of endonucleolytic cleavage in the coding region (Szádeczky-Kardoss, et al., 2018). Highly conserved Pelota (a homolog of Drosophila Pelota protein), HBS1 (HSP70 SUBFAMILY B SUPPRESSOR 1, also named SUPER KILLER 7 (SKI7)) and SKI2 are required for NSD in plants. SKI7 will recruit the exosome to perform 3' to 5' degradation. In plants, as an endonucleolytic cleaved fragments, the 5' cleavage fragments

by RISC-complex requires NSD machinery to be eliminated (Szádeczky-Kardoss, et al., 2018). 3) NGD pathway eliminates mRNAs with stalled translating ribosomes. In mammals, Ribosome stalling triggers the ubiquitination of ribosomal proteins, which further lead to endonucleolytic cleavage by a nuclease, then the 5' cleaved product is degraded by exosome like in the NSD mechanism while 3' cleaved product is degraded by XRN1 (Simms, et al., 2017; Liang, et al., 2019; Tatosyan, et al., 2020).

No matter which RNA decay pathway is used, the prerequisites of RNA degradation includes deadenylation and decapping. Deadenylation involves progressive shortening of 3' poly(A) tails mediated by several deadenylases including the conserved poly(A)-specific ribonuclease (PARN) and CARBON CATABOLITE REPRESSOR 4-NEGATIVE ON TATA (CCR4-NOT) complex (Liu and Chen, 2016; Tatosyan, et al., 2020). Impairment of PARN and CCR4 can enhance S-PTGS (Moreno, et al., 2013). After the initiation step of deadenylation, decapping is guided by conserved decapping enzymes and enhancers including DECAPPING 1 (DCP1), DCP2, DCP5, VARICOSE (VCS, also named ENHANCER OF mRNA DECAPPING4 (EDC4)), SM-LIKE (LSM) 1-7 complex and PROTEIN-ASSOCIATED WITH TOPOISOMERASE1 (PAT1) (Liu and Chen, 2016; Chantarachot and Bailey-Serres, 2018). Mutations in DCP1, DCP2 and VCS provoke an enhancement of RDR6-dependent transgene PTGS (Martinez de Alba, et al., 2015). After deadenylation and decapping, the "naked" mRNAs will be digested from 5' to 3' by exoribonucleases of the XRN family (XRN2 and XRN3 in nucleus and XRN4 in cytoplasm) and from 3' to 5' by exosome complex and co-factors (Liu and Chen, 2016; Chantarachot and Bailey-Serres, 2018; Tatosyan, et al., 2020). In cytoplasm, XRN4

suppresses PTGS by 5’ to 3’ degradation to the decapped RNA fragments cleaved by sRNAs, consequently suppress RNA-dependent RNA synthesis. The mutation of XRN4 promotes RDRs-dependent RNA silencing (Souret, et al., 2004). In nuclear, XRN2 and XRN3 can individually suppress PTGS through targeting pri-miRNA loops (Gy, et al., 2007). 3’ (2’), 5’-bisphosphate nucleotidase/inositol polyphosphate1-phosphatase FIERY1 (FRY1, also known as SAL1 or HOS2) can decompose 3’-phosphoadenosine 5’-phosphate (PAP) into 5’ AMP and Pi (Quintero, et al., 1996). FRY1 also serve as a PTGS suppressor since the loss function of FRY1 will accumulate PAP and consequently suppress XRNs activity (Gy, et al., 2007). Impairment of exosome components RRP4, RRP6L1, RRP41 and RRP44A was also found to enhance S-PTGS, indicating exosome proteins are suppressors of PTGS (Moreno, et al., 2013). RPT2a, a subunit of the 26S proteasome complex, was found do promote transgenic S-PTGS indirectly through negatively regulating RQC component such as RRP45a (Kim, et al., 2019).

1.2 SGS3 and DRB4

SGS3 was discovered through an EMS system aiming at impaired silencing of 35S promoter (derived from cauliflower mosaic virus (CaMV))-driven β-glucuronidase (GUS) in PTGS (Mourrain, et al., 2000). *sgs3-1* showed a significant accumulation of *GUS* transcripts and enhanced susceptibility to Cucumber mosaic virus (CMV). SGS3 is a plant-specific protein and no similarity with other proteins have been found (Bateman, 2002). However, there are 14 SGS3 family proteins containing those three domains have been identified, such as factor of DNA methylation (FDMs) and in *de novo* 2 (IDN2, also

called RDM12) (Bateman, 2002; Xie, et al., 2012). In *Arabidopsis*, *sgs3* mutants show a down curved leaves like *rdr6* mutants (Peragine, et al., 2004). SGS3 contains three domains: Zinc finger (ZF) domain, rice gene X and SGS3 (XS) domain and Coiled-coil (CC, also named as rice gene X Homology (XH)) domain (Bateman, 2002). In tomato, a homolog SlSGS3 can complement *sgs3-1* Arabidopsis phenotype and restore RNA silencing. SlSGS3 is a target of V2 protein, an RNA-silencing suppressor from *Tomato yellow curl leaf geminivirus* (TYLCV), and their interaction is indispensable for RNA-silencing suppression (Glick, et al., 2008). SGS3 was believed to function upstream of RDR6, and was demonstrated to stabilize the single-stranded fragments after primary siRNA cleavage (Yoshikawa, et al., 2005). SGS3 can interact with RDR6 and co-localize in cytoplasm to form granules adjacent to Processing-bodies (P-bodies) (Kumakura, et al., 2009). SGS3 itself does not affect RDR6 activity (Fukunaga and Doudna, 2009). SGS3 functions as a homodimer and this dimerization is important in the formation of cytoplasmic foci (Elmayan, et al., 2009). The XS domain is conserved in plants and is critical for RNA-binding activity. The CC domain is important for protein-protein interaction and homodimerization. Both XS and CC domains are critical for the localization in cytoplasm (Yoshikawa, et al., 2005; Elmayan, et al., 2009; Fukunaga and Doudna, 2009; Kumakura, et al., 2009). The truncation form containing N-terminal domain alone located mainly in cytoplasm as granule-like foci, while truncated SGS3 containing ZF domain alone mainly located in nucleus (Cheng and Wang, 2017). All three domains (XS, CC, and ZF) are important for the function of SGS3 in RNA silencing (Kumakura, et al., 2009). The XS domain is predicted to be a single-stranded RNA-

binding domain (RBD) with a unique version of a RNA recognition motif (RRM) fold (Zhang and Trudeau, 2008). While the in vitro assay showed that SGS3 alone does not bind to ssRNA, but prefers to bind to dsRNA with 5' overhang. The removement of ZF domain somehow seems promote the RNA binding affinity (Fukunaga and Doudna, 2009) and depletion of the ZF domain can increase SGS3 granule numbers in cytoplasm (Kumakura, et al., 2009). SGS3 also interacts with AGO1 and associates with miR173-RISC-target RNA. In tobacco, depletion of NtSGS3 destabilizes miR173-RISC-target cleavage fragment complex (Yoshikawa, et al., 2013). However, in the in vitro experiment, depletion of NtSGS3 does not affect the stabilization of cleavage fragment of *GFP* digested by gf698siRNAs (Yoshikawa, et al., 2013). SGS3 is targeted by virus proteins. A viral genome-linked protein (VPg) from Potyvirus can interact with SGS3 and mediates its degradation through 20S ubiquitin-proteasome and autophagy. Interestingly, even VPg itself localize mainly in nucleus, it can interact with SGS3 in cytoplasm (Cheng and Wang, 2017). But so far, how does SGS3 get involved in a wide-range of RNA silencing is not fully studied.

dsRNA BINDING PROTEIN4 (DRB4) is one of five dsRNA-binding proteins (DRB1-5). DRB1 is best known as HYL1, which specifically interacts with DCL1 to synthesize miRNAs (refer to section 1.1.1). DRB4 interacts with DCL4 to generate 21-nt siRNAs from TAS precursors and transgene-derived long dsRNAs (Fukudome and Fukuhara, 2017). DRB4 is required for the generation of exogenous 21-nt siRNAs through DCL4 and its dsRNA-binding domain is essential to facilitate DCL4 dicing activity (Fukudome, et al., 2011). Besides, the nuclear localization of ancestral DCL4 require its

co-factor DRB4 (Pumplin, et al., 2016). DRB2, 3 and 5 were reported not be involved in siRNA biogenesis (Curtin, et al., 2008), while later, DRB2 was found to be involved in the biogenesis of a specific miRNA subsets and DRB3 and DRB5 was involved in mediating RNA silencing triggered by DRB2-derived miRNAs (Eamens, et al., 2012). Loss of DRB2 results in an exclusive accumulation of p4-siRNAs while loss of DRB4 displays an opposite effects, indicating the DRB2 functions antagonistically to DRB4 (Pélissier, et al., 2011).

Although the main biochemical themes for RNA silencing have been extensively studied and auxiliary factors that impact the processes have been identified (Stepien, et al., 2017; Song, et al., 2019), RNA silencing remains to be fully understood.

1.3 Forward genetic methods to identify mutants involved in RNA silencing.

Forward genetic methods have been widely used in finding new genes involved in RNA silencing. Screening based on morphological phenotypes is mainly used. For example, a reporter system was designed with the *SUCROSE-PROTON SYMPORTER 2* (*SUC2*) promoter-driven expression of inverted repeat of the *phytoene desaturase* (*PDS*) gene. This can silence *PDS e*xpression in phloem companion cell where *SUC2* expressed specifically. Thus, the *SUC-hpPDS* transgenic line showed a bleached phenotype in leaf vein. Through the mutagenesis to this line, two genes, *FLOWERING TIME CONTROL PROTEIN* (*FPA*) and *FLOWERING CONTROL LOCUS A* (*FCA*) were recovered as suppressors to transgenic silencing through TGS pathway (Baurle, et al., 2007).

Another method was developed based on external reporter genes. In earlier times, *GUS* gene is widely used in Arabidopsis. RDR6 and SGS3 were identified from EMS mutagenesis to L1 line, a *35S-GUS* transgenic line with silenced *GUS* expression (Mourrain, et al., 2000). For instance, a line that constitutively expresses green fluorescent protein (GFP) mRNA fused with a miR171 target site was used as an EMS parental line. Mutants were identified based on the GFP expression level in leaves. *mbd* (*miRNA biosynthesis deficient*) mutants and *mad* (*microRNA action deficient*) mutants were found based on increased GFP signal. Among the mutants identified, *MAD5* encodes *KATANIN (KIN1*), an important protein involved in miRNA-directed translational repression (Brodersen, et al., 2008). Additionally, *KIN1/VCS* is also found to be required in miRNA-directed translational repression. These finding suggest that RNA quality control could be conjunct with some plant miRNAs action like that in animal cells (Brodersen, et al., 2008). *LIL* (*LOW IN LUCIFERASE EXPRESSION*) was identified though two LUC-based reporters, LUCH (Won, et al., 2012) and YJ (Li, et al., 2016), which were transferred into *rdr6*-11 mutant to prevent post-transcriptional gene silencing. LIL associates with MBD7 (METHYL-CpG-BINDING DOMAIN 7) and LIL-MBD7 complex is involved in DNA-methylation mediated gene silencing (Li, et al., 2017).

Apart from native miRNAs target site and inverted repeats, artificial miRNAs are also widely used in system design in Arabidopsis. For example, a reporter system was developed by expressing 35S promoter-driven artificial miRNA targeting three R3 MYB genes: *CAPRICE (CPC), TRIPTYCHON (TRY), and ENHANCER of TRIPTYCHON AND CAPRICE2 (ETC2*) regulating trichrome synthesis. Mutations in these genes showed an

increased trichrome density. So, the clustered trichrome was used as an indicator of miRNA activity. A gene named *Enhanced miRNA Activity 1* (*EMA1*) encodes an Importin ß Protein (also known as SUPER SENSITIVE to ABA and DROUGHT 2 (SAD2), which play a negative role in miRNA activity by interfering the loading of miRNAs into AGO1 (Wang, et al., 2011). In 2012, Manavella et al. designed a 35S promoter-Firefly luciferase (LUC) and then silenced it with an artificial miRNA (miR-LUC) which can be ubiquitously expressed. The purpose is to avoid unwanted influence of endogenous genes. *C-TERMINAL DOMAIN PHOSPHATASE-LIKE 1* (*CPL1*) was identified, which can regulate HYL1 activity. Full HYL1 activity requires CPL1-dependent dephosphorylation (Manavella, et al., 2012). Recently, Zhang et al. screened an allele of THP1 through EMS mutagenesis screening of a reporter system: *pSUC2: amiR-SUL* (*amS*) line, which expresses artificial miRNA targeted to *SULFUR* (*SUL*) under *SUC2* promoter. *THP1* belongs to transcription-coupled export 2 (TREX-2) complex and regulating several steps of miRNA biogenesis (Zhang, et al., 2020).

Enlightened by the forward genetic screening methods above, and combined with the previous discovery in our lab (Zhu, et al., 2011), we designed a unique reporter system and started our screening of new components involved in RNA silencing.

1.4 FVE

FLOWERING LOCUS VE (*FVE*), also known as *ALTERED COLD-RESPONSE GENE* (*ACG1*) (Kim, et al., 2004), and *MULTICOPY SUPPRESSOR OF IRA1 4* (*MSI4*), has been repeatedly recovered through independent genetic screenings for later flowering

mutants and cold response sensitivity (Koornneef, et al., 1991; Ausin, et al., 2004; Kim, et al., 2004). FVE is a plant homolog of mammalian retinoblastoma-associated protein (RbAp48) and yeast MSI (Kenzior and Folk, 1998). RbAp48 acts through multiple epigenetic complexes to impact tumorigenesis, cytoskeletal organization, age-related memory loss and cardiomyocyte hypertrophy (Nicolas, et al., 2000; Pavlopoulos, et al., 2013; Kosmidis, et al., 2018; Sunagawa, et al., 2019). In mammals, RbAp48 appears to function in different complexes. RbAp48 is recovered from the Histone Deacetylase Complex which contains Histone Deacetylase 1 (HDAC1) and Rb protein (Nicolas, et al., 2000; Laubinger, et al., 2010). RbAp48 is also a member of polycomb repressive complexes 2 (PRC2) that deposit a repressive mark of H3K27me1/2/3 in chromatin (Müller, et al., 2002). RbAp48 also has direct interaction with histones H3-H4 (Zhang, et al., 2013), and is believed to be a subunit of the chromatin assembly factor 1(CAF-1) complex (Loyola and Almouzni, 2004). In addition, RbAp48 is also recovered in an nucleosome remodeling deacetylase complex containing chromatin remodeling ATPase and chromatin deacetylation enzymatic activity (Allen, et al., 2013).

Arabidopsis contains five members of *MSI*-like gene family. *MSI1*, *MSI2* and *MSI3* are genetically closer to animal homologs compared to *MSI4* and *MSI5* that have high sequence similarity to each other (Ausin, et al., 2004). Loss of function mutant of *FVE* flowers late under all photoperiods (flowering delay more under short-day condition compared with that under long-day condition) and has greater tolerance of freezing (Kim, et al., 2004). Overexpression of *FVE* can only partially recover the late flowering phenotype (Ausin, et al., 2004). Apart from late flowering, *fve* mutant also displays a

longer life span and a dramatic increase of biomass (Abou-Elwafa, et al., 2011). Until now, there are 7 *five* alleles has been published: *five-1* and *five-2* with amino acid changes caused by EMS (Ausin, et al., 2004); *five-3* and *five-4* with premature terminating codons induced by fast-neutron (Ausin, et al., 2004); *five-5* with a premature terminating codon caused by EMS (Kim, et al., 2004); *five-6* and *five-7* made by T-DNA insertion (Morel, et al., 2008; Abou-Elwafa, et al., 2011). FVE contains six WD40 domains. The fourth WD repeat contains a putative retinoblastoma-binding motif (L-X-C-X-D) (Williams and Grafi, 2000). Besides, a potential zinc-binding site localizes in the sixth WD40 domain (Kenzior and Folk, 1998). WD40 domain is one of the most abundant domains in eukaryotes (Xu and Min, 2011). WD40 repeats can fold into a β-propeller structure (Xu and Min, 2011) (Figure 6). Like other MSI-like proteins or other WD40-enriched proteins, FVE has been known to act as a structural scaffold for the assembly of large complexes (Abou-Elwafa, et al., 2011).

FVE gene is known as one of seven genes in an autonomous flowering pathway in plants and FVE is required for histone deacetylation on *FLC* chromatin (Ausin, et al., 2004; Kim, et al., 2004). To a certain degree, MSI5 works redundantly with FVE (Gu, et al., 2011). HDAC complex containing FVE is involved in H3K9K14 deacetylation and H3K4 demethylation at the *FLC* loci (Figure 7) (Luo, et al., 2015).

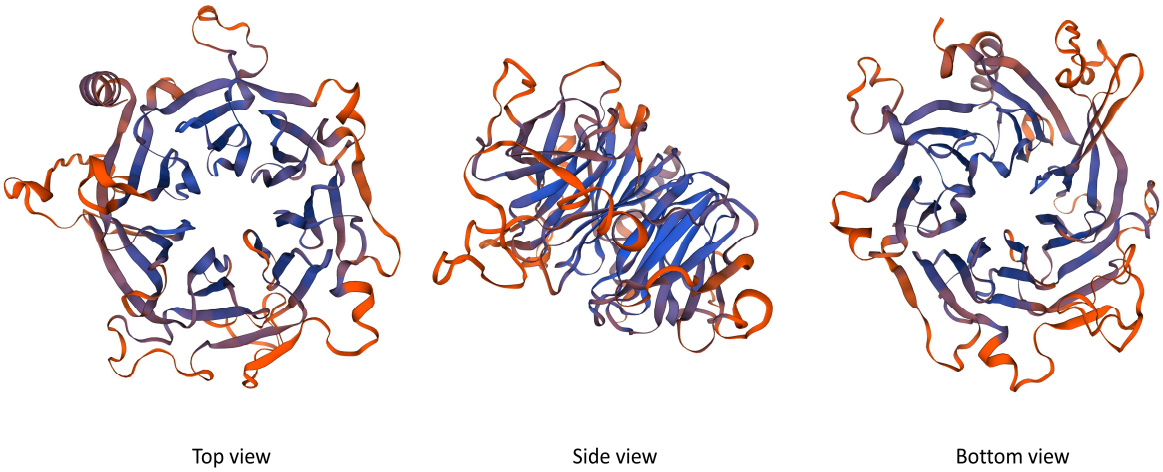

Figure 6 FVE structure prediction by SWISS-MODEL (https://swissmodel.expasy.org/)

With a typical feature of WD40-containing DDB1 and CUL4-associated factors (DCAFs), FVE also acts as a substrate receptor in CUL4-DDB1 ubiquitin E3 ligases. CUL4-DDB1^{MSI4} complex is present at *FLC* chromatin and interacts with a polycomb repressive complex 2 like complex (PRC2-like complex), mediating H3K27 trimethylation (H3K27Me3) of *FLC* (Figure 7) (Pazhouhandeh, et al., 2011), reminiscent of mammalian *RbAp48*. Two key components, FVE and CLF can be downregulated under UV-B radiation and cause decreased H3K27Me3 histone methylation level of *MIR156* loci (Dotto, et al., 2018). It has been reported that FVE/MSI5 form a complex with FLOWERING LOCUS D (FLD), a putative H3K4 demethylase, and HDA6 and HDA5. FVE-containing HDAC complex works on some RdDM target loci through mediating H3K9K14 deacetylation and H3K4 demethylation as repressive chromatin markers that positively regulate cytosine methylation (mainly CHG and CHH methylation), which may

promote the repressive histone modifications as a reinforce-loop (Gu, et al., 2011; Luo, et al., 2015; Yu, et al., 2016).

FVE also interact with HIGH EXPRESSION OF OSMOTICALLY RESPONSIVE GENE1 (HOS1) and is involved in HOS1-mediated activation of *FLC* transcription (Jung, et al., 2013). FVE/MSI5 interact with TRANSPOSABLE ELEMENTSILENCING VIA AT-HOOK (TEK), which is also a member of HDAC complex (Xu, et al., 2013). FVE contributes to silencing of transposons such as *AtMu1* and *AtSN1* with a hypermethylation status of those loci (Baurle and Dean, 2008). Although the regulation of FVE to *FLC* is independent of FCA, FCA requires FVE to repress *AtMu1* (Baurle and Dean, 2008). This function is reported to be through interacting with DRB2 and modulating RNA-directed DNA methylation pathway (RdDM) in a negative feedback loop (Clavel, et al., 2015). Despite the well-appreciated function in the epigenetic level, whether and how the FVE/RbAP48 functions in PTGS is unclear.

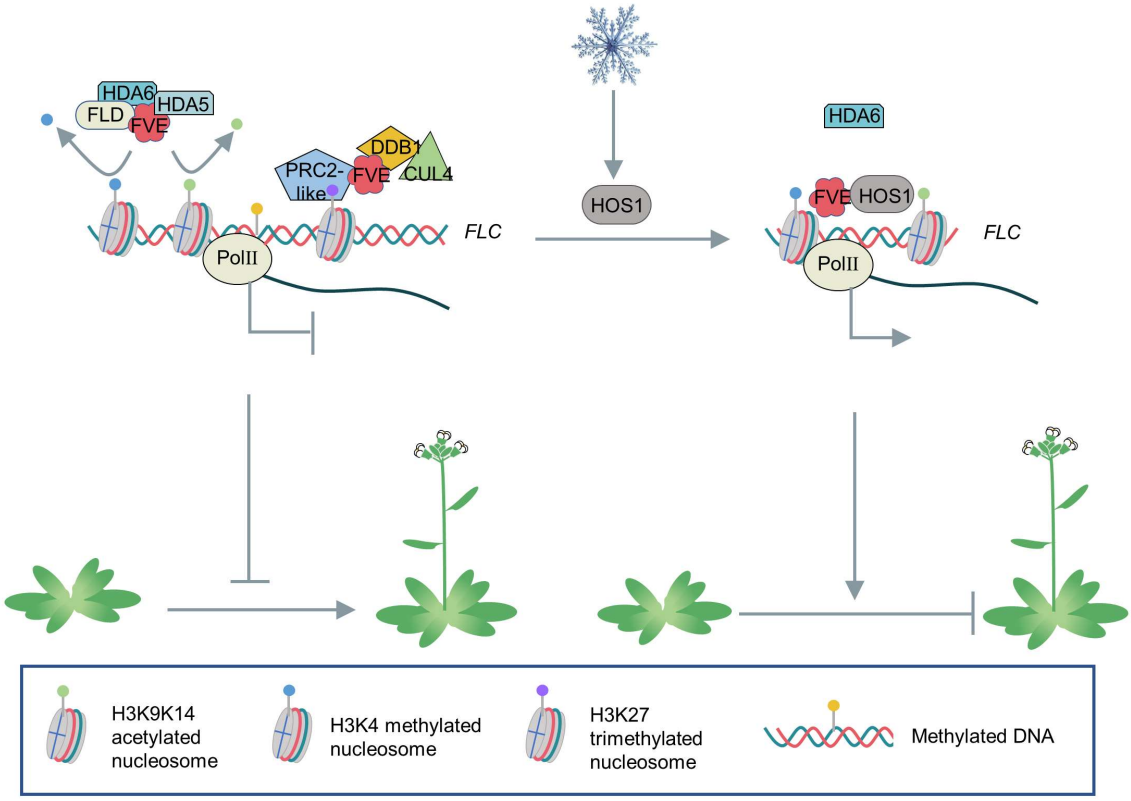

Figure 7 FVE is involved in multiple complexes.
FVE interacts with HDAC complex to perform H3K9K14 deacetylation and H3K4 demethylation to *FLC* chromatin, which are positive transcriptional marker. The suppression of *FLC* transcription will promotes the floral transition; FVE also interacts with DDB1-CUL4 and with PRC2-like complex to perform H3K27me3 to *FLC* chromatin to promote floral transition. In cold stress, HOS1 is induced and compete with HDA6 to interacts with FVE, which limits the accessibility of HDAC to FLC chromatin, therefore, suppress floral transition.

Even though WD40 proteins mainly function as an adaptor or platform in protein complexes, they may also bind with nucleotides (Xu and Min, 2011). Human Gemin5, a snRNA-binding subunit of SMN (survival of motor neuron) complex required for spliceosomal small nuclear ribonucleoparticle, contains 14 tandem WD40 domains. The WD40 domain mediates the specific binding to the Sm site [$A(U)_{4-6}G$] and m^7GpppG cap

of pre-snRNAs (Jin, et al., 2016; Xu, et al., 2016). Also, it has been predicted but not tested that RbAp48, the mammalian homolog of FVE, may also have the potential to bind to RNA (Bellucci, et al., 2011).

1.5 Dissertation review

Although biochemical themes for RNA silencing have been extensively studied and auxiliary factors have been identified to impact the processes (Stepien, et al., 2017; Song, et al., 2019), RNA silencing remains to be fully understood. My general research interest is to identify the new components involved in RNA silencing. This dissertation is composed of 3 main parts. The first part (Chapter II) presents how a *five* mutant is screened and what pathway it affected to increase reporter gene expression. In the second part (Chapter III) I examine how FVE affects this pathway. In the third part (Chapter IV) I introduce some other mutants screened from the same system but for which following study was stopped or paused.

Chapter II presents the discovery of a new allele of *five*. In this study, we designed a well-verified dual reporter system and used a forward genetic screening system to identify a new allele of *five* (*five-8*) with enhanced reporter gene transcripts level. FVE is localized in both nucleus and cytoplasm but cytoplasmic portion of FVE could fully rescue *five* defect in PTGS. These results shed new light on a non-canonical character of FVE involved in PTGS pathway.*five-8* displayed restricted effects on endogenous miRNA and tasiRNAs pathway, but had reduced siRNA production from sense and hairpin transgenes.

In Chapter III, we explored the mechanism of how FVE promotes RNA silencing through siRNA PTGS pathway. We found that FVE can interact with SGS3 and promote its homodimerization. Unexpectedly, FVE binds ssRNAs and dsRNAs with moderate affinity while FVE-8 has a significantly increased binding affinity to dsRNA, and these features impact SGS3/RNA association and routing to DRB4/DCL2/4 complexes. FVE and SGS3 also interact with DRB4 separately. In turn, FVE promotes whereas FVE-8 suppresses DRB4/DCL2/4 activity in generating siRNAs in vitro. We concluded that FVE synchronizes SGS3-DRB4-DCL2/4 channel to promote siRNA production whereas FVE-8 hijacks dsRNA substrates to prevent their downstream processing. Thus, this study reveals an uncanonical role of the epigenetic element FVE in transgene-PTGS and sheds light on a new regulatory layer in RNA silencing.

In chapter IV, two other mutants screened from the same system are introduced. They were put aside due to either failure in mapping or ununiform LUC signal.

CHAPTER II

FVE ENHANCE TRANSGENIC GENE SILENCING THROUGH A SIRNA MEDIATED PTGS PATHWAY

2.1 Summary

As a powerful and complicated network for regulating endogenous and invading RNA homeostasis, PTGS has been studied for decades. While the genetic and biochemical framework has been studied well, many new auxiliary factors and fundamental mechanism remain unclear. To further study PTGS, we designed a new genetic screening system (PAGO10-GFP-PHB-LUC) and validated the robustness of the reporter system because introduction of the reporter lines into several landmark mutants of miRNA and siRNA pathways could significantly increase the LUC signal. We screened an allele of *FVE* (*fve-8*) which is responsible for the upregulation of LUC transcripts and protein level. FVE was found to show dual roles of TGS and PTGS but cytoplasmic portion of FVE could fully rescue LUC signal in *fve-8*. Furthermore, loss-of-function of *fve* mutants had reduced siRNA production from sense and hairpin transgenes. We propose a non-canonical function of FVE in cytoplasm.

2.2 Introduction

Arabidopsis SAM development is regulated by several factors. Among them, there is a class III HD-ZIP family containing 5 transcription factors including PHB (Barton, 2010). Those genes are target of miR166/165. miR166/165 can be loaded into AGO1-

RISC complex, and then recruit HD-ZIP gene RNAs and perform cleavage. AGO10 has a higher affinity to bind with miR166/165 compared to AGO1. AGO10 sequesters miR166/165 by a higher binding affinity to forbid its binding with AGO1-cored RISC complex, leading to the upregulation of *HD-ZIP III* gene expression (Zhu, et al., 2011; Zhou, et al., 2015). Since there are still numerous unknown proteins participating in this RNA silencing pathway, we generated a dual reporter system for miRNA and siRNA pathways by placing a segment of miR166 target, *PHB*, flanked by *GFP* and luciferase (*LUC*) transcripts driven by *AGO10* promoter. After we obtained the single-copied, homozygous transgenic lines containing the report genes, we crossed them with known mutants of miRNA/siRNA pathway to verify the system. Through EMS mutagenesis to this report system, we recovered an allele of *FVE* displaying an enhanced LUC transcript and protein level traditional mapping and next generation sequencing (NGS). We further validated *FVE* mutation as a *bona fide* cause as wild-type *FVE* could fully rescue the *fve-8* phenotypes of enhanced LUC signal and late flowering-time.

As a well-known epigenetic element, FVE can participate in the formation of several epigenetic complexes and play a role as a scaffold for protein-protein interaction. We use chemical treatment and ChIP-PCR exclude that the LUC signal increase is result from the canonical role of FVE in TGS. However, whether and how does FVE is involved in PTGS is poorly understood. FVE was reported and observed to be localized mainly in nucleus and also in cytoplasm. Replacement of nucleus localization signal (NLS) with nucleus export signal (NES) of FVE led to the exclusive distribution of FVE_{NES} in cytoplasm. Surprisingly we found that cytoplasmic FVE can sufficiently rescue LUC level

but not late flowering phenotype. These results indicated that FVE has a non-canonical function in cytoplasmic PTGS, in addition to its well-known role in epigenetic silencing.

We then found that FVE has limited effect in endogenous PTGS through RNA seq but got a hint from small RNA seq that FVE may affect transgenic siRNA biogenesis. We use other transgene lines double confirmed our hypothesis and found that FVE does affect S-PTGS and IR-PTGS in those reporter lines.

These findings provide new insight of the role of FVE, which is a new member carrying out the crosstalk between TGS and PTGS in *Arabidopsis*.

2.3 Materials and methods

2.3.1 Vector construction and transgenic plants

Most of constructs were generated by a gateway system. To obtain pENTR-GFP-PHB-LUC, a truncation form of PHB containing exon 4 and 5 was amplified from Ler genomic DNA by KOD DNA polymerase (Novegen). PHB fragment was fused with GFP, LUC and pENTR by DNA fragments assembly (NEB HiFi DNA Assembly Master Mix) to generate pENTR-GFP-PHB-LUC. Then pENTR-GFP-PHB-LUC was transferred into gateway compatible binary vector of pBA002a-Multi Cloning Sites (MCS)-DC by LR Clonase (Invitrogen). *AGO10* promoter were amplified with primers P_{AGO10} BamHI For and P_{AGO10} XhoI Rev (Table 1). The PCR products were digested with BamHI and XhoI (NEB) as an insert. Meanwhile, pBA002a-MCS-GFP-PHB-LUC were digested with the same enzymes as backbones. The two parts were ligated by T4 DNA ligase (NEB) and

amplified by DH5α. To obtain pENTR-GFP-cPHB-LUC, a truncation form of cPHB containing exon 4 and 5 was amplified from wild-type cDNA by KOD DNA polymerase. After digested with BamHI and KpnI, pENTR-GFP-PHB-LUC and cPHB fragment was ligated to get pENTR-GFP-cPHB-LUC. pENTR-GFP-cPHB-LUC was transferred into gateway compatible binary vector of pK-35S-FM-DC by LR Clonase. The final vectors were transformed into *A. tumefaciens* strain ABI and then transferred to Ler *Arabidopsis* by flower dipping (Zhang, et al., 2006), respectively. Matured seeds were collected and positive transgenic lines were selected on standard MS medium containing 10 mg/l phosphinothricin (for pBA vector, Sigma-Aldrich) or 50 mg/l kanamycin (for pK vector, Sigma-Aldrich) together with 100 mg/l carbenicillin (Sigma-Aldrich). Single copy homozygous transformants were selected according to the Mendelian segregation ratio.

To obtain pK-DC-FM, pK-FM-DC was digested with XbaI and XhoI. The ends were blunted by DNA ploymerase I Large (Klenow) (NEB) and ligated to generate an intermediate vector. Then this intermediate vector and pBA002a-DC-FM were digested with SmaI and PacI. The longer fragment of the former digest product and the short fragment of the latter digest product were recovered, respectively. The two recycled fragments were ligated to generate pK-DC-FM. For the several candidate genes, full-length genomic DNAs including promoters and gene bodies were amplified by KOD DNA polymerase and were cloned into AscI/NotI-digested pENTR vector fragment through DNA fragments assembly. For *At2g16950*, the cDNA was cloned to pENTR™/D-TOPO™ (Invitrogen). In parallel, the promoter was ligated into the destination vector of pK-DC-FM to make pK-$P_{At2g16950}$-DC-FM. After sequencing confirmation, the pENTR-

At2g16950 vectors were transferred into gateway compatible binary vector of pK-$P_{At2g16950}$-DC-FM by LR Clonase (Invitrogen). The final constructs were transformed into *A. tumefaciens* strain ABI and then transferred them to *fve-8* (Zhang, et al., 2006), respectively. Transformants were selected on standard MS medium containing 50 mg/l kanamycin (Sigma-Aldrich) together with 100 mg/l carbenicillin (Sigma-Aldrich) and Luciferase pictures were taken on the 5th day, together with the parental line and *fve-8*. The luciferase signals were re-confirmed with T2 transgenic lines.

For pENTR-cFVE, cDNA of *FVE* with and without stop codon was amplified by KOD DNA polymerase (Novegen) and cloned into pENTR™/D-TOPO™ vector. The vectors were confirmed by sequencing. For pENTR-cFVE_{NES}, the nuclear localization signal (NLS) nucleotides were substituted with nuclear export signal (NES) nucleotides by several steps: Firstly, with the prerequisite of no amino acid change, two restriction digestion sites (KpnI and BglII, NEB) were introduced to the two sides of NLS by PCR with pENTR-cFVE as the template and NLS mutation KpnI For and NLS mutation BglII Rev as primers (Table 1). PCR products were digested with DpnI (NEB) and transformed into *E. coli* strain DH5α. After sequencing confirmation, the new plasmid was digested with KpnI and BglII. The digested fragment was extracted as the backbone; Meanwhile, oligos NES For and NES Rev were equally mixed in a 1x T4 ligation buffer, and annealed by denaturing at 95°C for 10 min followed by naturally cooling down to room temperature. The two parts were ligated by DNA T4 ligase (NEB) and transformed into DH5α. pENTR-cFVE and pENTR-cFVE_{NES} were cloned to both pK-MCS-FM-DC and pK-35S-DC by LR clonase. *FVE* promoter were amplified with Primers P_{FVE} BamHI For and P_{FVE} XmaI

Rev (Table 1). The PCR products were digested with BamHI and XmaI (NEB) as an insert. Meanwhile, pK-MCS-FM-cFVE and pK-MCS-FM-cFVE$_{NES}$ were digested with the same enzymes as backbones. The two parts were ligated with T4 DNA ligase and amplified by DH5α. For pK-gFVE$_{NES}$, the fragment containing NES motif was cut from pENTR-cFVE$_{NES}$ and swapped to pK-gFVE used for complementation experiment. The final plasmids were transformed into ABI and then transferred them to *five-8*. For pENTR-FVE-8, a CDS region was amplified by KOD enzyme with cDNA from *five-8* served as the template. The DNA fragment containing a point mutation was replaced with the WT fragment in pENTR-FVE using XhoI and HindIII. pENTR-FVE-8 was verified by sequencing. For pENTR-FVE$_{5+6}$, a CDS region was amplified by KOD with cDNA from E5-4 and ligated to pENTR vector.

For pCambia-P$_{MIR166b}$-FM-CNA, Promoter MIR166b was amplified by KOD hot-start DNA polymerase and digested by BamHI and XbaI. Digested fragment was ligated to the same enzymes digested backbone of pCambia-35S-Myc-CNA (Li, et al., 2013). pCambia-P$_{MIR166b}$-FM-CNA, pCambia-35S-Myc-PHB(m) and pCambia-35S-Myc-PHB (Li, et al., 2013) were transformed into *A. tumefaciens* strains GV3101 and then transferred into E5-4 × *five-8* F2 heterozygous lines. Positive transgenic lines were selected on MS medium with 50 mg/l Kanamycin and 40 mg/l Hygromycin (Sigma-Aldrich) respectively. Also, those lines were genotyped with dCAPS primers and corresponding restriction enzymes showed in Table 2. The wild-type PCR fragment can be digested by BamHI while that of mutant cannot.

Table 1 Primers used for constructs in Chapter II.

Primer name	Sequence
PHB Exon 4 For	GACGAGCTGTACAAGGGATCCCTCCTTTCTATAGCAGAGG
PHB Exon 5 Rev	TTTGGCGTCTTCCATACCTCCGGTACCCTTCATGGGT
GFP fusion For	GCCGCCCCCTTCACCATGGTGAGCAAGGGCGAGCTGTAC
GFP Rev	CTTGTACAGCTCGTCCATGCC
LUC For	ATGGAAGACGCCAAAAACATAAAG
LUC fusion Rev	GGCGCGCCCACCCTTCAATTTGGACTTTCCGCCCTTC
P_{AGO10} BamHI For	CAGGATCCTCGTACCAGAAGGAAACT
P_{AGO10} XhoI Rev	CCGCTCGAGATCCTCTAGATTTGTTGTTTGGATTTTC
5 Infu At2g18100 NotI For	AAAAAAGCAGGCTCCGCGGCCGCGGTATGGTTATATGGAGATCCAG
3 Infu At2g18100 AscI Rev	AAGAAAGCTGGGTCGGCGCGCCCACCCTTGAGAGTGTTTCGTAAAACAGG
At2g18100 2881 For	GAGACAATGTCTGCATGCTCTGC
At2g18100 2881 Rev	GCAGAGCATGCAGACATTGTCTC
5 Infu At2g18330 NotI For	AAAAAAGCAGGCTCCGCGGCCGCGCTTCCAGTTCAATGAGCACCTC
3 Infu At2g18330 AscI Rev	AAGAAAGCTGGGTCGGCGCGCCCACCCTTCGGAAACGATTGGCCACCTTC
5 Infu At2g19520 NotI For	AAAAAAGCAGGCTCCGCGGCCGCGAACCACTAGGAGATCGTCGTCC
3 Infu At2g19520 AscI Rev	AAGAAAGCTGGGTCGGCGCGCCCACCCTTAGGCTTGGAGGCACAAGTCAT
At2g19520 3030 For	GTTGACGAGAAGTACTCTCAGTGG
At2g19520 3030 Rev	CCACTGAGAGTACTTCTCGTCAAC
5 Infu At2g21300 NotI For	AAAAAAGCAGGCTCCGCGGCCGCGAAGAAAATCCAAAGAGAAAGCCTG
3 Infu At2g21300 AscI Rev	AAGAAAGCTGGGTCGGCGCGCCCACCCTTGAACAGTGTGGCCATGCTTTT
At2g21300 3617 For	CATGTTGCCCGGGAAGAGAAG
At2g21300 3617 Rev	CTTCTCTTCCCGGGCAACATG
5 Infu At2g21430 NotI For	AAAAAAGCAGGCTCCGCGGCCGCGTAATCGTTTTGGTTATCTCTGCAGAG
3 Infu At2g21430 AscI Rev	CAAGAAAGCTGGGTCGGCGCGCCCACCCTTAGAAGTGGTAGCAGCGACGG
5 Infu At2g18640 NotI For	AAAAAAGCAGGCTCCGCGGCCGCTCCGAATGCGGTTTTGATCC
3 Infu At2g18640 AscI Rev	AAGAAAGCTGGGTCGGCGCGCCCACCCTTGTGGTTTCTGTTGGCAATGAA
5 Infu At2g17150 NotI For	AAAAAAGCAGGCTCCGCGGCCGCATCCGTCTGTGCATCTTCTCAATG

Table 1 Continued

Primer name	Sequence
3 Infu At2g17150 AscI rev	AAGAAAGCTGGGTCGGCGCGCCCACCCTTGGAAAGAC CAGTGTTGCCAAA
AT2G16950 Promoter-EcoRI Rev	CGGAATTCGATTGTTGTGGCAAAAAGGTAAAT
AT2G16950 Promoter-EcoRI For	GGAATTCTGTTAAACCGGCAAAAACGGT
AT2G16950 cDNA For	CACCATGGCGGCGACGGCGGTGGTC
AT2G16950 cDNA Rev	TTACACTTGATATCTCGCAAG
AT2G19520-ATG For	CACCATGGAGAGCGACGAAGCAGC
AT2G19520-cDNA-3end Rev -nostop	AGGCTTGGAGGCACAAGTCAT
AT2G19520-cDNA-3end Rev -stop	TTAAGGCTTGGAGGCACAAGTC
AT2G19520-Promoter-BamHI For	CGGGATCCGAACCACTAGGAGATCGTCGTCC
AT2G19520-Promoter-SacI Rev	CGAGCTCTTTCCTCTCTCTGTCTTTCAGTTTTTTTTTTTT GGTC
AT2G19520-Promoter-EcoRI For	CGGAATTCGAACCACTAGGAGATCGTCGTCC
AT2G19520-BamHI-ATG For	CGGGATCCATGGAGAGCGACGAAGCAGC
AT2G19520-cDNA-XhoI Rev -stop	CCGCTCGAGTTAAGGCTTGGAGGCACAAGTC
AT2G19520-Promoter-SacI For	CGAGCTCGAACCACTAGGAGATCGTCGTCC
NLS: mutation sites primers KpnI For	ACCGGAGCTTCTGGTACCAAGAAGAGAGGTCGGAGAT CTAAAACCAAGGAAG
NLS: mutation sites primers BglII Rev	CTTCCTTGGTTTTAGATCTCCGACCTCTCTTCTTGGTAC CAGAAGCTCCGGT
NES nucletide For	CCTGCAGCTGCCGCCGCTGGAACGCCTGACCCTGA
NES nucletide Rev	GATCTCAGGGTCAGGCGTTCCAGCGGCGGCAGCTGCA GGGTAC
BamHI $P_{MiR166b}$ For	CTCGGATCCTCTTTGTTTCTCTCTTCCAAG
XbaI $P_{MiR166b}$ rev	CGCTCTAGATCCTCTTCTTCTTCTTCTTTAAGAAAC
HindIII-FVE-For	CCCAAGCTTACCGCTAATGGAGTTGGT
XhoI-FVE-Rev	CCGCTCGAGTTAAGGCTTGGAGGCAC
gsRNA1 For	ATTGGCAGAATTCACACCTCTCCA
gsRNA1 Rev	AAACTGGAGAGGTGTGAATTCTGC
gsRNA2 For	ATTGCCTCAAGCAACGACACCGAG
gsRNA2 Rev	AAACCTCGGTGTCGTTGCTTGAGG

For CRISPR-cas9-FVE constructs, two guide sequences targeting *FVE* were chosen based on website design http://crispr.hzau.edu.cn/CRISPR2/. The guide sequences without PAM and its corresponding complementary strand sequences were designed to be annealed with a BsaI digested sticky end added at the 5' and 3' ends. The annealed duplexes were ligated to a BsaI digested AtU6-26-sgRNA vector by T4 ligase, respectively. After sequencing confirmation, AtU6-26-sgRNA1 was digested by SpeI and U6-sgRNA1 fragment was recovered and ligated to fragments of AtU6-26-sgRNA2 digested by SpeI and NheI. The tandem sgRNAs sequences were extracted from AtU6-26-sgRNA1-U6-26-sgRNA2 digestion with SpeI and NheI and ligated to SpeI digested pCambia1300-pYAO-cas9-MCS. Digestion confirmed pCambia1300-pYAO-cas9-U6-sgRNA1-U6-sgRNA2 were transformed to GV3101 and then transformed to L1 line and *35S-hpCHS* line. T0 plants were selected by standard MS medium containing 40 mg/l Hygromycin B (Sigma-Aldrich) together with 100 mg/l carbenicillin (Sigma-Aldrich). Mutation in Positive plants were confirmed by sequencing.

0.5 g homozygous T4 generation of *Ler; P_{AGO10}-GFP-tPHB-LUC* transgenic seeds were cleaned with 0.1% Tween-20 followed by at least 4 times wash with water. Soak the seeds in a 50 ml tube with 40 ml water at 4 ℃ overnight. Those seeds were treated with 4% EMS for 8 h with rotating. After 20 times wash and 2 days fertilization in 4 ℃, M_0 seeds were suspended in 0.1% agar and sowed to soil. Plants were grown in LP5 Metromix (SunGro, Canada) in a growth chamber at 22 ℃ with a 50% humidity under mid-day conditions (12 h light/ 12 h dark). Keep light illumination at 110 mmol photons/m^2s. After about 3 months, M_1 seeds were collected in the unit of tray. Based on germinated plants

number, I randomly take that number times 8 seeds to sterilize and sow on MS medium plates, with parental line and WT Ler seeds as positive and negative control, respectively. Then I used an electron multiplying charge-coupled device (EMCCD) camera (Princeton) to capture LUC fluorescence of 5-day seedlings after sprayed with 10 mM Luciferin (Goldbio). The images were processed by Winview32 or Lightfield. The plants showing stronger fluorescent signal were selected and transferred to soil. M_2 seeds were collected individually when plants matured. A second-round screening was performed as above. Seedlings showing stable uniform LUC signal were transferred to soil. Mutants were crossed with E5-4 and Col-ecotype WT plants, respectively.

2.3.2 Plant materials and growth conditions

Arabidopsis thaliana ecotype Landsberg (Ler), Columbia (Col-0), E5-4 (Ler; PAGO10-GFP-PHB-LUC), *hyl1-2* (SALK_064863), *dcl2-1 dcl4-2* (SALK_064627 CS9969), *ago1-27*, *sgs3-1, rdr6-11* (CS24285), *ago10-3* (SALK_519738), *pnh2 (*CS3853*),* and *drm1 drm2 cmt3* (Cao, et al., 2003) were used for this study. Plants were grown on soil at 22°C or MS plates in 12 h light/ 12 h dark.

E5-4 was crossed with Col-0 for seven generations to get Col-0 background E5-4 (Ec5-4). Ec5-4 in *se-2*, *hyl1-2*, *dcl2-1 dcl4-2* background plants were obtained by crossing Ec5-4 with the mutants, respectively. M17-1 in *ago1-27*, *hyl1-2*, *rdr6-11* and *sgs3-1* background plants were obtained by crossing M17-1 with the mutants, respectively. In the F2 generation, homozygous *rdr6-11* and *sgs3-1* mutants were identified by PCR using primers listed in Table 2.

Table 2 Primers used for genotyping.

For genotyping	Sequence	Enzyme (if needed)
dCAPS FVE For	GATCGTAGGAAGCTTACCGCT	BamH I
dCAPS FVE Rev	ACTATGTACACACCCTGTCAGGATC	
salk_013789c LP	CAACCCGAGTAGTTTTGCTTG	
salk_013789c RP	CGATTCTTGTAGGTTGCTTGC	
LBb1.3	ATTTTGCCGATTTCGGAAC	
dCAPS rdr6-11 For	TACTGTCCCTGGCGATCTCT	Taq I
dCAPS rdr6-11 Rev	CCACCTCACACGTTCCTCTT	
dCAPS sgs3-1 For	GAACGTTCAGGGTGGTTATAG	Rsa I
dCAPS sgs3-1 Rev	GTTCTTGTTCTTCTTGGAAATGACCTCG	

2.3.3 EMS mutagenesis, mutant screen and Luciferase Assays

EMS mutagenesis was done as described with minor modifications (Wang, et al., 2011). 0.4% EMS was used to treat 20000 seeds of E5-4 for 8 h at room temperature. About 7000 M1 plants survived. Approximately 56000 5-day-old M2 seedlings were assayed for LUC activity with EM CCD camera (Princeton) and Winview 32 and Lightfield, of which showing enhanced LUC luminescent were picked. M2 seedlings were outcrossed with Col-0. Genomic DNA was extracted with CTAB (Hexadecyltrimethylammonium bromide). Traditional mapping markers were designed based on an *Arabidopsis* mapping platform. The DNA seq library was constructed according to manufacturer's (NEB) instructions with modifications. NGS was performed by Illumina and sequence data were analyzed with SHOREmap v2.0 (Schneeberger, et al., 2009) and NGM (Li, et al., 2008).

2.3.4 Chop PCR and Aza-dc treatment

Genomic DNA of Arabidopsis seedlings were extracted with CTAB method. Concentration was measured by Nanodrop and normalized by agarose gel electrophoresis. For each sample, 1 μg DNA was taken to digest with McrBC restriction enzyme (NEB) as manufacturer's instruction. Digestion products were purified by phenol/chloroform. Another 1 μg DNA was used as control.

For AZA (5-aza-2'-deoxycytosine (aza-dC)Aza-dC) assay, AZA dissolved in water was added to MS medium to a final concentration of 7 μg/ml (Chang and Pikaard, 2005). Aza-dc was dissolved in water and added to MS medium to a final concentration of 4 μM (Mathieu, et al., 2007). Seeds were germinated on MS medium with or without aza for 5 days before LUC activity assay. After LUC activity was recorded, seedlings were harvested for RT-PCR. PCR was performed with primers showed in Table 3.

Table 3 Primers used for RT-PCR.

For qRT-PCR	**Sequence**
LUC RT For	ACAATCCGGAAGCGACCAAC
LUC RT Rev	CAATTTGGACTTTCCGCCCTTC
EF1α-qRT For	GATTTGCTGTTGTAACAAGATGGATG
EF1α-qRT Rev	AGGGTTGTATCCGACCTTCTTCA
AtMU1 F	GTGGATATACCAAAAACACAA
AtMU1 R	CTTAGCCTTCTTTTCAATCTGA
AGO10 For	ATGCCGATTAGGCAAATGAAAG
AGO10 Rev	CAAATCCTTGGTAGGCAAATCAGC

2.3.4 RT-PCR and quantitative RT-PCR

Total RNA was extracted using TRI reagent (Sigma-Aldrich) from 5-day-old seedlings. Total RNA was treated with DNase I (Sigma-Aldrich AMPD1) and reversed transcribed with Superscript III reverse transcriptase (Invitrogen Cat #18080093) primed by oligo $_{d}$(T) as manufacturer's instructions. *Actin* or *EF1α* gene was used as internal controls. For analysis using regular PCR, the PCR products were fractioned on agarose gels. qRT-PCR was performed by CFX384 touch^{TM} Real-time PCR detection system (Bio-Rad). Primers were listed in Table. 3.

2.3.5 RNA-seq and sRNA-seq

Total RNA was prepared from 5-day-old seedlings grown on MS medium using TRI Reagent. Construction of RNA and sRNA libraries, Illumina sequencing and bioinformatic analysis were performed as described (Ma, et al., 2018).

2.3.6 RNA blot and sRNA blot

Total RNA was extracted using TRI reagent from 5-day-old seedlings. RNA blot hybridizations of low molecular weight RNAs (sRNA blot) and high molecular weight RNAs (Northern blot) were performed as described previously (Zhang, et al., 2006). For miRNAs and ta-siRNA blot, the probes, which are 21-nt DNA oligos complementary to the corresponding sRNAs (The probes were listed in Table. 4), were labeled by [γ-32P] ATP (Perkin Elmer) with T4 PNK (NEB). For northern blot and transgenic sRNA blot, the probes were PCR products amplified with primers listed in Table. 4 then labeled by

[α-32P] dCTP (Perkin Elmer) with Klenow fragment (3' to 5' exo-, NEB). Hybridization signals were detected with Typhoon FLA7000 (GE Healthcare). Primers and probes used are listed in Table 4.

Table 4 Primers and probes used in RNA blot and sRNA blot.

Primers for probes and probes	**Sequence**
GFP For	ATGGTGAGCAAGGGCGAGCTGTAC
GFP middle Rev	GTTGCCGTCCTCCTTGAAGTCGA
U6	TCATCCTTGCGCAGGGGCCA
Anti miR166	GGGGAATGAAGCCTGGTCCGA
Anti miR156	GTGCTCTCTTTCTTCTGTCA
Anti miR398	AAGGGGTGACCTGAGAACACA
Anti miR167	TAGATCATGTTGGCAGTTTCA
Anti miR390	GGCGCTATCCCTCCTGAGCTT
Anti miR164	TGCACGTGCCCTGCTTCTCCA
Anti miR159	TAGAGCTCCCTTCAATCCAAA
Anti miR168	TTCCCGACCTGCACCAAGCGA
Anti miR171	GATATTGGCGCGGCTCAATCA
GUS1-300 For	ATGTTACGTCCTGTAGAAACCCCA
GUS1-300 Rev	ATTGACCCACACTTTGCCGTAAT
GUS560-786 For	TCACCGTGGTGACGCATGT
GUS560-786 Rev	ACACTCTGTCTGGCTTTTGGCT
GUS1103-1354 For	GCAACAAGCCGAAAGAACTGTAC
GUS1103-1354 Rev	TGTGAGCGTCGCAGAACATTAC
hpCHS H1 For	GCACTGCTAACCCTGAGAACCAT
hpCHS H1 Rev	GAAGCAACCTTGCTGGTACATC
hpCHS H2 For	GATGTACCAGCAAGGTTGCTTC
hpCHS H2 Rev	TGAGGAGATGGAAGGTGAGACCA

2.3.7 Western blot

Western blot analyses were performed as described (Zhu, et al., 2011). Blots were detected with antibodies against Myc (Sigma-Aldrich C 3956), YFP (Roche and Agrisera

AS15 2987), Actin (Sigma-Aldrich A0480), Histone 3 (H3, Agrisera AS10 710), AGO10 (Agrisera AS15 3071), SGS3 (Agrisera AS15 3099), Flag (Sigma-Aldrich, F1804) and HA (Sigma-Aldrich H9658). Secondary antibodies were goat-developed anti-rabbit (GE Healthcare, Cat#: NA934) and anti-mouse IgG (GE Healthcare, Cat#: NA931). Western blots membranes were developed with ECL+, and signals were detected with ChemiDoc XRS+ and captured with the ImageLab Software (Bio-Rad) as manufacturer's instruction.

2.3.8 ChIP-PCR

ChIP assay was performed as described (Castillo-Gonzalez, et al., 2015). 3 grams of 5-day-old seedlings were harvested from MS medium. Materials were soaked into Crosslink buffer (0.4 M sucrose, 10 Mm Tris-HCl pH 8.0, 1 mM PMSF, 1 mM EDTA and 1% formaldehyde) and crosslinked by vacuum infiltration for seven min and slowly released for 2 min at room temperature. Repeat once as needed. The reaction was stopped with 2M Glycine to a final contraction of 100 mM at room temperature. Materials were rinsed 4 times with ice cold water and flash-frozen in liquid nitrogen. After grounded into fine powder, the materials were suspended in 6 volumes of cold fresh Honda buffer (20 mM Hepes-KOH pH 7.4, 0.44 M sucrose, 0.5% Triton X-100, 10 mM $MgCl_2$, 1.25% Ficoll, 2.5% Dextran T40, 5 mM DTT, 1 mM PMSF, 1 pellet/15 ml Complete EDTA-free Protease inhibitor [Roche]). Vortex briefly and keep samples on ice for 15 min until complete homogenization is achieved. Sample-buffer were filtered through two layers of Miracloth and centrifuge at 2000 g for 15 min at 4°C. Resuspend the pellet in 2 volume Honda buffer. Centrifuge at 1500 g for 15 min at 4°C. Repeat resuspending until the pellet

is not green. Resuspend the pellet in (250 µl/ g starting material) nuclei lysis buffer (50 mM Tris-HCl pH 8.0, 10 mM EDTA, 1% SDS, 1 mM PMSF, 1 pellet/15 ml Complete EDTA-free Protease inhibitor). Sonicate by biruptor (30 s Hi energy, 90 s pause for 10 cycles) at 4°C. Centrifuge the samples for 10 min at 15000 rpm at 4°C. 100 µl sonicated chromatin was diluted 10-fold with lysis buffer. The immunoprecipitation was accomplished by the addition of 36 µl Protein A Dynabeads (Invitrogen) and 3 µl of anti-H3K27me3 antibody (Millipore Cat# 07-449), followed by overnight incubation at 4°C on mild rotation. The beads conjugated complexes were washed with 1 ml Binding/Washing buffer (150 mM NaCl, 20 mM Tris-HCl pH 8.0, 2 mM EDTA, 1% Triton X-100, 0.1% SDS and 1mM PMSF) under 5 min rotation for 4 times and then washed with 1 ml TE buffer (1 mM EDTA, 10 mM Tris-HCl pH 8.0) for 4 times. The samples were eluted twice with 250 µl elution buffer (0.5% SDS, 0.01 M $NaHCO_3$) at room temperature for 15 min and 30 min, respectively. Reverse crosslink was performed by 100 mM NaCl at 65°C for at least 4 hours. Proteinase K was added to digest proteins for 1.5 h at 45°C. The DNA was purified by Phenol: Chloroform: Isoamyl alcohol (25:24:1) and precipitated in 2.5-fold ethanol. IP was developed with an anti-H3 antibody. PCR primers were listed in Table 5.

Table 5 Primers used for ChIP-PCR.

Primers for ChIP assay	Sequence
FLC ChIP For	GTCATTCACGATTTGTTTGATACGATCTG
FLC ChIP Rev	GATCTCCCGTAAGTGCATTGCA
LUC-5 For	AAGACGCCAAAAACATAAAGAAAG
LUC-225 Rev	ATTTGTATTCAGCCCATATCGTTT
LUC-774 For	TGGATTTCGAGTCGTCTTAATGTA
LUC-1037 Rev	GTAGTCTCAGTGAGCCCATATCCT
LUC-1370 For	TATTGTTACAACACCCCAACATCT
LUC-1617 Rev	GAGGATCTCTCTGATTTTTCTTGC
Pro AGO10 For	TTCGTGAACGGCTACACATCCAT
Pro AGO10 Rev	TGTGTTTGGTTTATGGCAGCAACT
AGO10 5'UTR For	CTAATTTCATGGTTTCTTGTC
AGO10 5'UTR XbaI Rev	CGTCTAGATTTGTTGTTTGGATTTTCA

2.3.9 GUS staining

F2 seedlings of FVE (+/) and FVE (-/-) in L1 background were isolated by segregation and genotyping (primers used are listed in Table 1). 10-day-old seedlings of F2 and were harvested and developed with GUS staining was performed as described (Wang, et al., 2018). Seedlings were soaked into GUS staining buffer (200 mM NaH_2PO4-Na_2HPO4 pH 7, 2 mM $K_3[Fe(CN)_6]$, 2 mM $K_4[Fe(CN)_6]$ and 2 mM X-Gluc) and vacuumed for 10 min at room temperature and incubated at 37 °C for several hours to overnight depending on GUS expression intensity. The reaction was stopped and the plant materials were cleared by rinse and incubation with 70% ethanol overnight at 37℃. 70% ethanol may need to be changed until the chlorophyll are gone.

2.3.10 Nuclear-cytoplasmic fractionation assay

5-day-old seedlings on MS medium were harvested for nuclear-cytoplasmic separation as described previously (Zhang, et al., 2017). 0.5 g fine ground powder was mixed with 1 ml lysis buffer (20 mM Tris-HCl pH 7.5, 20 mM KCl, 2 mM EDTA, 2.5 mM $MgCl_2$, 25% glycerol, 250 mM Sucrose and 5 mM DTT and 1× Complete EDTA-free protease inhibitor (Roche)). The homogenate was filtered through two-layer Miracloth. After a centrifuge of 1500 g for 10 min at 4°C, the supernatant containing cytoplasmic fraction was centrifuged at 10000 g for 10 min at 4°C and the supernatant was use as cytoplasmic fraction for western blot; while the pellet was washed four times with 1 ml of nuclear resuspension buffer 1 (20 mM Tris-HCl, pH 7.4, 25% glycerol, 2.5 mM $MgCl_2$, and 0.2% Triton X-100) each, then resuspended with 500 µl nuclear resuspension buffer 2 (20 mM Tris-HCl, pH 7.5, 0.25 M sucrose, 10 mM $MgCl_2$, 0.5% Triton X-100, 5 mM β-mercaptoethanol and 1 × Complete EDTA-free protease inhibitor (Roche)). Then carefully overlay the resuspends on top of 500 µl nuclear resuspension buffer 3 (20 mM Tris-HCl, pH 7.5, 1.7 M Sucrose, 10 mM $MgCl_2$, 0.5% Triton X-100, 5 mM β-mercaptoethanol and 1 × Complete EDTA-free protease inhibitor (Roche)). After a centrifuge at 16000 g for 45 min at 4°C, the pellet containing nuclear fraction was resuspended in 400 µl lysis buffer and collected for western blot assays. Rubisco stained with ponceau S and Histone3 protein level were used for fractionation quality validation and internal control.

2.4 Results

2.4.1 A new mutant of attenuated RNA silencing (ars) identified from a forward genetic screen system

We previously discovered that AGO10 antagonizes AGO1 silencing activity by sequestering miR165/166 to regulate shoot apical meristem development (Zhu, et al., 2011; Zhou, et al., 2015). To identify genes that regulate miR165/166 activity, we designed a reporter system containing a section of genomic *PHB* (exon4, intron4 and exon5) which harbors miR165/166 complementary sequence once spliced. The miR165/166 targeted site is flanked by *GFP* and *Luciferase* (*LUC*) genes and driven by the *AGO10* native promoter (P_{AGO10}-*GFP-PHB-LUC*), or constitutive promoter (*35S-GFP-cPHB-LUC*) (Figure 8A). These constructs were transformed into *Arabidopsis thaliana* Landsberg (Ler) ecotype and single-copy homozygous transgenic lines with a moderate level of luciferase activity were selected for further genetic analysis. The resulting parental lines for P_{AGO10}-*GFP-PHB-LUC* and *35S-GFP-cPHB-LUC* were termed E5-4 and M17-1, respectively. We hypothesized that LUC activity would increase when miRNA-mediated silencing is impaired. To test this, we crossed Ec5-4 (E5-4 in Col-0 background) with *se-2* and *hyl1-2* mutants, and M17-1 with *ago1-27* and *hyl1-2* mutants. Examination of F2 population indicated that LUC signal was substantially increased in the mutant background compared with that of wild-type (WT) background, validating the feasibility of the screening strategy (Figure 8B and 8C). Interestingly, the introgression of E5-4 into *dcl2-1 dcl4-2* and M17-1 lines into *rdr6* and *sgs3-1*, all of which are landmark mutants in transgene-PTGS

pathway, could also dramatically increase LUC signal (Figure 8B and 8C). These results indicated that the dual reporter system could be exploited to systematically recover genes that are involved in either miRNA or transgene-PTGS pathways.

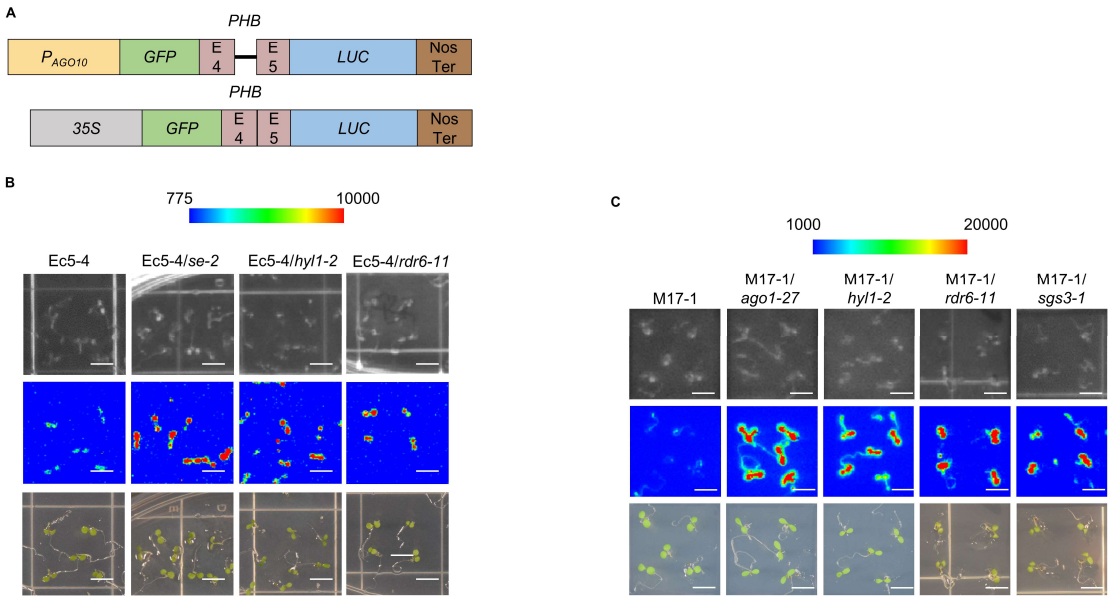

Figure 8 A new screening system was designed and verified.
(A) Schematic constructs of transgenic lines E5-4 and M17-1 used for the EMS screening in this study. E4 and E5: the 4th and 5th exons of *PHB*, respectively. Nos Ter: nopaline synthase terminator.
(B) Mutations of known miRNA and siRNA machinery increased LUC luminescence. 5-day seedlings of Ec5-4/se-*2*, M17-1/*hyl1-2*, Ec5-4/*rdr6-11* were photographed in bright field (Top panel); under CCD camera for LUC signal (middle panel); and under regular camera (bottom panel). Scale bars, 0.5 cm.
(C) The crossing lines of M17-1 with the indicated mutants displayed similar pattern with (B). Scale bars, 0.5 cm.

We performed the ethyl methanesulfonate (EMS) mutagenesis on E5-4 seeds. After selfing of EMS treated plants, five-day-old M2 seedlings were screened for

increased luminescence. In the M2 individuals, several dozens of lines were found with increased LUC activity. Since numerous essential mutants recovered in earlier genetic screening for PTGS defects display severe development defects, we focused on the lines with normal or mild morphological phenotypes. A mutant, here we named attenuated RNA silencing 1-1 (*ars1-1*), displayed a stronger LUC luminescent signal compared with that of E5-4 (Figure 9A). Further RNA blot assay showed that *LUC* expression level was as high as 4-fold in *ars1-1* mutant compared with that in E5-4 (Figure 9B).

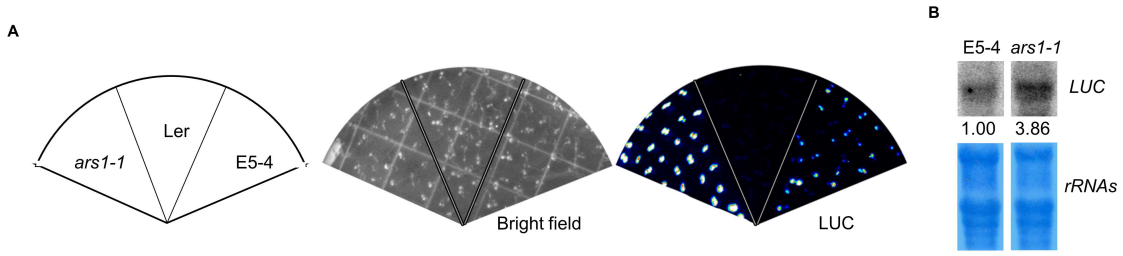

Figure 9 Isolation of a new mutant of attenuated RNA silencing through a forward genetic screening.
(A) Mutation in *FVE* caused increased LUC luminescence. 5-day seedlings of E5-4, *ars1-1* and *Ler* were photographed in bright field (top panel) and under CCD camera for LUC signal. The signals were displayed by Winview32 software.
(B) Northern blot showed that *LUC* transcripts accumulated in *ars1-1*(*fve-8*) compared with E5-4. rRNAs serve as an internal control.

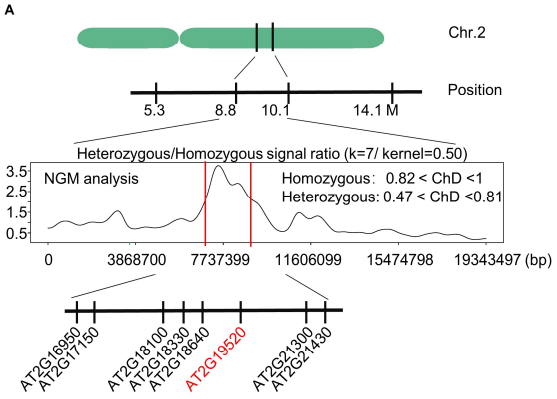

B

Position	Accession	Ref. codon	SNP codon	AA change
7127168	AT2G16950.1	GCA	ACA	A->T
7237715	AT2G17150.1	CGG	TGG	R->W
7618807	AT2G18100.1	GGT	GAT	G->D
7713024	AT2G18330.1	GGT	AGT	G->S
7827885	AT2G18640.1	CGT	TGT	R->C
8191743	AT2G19520.1	TGG	TGA	W->*
8841974	AT2G21300.1	CCG	CTG	P->L
8897739	AT2G21430.1	TCT	TTT	S->F

Figure 10 Eight candidates were recovered from NGM analysis.
(A) NGM analysis of F2 mapping population delineated eight candidates in 2.3Mb of Chromosome 2.
(B) A summary of 8 candidates including physical positions, annotations, mutation codons and amino acid (AA) changes.

The *ars1-1* mutant was outcrossed with Col-0 to generate F2 mapping populations. We first performed rough genetic mapping followed by next-generation sequencing (NGS) and delineated the mutations to a 1.3-megabase interval on chromosome 2 that harbors eight candidate genes (Figure 10A). Among the candidates, *TRANSPORTIN1(TRN1*, *At2g16950*) was reported to promote loading of miRNAs into AGO1-RISC complex (Figure 10B) (Cui, et al., 2016). However, introduction of wild-type *TRN1* into *ars1-1* mutants did not bring LUC signal back to the level in E5-4 (Figure 11A), referring that here the Ala to Thr substitution of *TRN1* is a weak allele, different from the previously reported strong allele *trn1*, and does not account for the increased *LUC* expression in the *ars1-1* mutant. We then extended complementation experiments to the rest seven loci and found that only *AT2g19520 (FVE)* could recover the LUC luminescence back to the parental level (Figure 11A). The late flowering phenotype of the mutant was also fully

rescued in FVE-complementation line (Figure 12). These results indicated that the mutation in *FVE* is responsible for the increased LUC activity in the mutant. In *ars1-1*, a G-to-A mutation creating a pre-mature stop codon at the middle of 12th exon of *AT2g19520* was pinpointed (Figure 11B). Since there are several *fve* mutants identified in previous literature, we renamed *ars1-1* as *fve-8*.

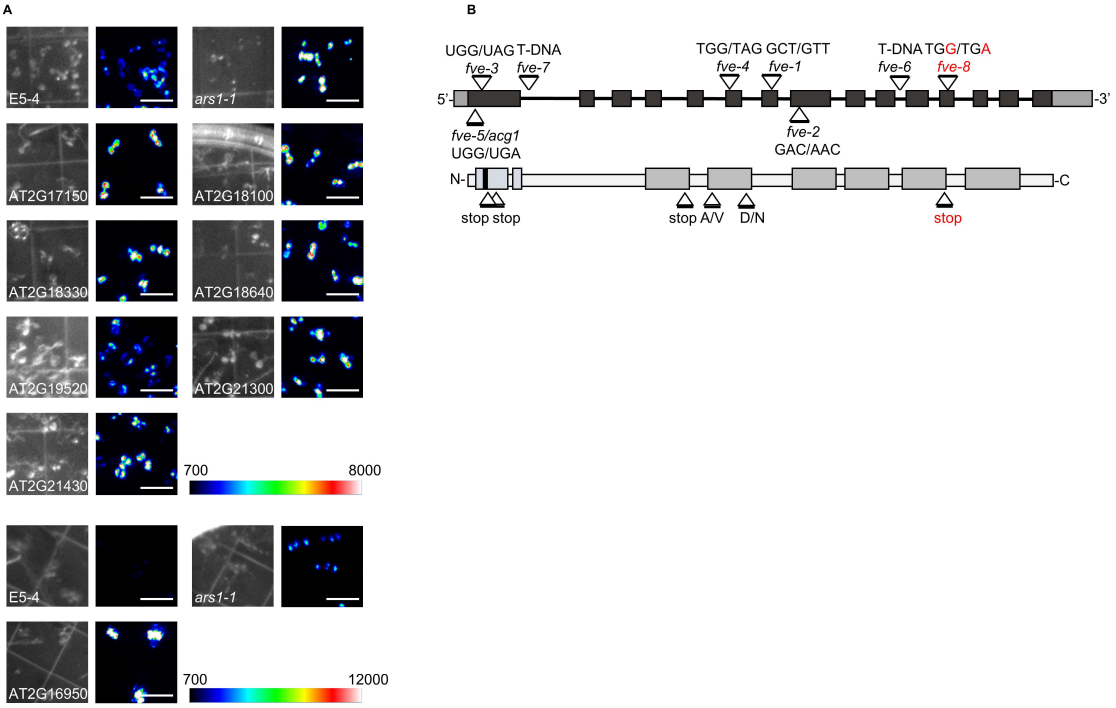

Figure 11 *ars1-1* is a new allele of *fve*.
(A) Complementation assay of LUC luminescence. Five-day seedlings of E5-4, *ars1-1* and transformants of 8 candidates expressed in *ars1-1* were photographed in bright field (left panel) and under CCD camera for LUC signal. The signals were displayed by Lightfield software. Scale bars, 1 cm.
(B) Gene structure of *FVE* includes UTRs (grey boxes), exons (black boxes), introns (lines) and mutations of *fve* alleles (triangles). The new allele *fve-8* was colored by red. Bottom, the protein schematic shows low complexity region (light grey boxes), 6 x WD40 domains (dark grey boxes), putative nuclear localization signal (NLS, black box) and *fve* alleles (triangles).

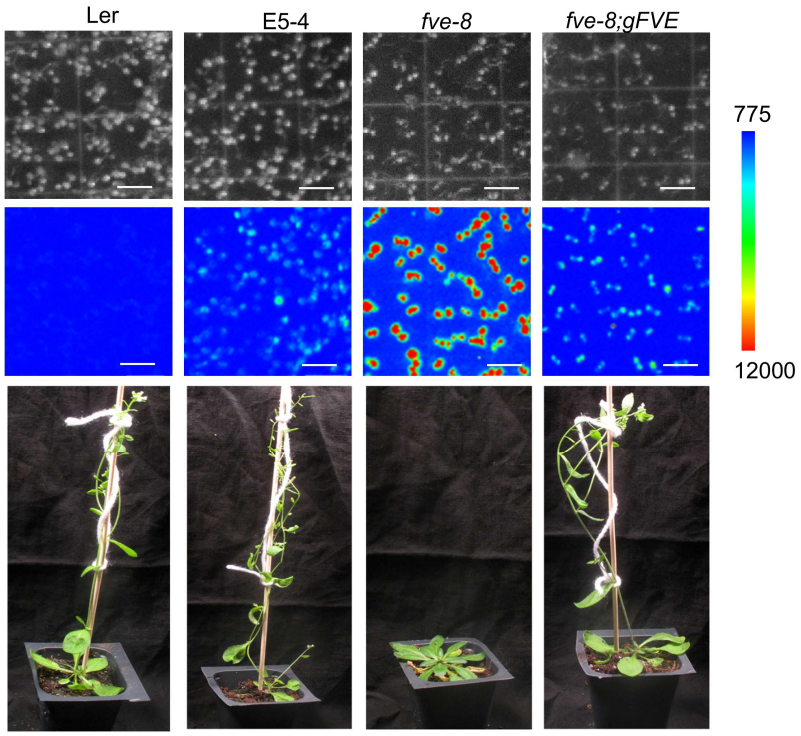

Figure 12 FVE can recover both LUC and late flowering phenotype.
Mutation in *FVE* caused increased LUC luminescence. 5-day seedlings of E5-4, *ars1-1* (*fve-8)* and *fve-8; gFVE* were photographed in bright field (top panel) and under CCD camera for LUC signal (middle panel). The signals were displayed by Lightfield software. Scale bars, 1 cm; bottom: 6-week-old *fve* and complementation lines displayed later flowering and normal flowering phenotypes. Scale bars, 1 cm.

2.4.2 FVE plays dual roles in TGS and PTGS pathways.

To test if *fve-8* upregulates *LUC* expression level through a TGS pathway, we first treated *fve-8* with 5-aza-2'-deoxycytidine (aza-dc), a chemical that can abolish DNA cytosine methylation. The transposon element *AtMu1* served as a positive control as it is suppressed by *FVE* at the TGS level (Baurle, et al., 2007; Gu, et al., 2011). Indeed, *AtMu1* displayed significantly increased expression in *fve-8* compared with E5-4, but this increase

was abolished by the aza-dc treatment. However, this scenario did not happen with LUC signal and transcripts (Figure 13A and 13B). We also performed an H3K27me3-ChIP assay with *FLC* and *EF1α* as positive and negative controls, respectively (Pazhouhandeh, et al., 2011). We did not observe a noticeable difference of H3K27me3 signal in the *LUC* gene body between *fve-8* and E5-4 lines (Figure 13C). A marginally reduced H3K27me3 ChIP signal in the *AGO10* promoter and 5' UTR was detected in *fve-8*, referring that FVE might have some repressive effect on expression of endogenous *AGO10* and arguably transgene *LUC* expression at certain levels. This result is in line with a previous report that endogenous *AGO10* promoter locus contains relatively lower levels of mCHG and mCHH DNA methylation in *fve* (Stroud, et al., 2013). Notwithstanding, the endogenous AGO10 protein level was not affected (Figure 13D), referring that enhanced LUC signal in *fve-8* did not result from the possible change of AGO10 ability to decoy miR165/166 (Zhu, et al., 2011; Zhou, et al., 2015).

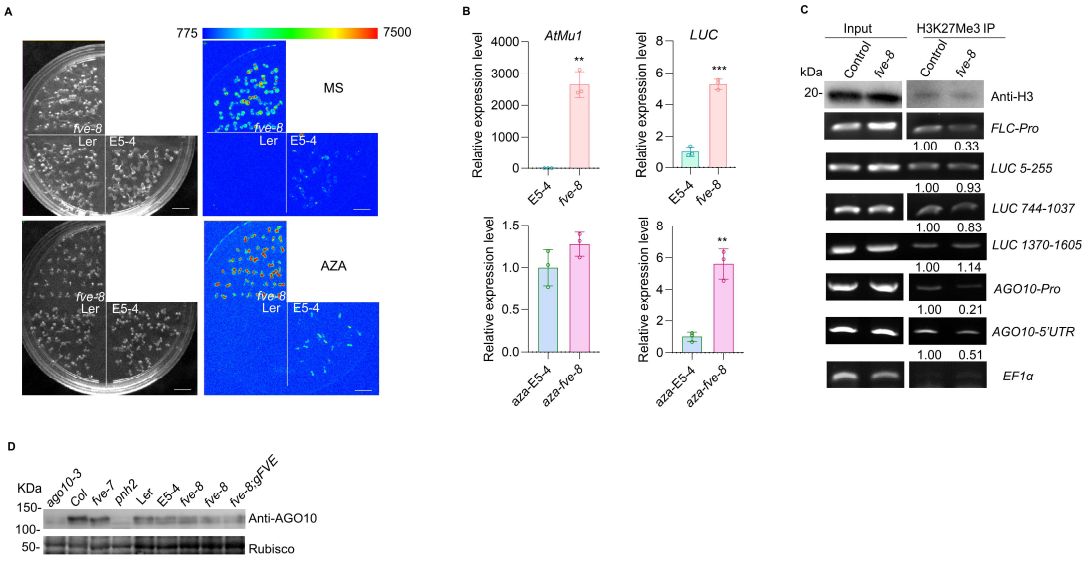

Figure 13 *fve-8* doesn't regulate LUC expression through TGS pathway.
(A) AZA treatment did not alter the patterns of LUC luminescence in E5-4 and *fve-8* compared with mock. 5-day-old seedlings of Ler, E5-4, *fve-8* and *fve-8; gFVE* on Mock medium and AZA medium were photographed, respectively. Scale bars, 2 cm.
(B) qRT-PCR of *LUC* and *AtMu1* transcripts in materials collected from (A). The data were presented as mean ± s.d. (n=3) biologically independent replicates. *EF-1α* serves as an internal control. The asterisks indicate a significant difference between mutants and E5-4 (unpaired two-tailed Student's *t*-test, $^{**}P< 0.01$; $^{***}P< 0.001$).
(C) The ChIP-PCR assay did not show the significant change of H3K27me3 in 5-day-old seedlings of WT and *fve-8*. Western blot assay using an anti-Histone 3 (H3) antibody validated the IP enrichment of H3K27me3. PCR with primers from *LUC* coding regions and P_{AGO10} was performed. P_{FLC} and *EF-1α* were amplified as positive and negative controls, respectively.
(D) Western blot analysis showed that endogenous AGO10 protein level was not altered in *fve* mutants. Western blot was conducted with 5-day-old seedlings of lines as indicated using an anti-AGO10 antibody. Coomassie blue stained Rubisco was used as an internal control. *ago10-3* and *pnh2* were used as negative controls.

To further clarify the role of FVE in suppressing *LUC* expression, we examined the cellular localization of FVE protein. FVE protein was highly enriched in nuclei but also distributed in cytoplasm (Figure 14A and 14B). Computational analysis predicted the presence of the nuclear-localization signal (NLS) in FVE (GPKKRGRK) (Ausin, et

al., 2004; Brameier, et al., 2007). We then replaced the NLS at the N terminal of FVE with a nuclear export signal (NES, LQLPPLERLTL) (Ye, et al., 2012)(Figure 14C), and transfected *35S-YFP-cFVE* and *35S-YFP-cFVE$_{NES}$* constructs into *Nicotiana benthamiana* (*N. benthamiana)* leaves and *Arabidopsis* protoplasts. The confocal microscopy imaging showed that YFP-FVE$_{NES}$, different from YFP-FVE, was exclusively expressed in cytoplasm (Figure 14A and 14B).

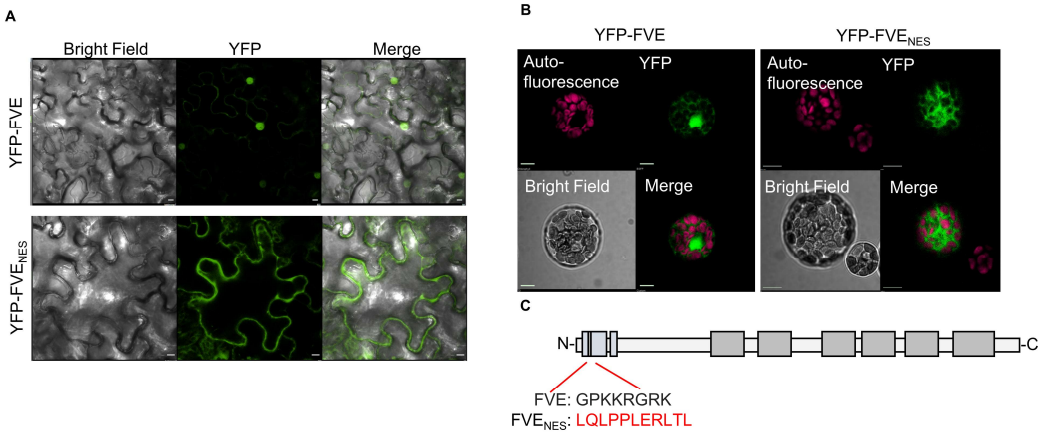

Figure 14 FVE expressed in both nucleus and cytoplasm while FVE$_{NES}$ exclusively expressed in cytoplasm.
(A) Confocal microscope imaging showed subcellular localizations of YFP-FVE and YFP-FVE$_{NES}$. The proteins were expressed in leaves of *N. benthamiana*. Scale bars, 50 μm. At least ten independent cells were tested with similar results.
(B) Confocal microscope imaging showed subcellular localizations of YFP-FVE and YFP-FVE$_{NES}$. The proteins were expressed in wildtype *Arabidopsis* protoplasts. Scale bars, 10 μm. Five independent protoplasts were tested with similar results.
(C) A schematic structure of FVE protein with NLS and NES sequence displayed.

To further validate this result, we generated stable *fve-8;35S-Flag4Myc(FM)-cFVE* and *fve-8;35S-FM-cFVE$_{NES}$* transgenic lines. Cell fraction assays showed that FVE

was present in both nucleus and cytoplasm in *fve-8;35S-FM-cFVE* lines, while the protein was only detected in cytoplasm in *fve-8;35S-FM-cFVE$_{NES}$* lines (Figure 15A-15C).

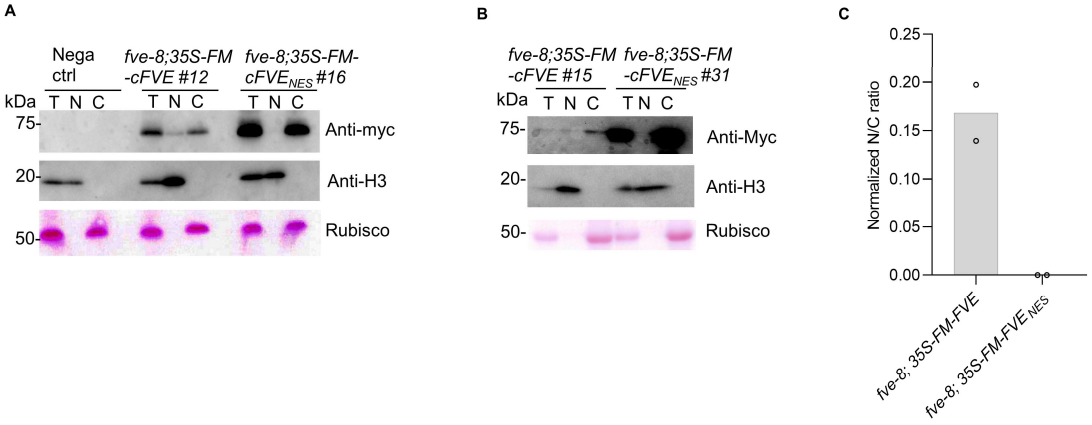

Figure 15 FVE expressed in both nucleus and cytoplasm while FVE$_{NES}$ exclusively expressed in cytoplasm.
(A and B) Cell-fractionation analysis showed FM-FVE and FVE-FVE$_{NES}$ amount in total extract (T), nuclear fraction (N) and cytoplasmic fraction (C) from five-day-old seedlings of *fve-8* (negative control), *fve-8; 35S-FM-cFVE* #12 or #15 and *fve-8; 35S-FM-cFVE$_{NES}$* #16 or #31. Western blot analysis of FVE was conducted with an anti-Myc antibody. H3 detected by an anti-H3 antibody and rubisco stained with Ponceau S were used as controls for the nuclear-specific and cytoplasmic-specific fractions, respectively.
(C) Quantification of the nuclear-cytoplasmic distribution of FVE and FVE$_{NES}$ proteins. The nuclear and cytoplasmic fraction (N/C) ratios of FVE($_{NES}$) proteins were sequentially normalized corresponding H3 or Rubisco signals. Data are presented as mean with two biologically independent replicates.

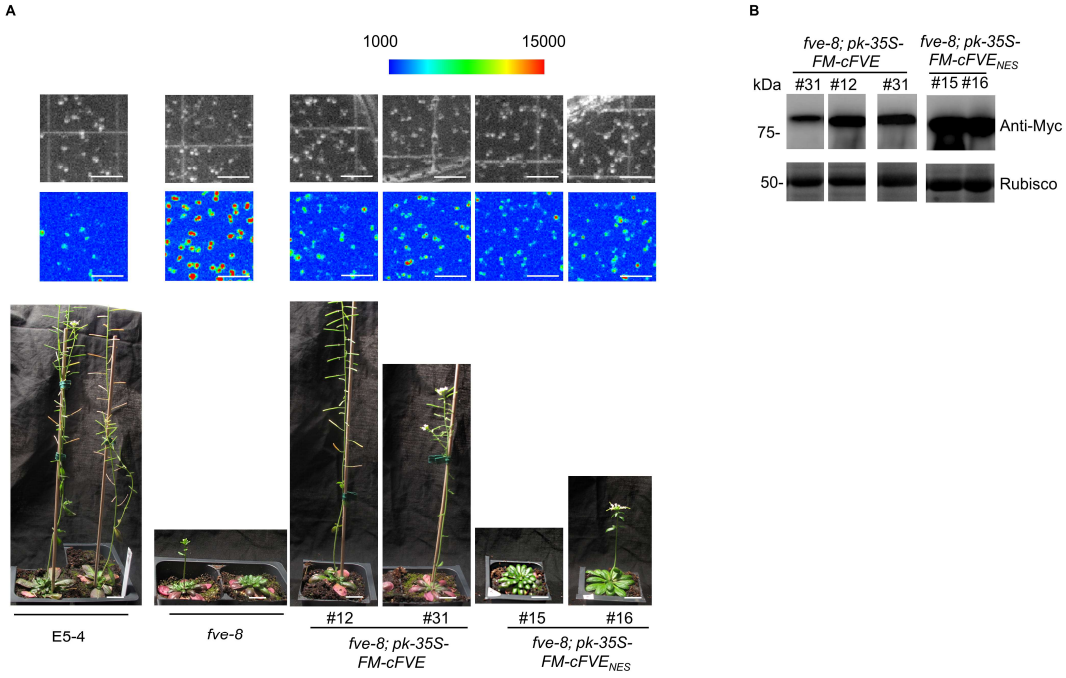

Figure 16 Both FVE and FVE$_{NES}$ can rescue LUC phenotype while FVE$_{NES}$ failed to recover late flowering.
(A) FVE$_{NES}$, different from FVE, could efficiently rescue LUC luminescence but not late-flowering phenotype of *fve-8* back to the parental level. Five-day old seedlings in (E) were photographed in bright field (top panel); and under CCD camera for LUC signal (middle panel). Scale bars, 1 cm. The signals were displayed by Lightfield software. Bottom: 6-week-old plants were captured. *fve-8* and E5-4 plants serve as controls. Scale bars, 1 cm. (B) Western blot analysis of FM-cFVE and FM-cFVE$_{NES}$ protein accumulation in overexpression lines. Western blot assay was conducted with an anti-Myc antibody. Coomassie blue stained rubisco was used as an internal control.

Of note, YFP-FVE distribution displayed different patterns in the confocal imaging and cell fraction experiments, referring that florescent signal is concentrated in nucleus but diluted in cytoplasm in the confocal imaging. Importantly, the late flowering phenotype in *fve-8* was only be recovered by *fve-8;35S-FM-cFVE* lines but not *fve-8;35S-FM-cFVE$_{NES}$* lines while FVE protein levels were abundant in two types of transgenic lines (Figure 16Aand 16B). However, both constructs could rescue the LUC signal in *fve-*

8 back to a normal level in E5-4. These results indicated that FVE has separate functions in nuclei and cytoplasm, and there must be a new function of FVE_{NES} in cytoplasmic RNA silencing.

To further validate this concept, we also generated *five-8; P_{FVE}-cFVE* and *five-8; P_{FVE}-$cFVE_{NES}$* transgenic lines and determined LUC luminescence in parallel. Again, a majority of transformants of the two constructs could recover LUC signal in *five-8* to the level in E5-4 (Figure 17A). In agreement with the changes of LUC signal, *LUC* transcripts were significantly reduced in two kinds of complementation lines (Figure 17B). This result indicated that cytoplasmic FVE is functionally sufficient to silencing *LUC* transgene. Of note, we observed that *LUC* expression was even marginally lower in *five-8; P_{FVE}-$cFVE_{NES}$* compared with that in *five-8; P_{FVE}-cFVE,* likely due to variations of FVE expression in independent lines (Figure 17B). To test if FVE_{NES} had a similar impact on *AGO10*, we next examined the expression of *AGO10*, the assumed proxy of the *LUC* transgene at an epigenetic status. Interestingly, the *AGO10* level was approximately 2-fold higher in *five-8* than that of E5-4; and was fully rescued in *five-8; P_{FVE}-cFVE*. However, the *AGO10* level was even increased to approximately 3- or 4-fold in *five-8; P_{FVE}-$cFVE_{NES}$* transformants (Figure 17B). These results indicated that nuclear FVE, but not cytoplasmic FVE, indeed repressed the transcription of *AGO10,* but not that of *LUC* transgene at an epigenetic level. This observation suggested that the slightly reduced H3K27me3 repressive mark would be likely from the promoter of endogenous *AGO10*, rather than the one for *LUC* transgene (Figure 13C). This result further suggested that FVE differently impacts native genes and transgenes at the epigenetic level. One plausible hypothesis for enhanced *AGO10*

expression in the *FVE$_{NES}$* complementation line is that FVE$_{NES}$ retains nuclear FVE cofactors from nucleus to cytoplasm, partially releasing the epigenetic suppression at the native *AGO10* promoter.

Altogether, we concluded that FVE has a noncanonical role in regulating *LUC* expression at a PTGS level in cytoplasm, in additional to its prototypical roles in epigenetic regulation of native genes in the nucleus.

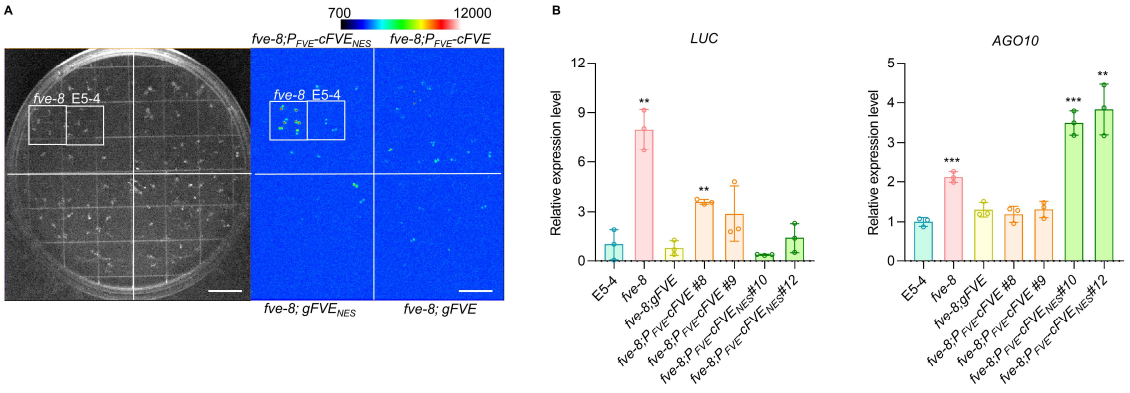

Figure 17 FVE regulates LUC expression through a PTGS pathway.
(A) FVE$_{NES}$ could efficiently rescue LUC luminescence in *fve-8* back to the parental level. Five-day-old seedlings or T1 transformants of E5-4, *fve-8, fve-8; gFVE, fve-8; P$_{FVE}$-cFVE, fve-8; P$_{FVE}$-cFVE$_{NES}$* and *fve-8; gFVE$_{NES}$* were photographed under CCD camera. Scale bars, 2 cm.
(B) qRT-PCR analysis showed that *LUC* transgene and endogenous *AGO10* were regulated differently by *FVE* and *FVE$_{NES}$*. Five-day-old seedlings materials of E5-4, *fve-8, fve-8; gFVE, fve-8; P$_{FVE}$-cFVE* and *fve-8; P$_{FVE}$-cFVE$_{NES}$* were used for assay. The data were presented as mean ± s.d. (n=3) biological independent replicates. *EF-1α* serves as an internal control. The asterisks indicate significant difference between mutants and E5-4 (unpaired two-tailed Student's *t*-test, **P*< 0.05; ***P*< 0.01; ****P*< 0.001).

2.4.3 fve-8 has limited impact on function of endogenous ta-siRNAs

Given that cytoplasmic FVE could promote PTGS, we evaluated the impact of *fve* mutations on miRNA pathway, sRNA blot assays showed that the accumulation of most tested miRNAs including miR166 was not significantly changed in the *fve* mutants compared with that in the corresponding controls (Figure 18A). Consistent with these results, there was no significant change in the accumulation of the majority of pri-miRNAs (Figure 18B). Similarly, RNA-seq did not reveal significant changes in the majority of miRNA targets except eight transcripts (Figure 18C and 18D). Interestingly, *At1G54260* and *At1G56650*, two of the affected transcripts were targeted by ta-si-RNAs (TAS1a-siR9(-) and TAS4a-siR81(-), respectively). Given that ta-siRNAs are just a tiny portion of endogenous siRNAs, the disproportionate impact of *fve* mutations on function of ta-siRNAs raised a possibility that FVE might have some impacts on ta-siRNA-mediated RNA silencing.

We next examined whether the attenuated LUC signal was due to miR166-mediated translation repression. Isogenic *fve-8 (-/-)* and heterozygous *(+/-)* lines containing *35S-PHB-Myc, 35S-PHBm-Myc* or $P_{MIR166b}$*-CNA-Myc* were generated. The accumulation of transgenic proteins was similar between *fve-8* (-/-) and *fve-8* (+/-) (Figure 18E). These results indicated that LUC signal increase in *fve* did not result from the defect of miR165/166 biogenesis and activity.

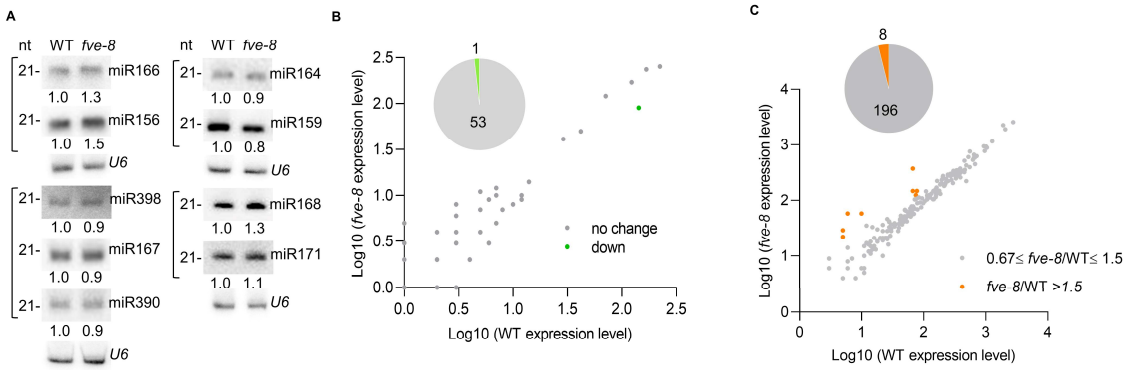

D

Gene Annotation	Corresponding miRNA/tasiRNA
AT5G55930	miR159
AT3G44860	miR163
AT5G47260	miR472
AT1G52040	miR846
AT1G52030	miR846
AT1G60110	miR846
AT1G54260	TAS1a-siR9(-)
AT1G56650	TAS4a-siR81(-)

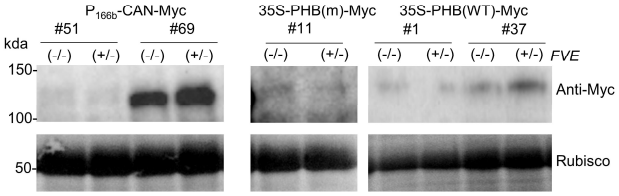

Figure 18 *FVE* has limited impact on the endogenous PTGS pathway.
(A) sRNA blot analyses of selected miRNAs in five-day-old seedlings of WT and *fve-8*. *U6* serves as a loading control. nt, nucleotides. The experiment was independently repeated twice with similar results.
(B) RNA sequencing analysis showed that the expression of most of *MIR* genes was not affected in *fve-8*. The *x* and *y* axes indicate the logarithms of *MIR* expression in WT and *fve-8*, respectively. *MIRs* with a significant decrease in *fve-8* relative to WT are shown by green dots. Grey dots refer to *MIR* genes without significant differences in expression. The pie in the top-left indicates the numbers of different categories of *MIR* genes. See also Table. S2.
(C) RNA sequencing analysis of miRNA target genes in *fve-8* and WT. The *x* and *y* axes indicate the logarithms of expression of miRNA targets in WT and *fve-8*, respectively. Orange and grey dots showed that increased (*fve-8*/WT >1.5) and rather stable (*fve-8*/WT <1.5) expression of target genes in *fve-8* compared with that of WT, respectively. The pie in the top-left indicates the numbers of different categories of target genes. See also Table. S2.
(D) A list of significantly upregulated genes targeted by miRNA/siRNAs including gene annotations and corresponding miRNA/siRNAs.
(E) Western blot analyses showed that protein levels of several miRNA targets were not changed in F2 of segregated *FVE* (+/) and *FVE* (-/-) using an anti-Myc antibody. Coomassie blue stained rubisco was conducted as an internal control.

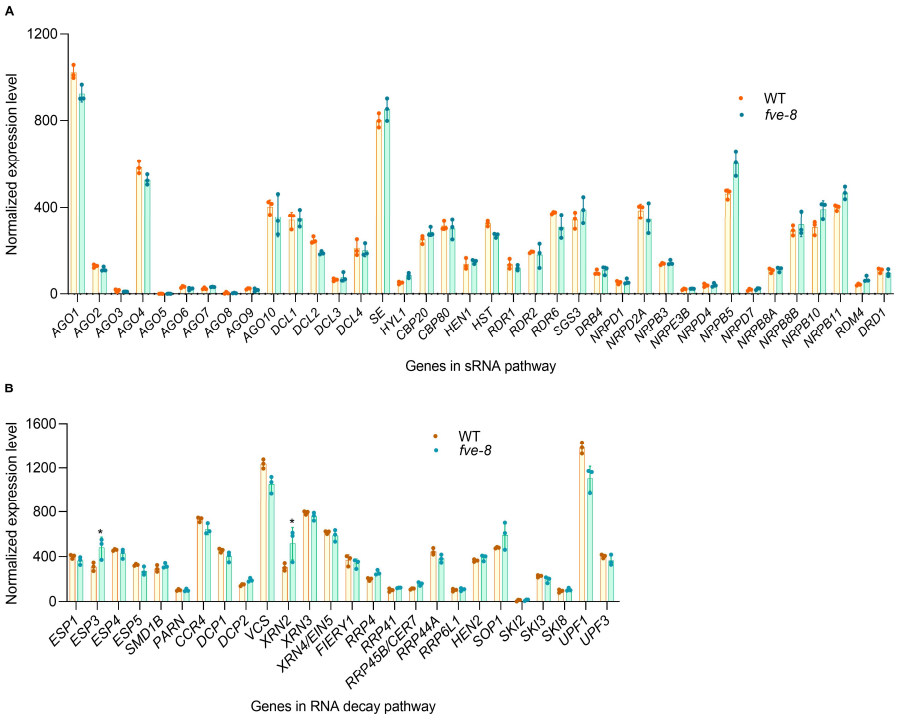

Figure 19 *FVE* has limited impact on the endogenous PTGS pathway and RNA decay pathway.
RNA sequencing analysis showed that the expression of the majority of RNA quality control genes (F) and sRNA pathway genes (G) was not significantly altered in *fve-8*. The *y*-axis indicates the normalized express level. The values were presented as the mean of 3 replicates of normalized reads amount ± s.d. (*adjusted *p*-value (*padj*) < 0.05). Individual data points were shown.

Also, the expression levels of key components in miRNA and RNA decay pathways were not affected except for a noticeable increase of *XRN2* and *ESP3* (Figure 19A and 19B). Thus, it is unlikely that LUC activity in *fve-8* was caused by indirect effect through alteration of miRNA and RQC pathways.

2.4.4 FVE promotes the accumulation of transgene-derived siRNA

We next hypothesized that FVE might impact transgene-PTGS pathway. We

conducted a Mi-seq and found that sRNAs derived from *GFP-PHB-LUC* transgene were reduced in *fve-8* compared with E5-4 and *fve-8; gFVE* (Figure 20). This result suggested that FVE may affect LUC accumulation through regulating of transgene-derived siRNAs.

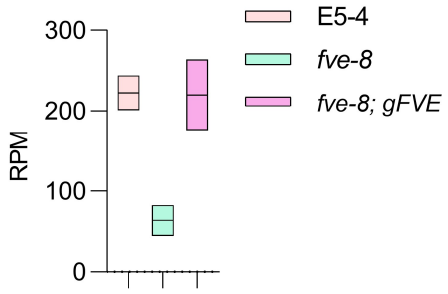

Figure 20 siRNA mapped to GFP-PHB-LUC loci is decreased in *fve-8*.
miSeq analysis showed that siRNA amount (reads per million, RPM) mapped to *GFP-PHB-LUC* region was reduced in *fve-8.* Lines in the middle of boxes indicate mean values from two independent biological replicates.

To further test this hypothesis, we crossed *fve-8* with L1 line, which contains a silenced *GUS* transgene and serves as a reporter for a sense transgene-PTGS pathway (Mourrain, et al., 2000). Genotyping was done for F2 population with a pair of dCAPS primers designed to distinguish homozygous *fve-8* and heterozygous or wildtype (Figure 21A). sRNA blot showed that the amount of *GUS* loci-derived siRNAs in *fve-8 (-/-)* decreased compared with that in heterozygotes or wild-type background (Figure 21B). Consistently, GUS activity was enhanced in *fve-8* (-/-) compared with that in a non-homozygous *fve-8* or L1 line (Figure 21C). Thus, this result further indicated that FVE is indeed engaged in the transgene-PTGS pathway.

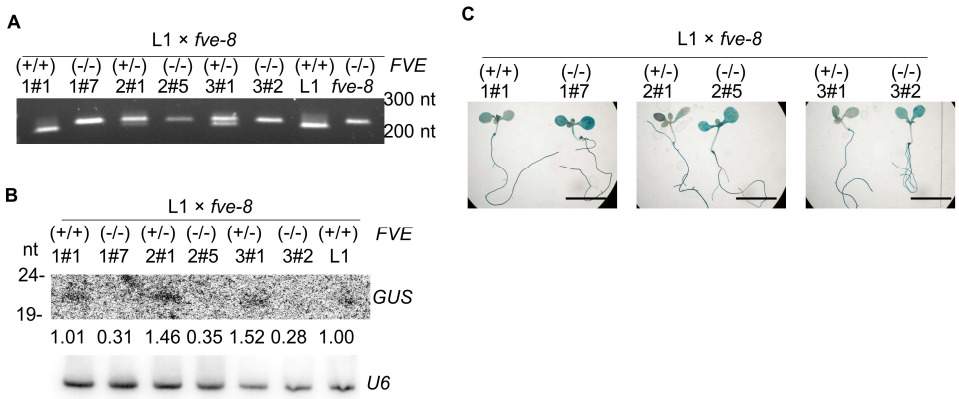

Figure 21 Transgene-derived S-siRNA is decreased in *fve-8*.
(A) Genotyping of different lines of L1 × *fve-8* F2 materials by PCR with dCAPS primers followed by digested by BamHI.
(B) sRNA northern blot assay of GUS-mapped siRNAs in ten-day-old seedlings F2 plants genotyped in (A). *U6* is a loading control. nt, nucleotides. This assay was done with three groups of isolated FVE (+/) and FVE (-/-) F2 materials.
(C) GUS staining assay with ten-day-old seedlings materials analyzed in (B). Scale bars, 1 cm. At least 3 independent cross lines were tested and showed similar results.

To further test whether *FVE* impacts the silencing of hairpin-transgene, we used CRISPR-cas9 technology to knock out *FVE* in a well-known *hpCHS* reporter line, lacking flavonoid pigments due to the PTGS of *CHS* expression (Wesley, et al., 2001) (Figure 22A). At least two biallelic homozygous mutants were obtained (Figure 22B). The *CHS* siRNA level in *fve* (-/-) background was remarkably decreased compared with that in *FVE (+/+)* background (Figure 22C). Correspondingly, the leaves became darker in *cas9-fve* mutants compared with that of the parental line due to the release of the silenced *CHS* (Figure 22D). Moreover, the seed coat of *cas9-fve* mutants turned to a brown color indicative of flavonoid production otherwise light-yellow color observed in the parental

line (Figure 22D). Both leave and seed phenotypes indicated that the endogenous *CHS* expression level was increased in the *fve* mutants compared with the parental line.

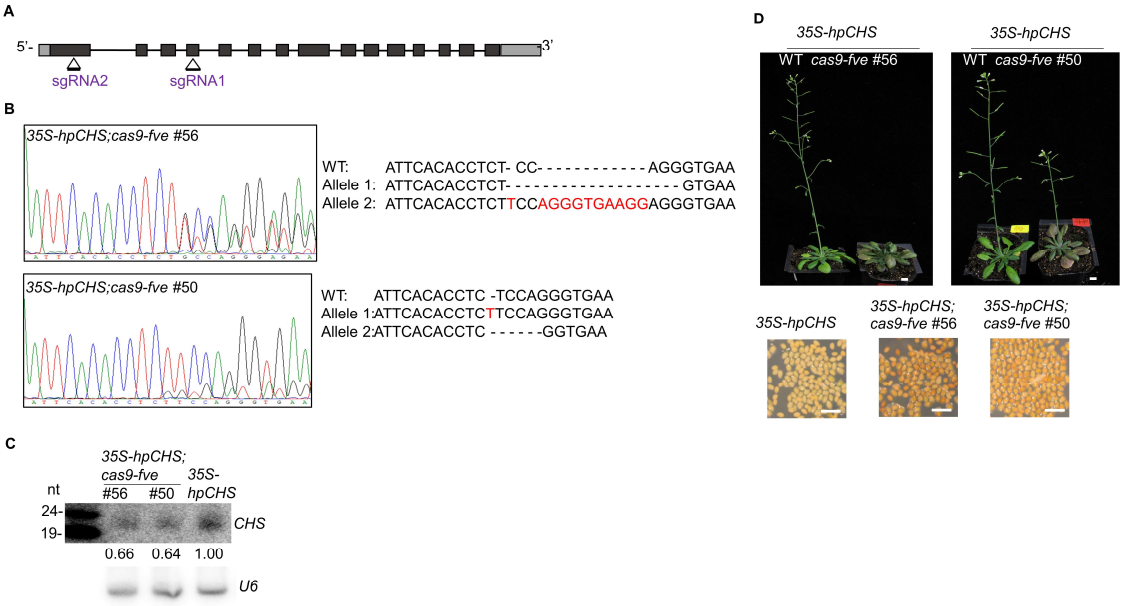

Figure 22 Transgene-derived IR-siRNA is decreased in *fve-8*.
(A) Targeting sites in *FVE* transcript with guide RNAs for CRISPR-Cas9 system.
(B) Sequence results of two independent *35S-hpCHS;cas9-fve* mutants. The edited DNA sequences were shown. Dashes in alleles and red nucleotides indicate deletion and insertion, respectively.
(C) sRNA northern blot assay showed transgenic *CHS*-mapped siRNAs were reduced in *fve* mutants in F2 plants genotyped in (B). *U6* is a loading control. nt, nucleotides. Three biological repeats were conducted with similar results.
(D) *CHS*-specific phenotypes of forty-five-day-old plants (top) and seeds color (bottom) of lines used in (C). Scale bars, 0.2 cm.

In conclusion, FVE participates in the silencing of both sense and double-stranded transgenes; and impacts transgene siRNA production.

2.5 Discussion

Here, we reported a newly developed dual reporter system for monitoring processes of both miRNA and siRNA-mediated RNA silencing. Our system is reminiscent of a screening system used by Kim et al (Kim, et al., 2019). Both our system and theirs can obtain mutants involved in miRNA and siRNA pathways. Using our system, we discovered FVE, a very classical epigenetic component, as a new player in PTGS pathway. Several pieces of evidence support our notion: First, loss-of-function of *FVE* compromised siRNAs from transgenic transcripts from several independent reporter lines. Second, FVE protein is well accumulated in cytoplasm, although it was previously thought to be exclusively in nucleus; moreover, cytoplasmic FVE could fully rescue the defect of *fve-8* in RNA silencing, indicating that the workplace for this function is indeed in cytoplasm where PTGS typically takes place.

As a well-known epigenetic element, FVE has evolved to secure a new role in PTGS. This feature allows FVE to shuttle between nucleus and cytoplasm to suppress gene expression at both TGS and PTGS levels. The fact that the very same protein has multiple functions in TGS and PTGS is reminiscent of several other well-known genes. Chromatin remodeling factor 2 (CHR2), best known to remodel chromatin structures to regulate gene transcription can also interact with SE to remodel pri-miRNAs and suppress miRNA production (Wang, et al., 2018). On the other hand, SE not only regulates RNA processing but also participates in epigenetic silencing of transposable elements (TE) and protein-coding genes (Ma, et al., 2018; Speth, et al., 2018). However, different from CHR2 and SE which likely act in different but co-transcriptional processes, FVE's functions are

spatiotemporally separated. This feature might allow FVE to regulate a broad spectrum of targets.

Interestingly, our study is reminiscent of an earlier report that the mutants of *FCA/FPA, FLD,* and *FVE*, which all coordinately regulate flowering time, can partially rescue the bleach phenotype of transgenic lines expressing *SUC2* promoter-driven hairpin transcripts *of PDS (SUC-hpPDS)*. The mechanism for *fca/fpa* in rescuing *SUC-hpPDS* phenotype was interpreted through the TGS pathway (Baurle, et al., 2007). However, there was no further following study to unravel whether this suppression is via TGS or PTGS regulation given that FVE was only mentioned as a minor element. Here, we primarily exclude that FVE regulates LUC signal through TGS pathway.

CHAPTER III

FVE REGULATE TRANSGENIC SIRNAS THROUGH SGS3/DRB4/DCL2/4 CHANNEL

3.1 Summary

In Chapter II, we demonstrated that FVE regulate LUC expression through promoting its corresponding transgene derived siRNAs. In PTGS pathway, siRNA synthesis requires RDR6/SGS3 to yield dsRNA precursor and then, the dsRNA are processed into siRNAs by DCL2/4. DRB4, a homolog of HYL1, is a co-factor of DCL4. Here, we found that FVE interacts with SGS3 in cytoplasm and promotes its homo-dimerization. Unexpectedly, FVE-8, the truncation form of FVE in *fve-8*, can bind to RNA. Following this clue, we found that FVE and FVE-8 show comparable binding affinity to ssRNA, while FVE shows similar binding affinity to dsRNA, FVE-8 shows a much stronger binding ability to dsRNA. We further found that both FVE and FVE-8 interacts with DRB4 and they play opposite roles in regulating DCL2/4 activity.

3.2 Introduction

Compared with miRNA pathway, siRNA pathway involves different proteins but also share some components with miRNA pathway. In S-PTGS pathway, the precursors of siRNAs are dsRNAs which are synthesized by RDR6/SGS3. RDR6 was reported to be a powerful polymerase: it can not only use ssRNA but also ssDNA as templates to synthesize the second strand; the reaction does not require primers and it won't be affected

by 5’ Cap or poly (A) structures; also template size and sequence don’t affect RDR6 activity (Curaba and Chen, 2008).These two proteins can form RDR6/SGS3-bodies in cytoplasm. However, we still do not know how they capture ssRNA as templates. After the synthesis, dsRNAs are channeled to DCL2/4 to be diced into siRNAs. How are dsRNAs delivered to DCL2/4 are not well explained.

Followed Chapter II, we would like to explore how does FVE affect transgenic-siRNA production. We found that FVE but not its truncated mutant, FVE-8, could interact with SGS3 and promote its homodimerization. Unexpectedly, FVE binds ssRNAs and dsRNAs with moderate affinity while FVE-8 has a significantly increased binding affinity to dsRNA, and these features impact SGS3/RNA association and routing to DRB4/DCL2/4 complexes. In turn, FVE promotes whereas FVE-8 suppresses DRB4/DCL2/4 activity in generating siRNAs in vitro. We concluded that FVE synchronizes SGS3-DRB4-DCL2/4 channel to promote siRNA production whereas FVE-8 hijacks dsRNA substrates to prevent their downstream processing. Thus, this study reveals an uncanonical role of the epigenetic element FVE in transgene-PTGS and sheds light on a new regulatory layer in RNA silencing.

3.3 Method and materials

3.3.1 Vector construction and transgenic plants

For split-YFP constructs, full length of CDS of FVE and SGS3 were cloned into pBA-35S-nYFP-DC and pBA-35S-cYFP-DC by LR reaction. For split-LUC constructs,

those CDS were cloned into pCambia1300-Myc-DC-nLUC and pCambia1300-cLUC-3HA-DC by LR reaction. Digestion confirmed plasmids were transferred to GV3101 for transit infection in tobacco leaves as described (Zhang, et al., 2017).

For Y2H vectors, full length of CDS of FVE, SGS3, RDR6, DCL2, DCL3, DCL4, DRB4, AGO1, DRD1 and RDR2 and truncation FVEs were cloned into vectors pGADT7-GW and pGBKT7-GW by LR recombination.

Table 6 Primers used for constructs in Chapter III.

Primers for constructs	**Sequence**
FVE_{5+6} For	CACCATGGGACACAAAGCTGCTGTTC
SGS3-1-For	ATGAGTTCTAGGGCTGGTCCAA
SGS3-220 Rev	TCAATTTATCTGCTCGATCGACAAGCT
SGS3-219 For	ATGAATGAACCACAGAGGCAGTGG
SGS3-270 Rev	TCACTTTTCTAAAACTTCAGCCAATTCT
SGS3-271 For	ATGGATCTACAGATGAGAGGCGCAT
SGS3-450 Rev	TCAGTAGTTCAGCTGCTGATTGTCCT
SGS3-449 For	ATGAACTACTTTAAGAACAAGCTCTCAAAAC
SGS3-625 Rev	TCAATCATCTTCATTGTGAAGGCCA
DRB4-BamHI For	CGGGATCCATGGATCATGTATACAAAGGTCAACTG
DRB4-XhoI Rev	CCGCTCGAGTTATGGCTTCACAAGACGATAGGCT
DRB4 For	ATGGATCATGTATACAAAGGTCAACTG
DRB4 Rev	TTATGGCTTCACAAGACGATAGGCT
DRB4 Rev-nonstop	TGGCTTCACAAGACGATAGG
1 nt deletion For	AATTCGGCCTCCATGGGGAGGCGCGCCGAGCT
1 nt deletion Rev	CGGCGCGCCTCCCCATGGAGGCCG
2 nt deletion For	CATGGGGCCGCGGCCGCGGAGGCGCGCCCTGCA
2 nt deletion Rev	GGGCGCGCCTCCGCGGCCGCGGCCC

For 6×His-SUMO-FVE/FVE-8/DRB4, FVE/ FVE-8/DRB4 CDS were amplified from corresponding pENTR-FVE/FVE-8/DRB4 and ligated to pET28a-Avi-6×His-

SUMO vector by BamHI/XhoI. Sequence confirmed plasmids were transferred to *E. coli* BL21 (DE3) cells for protein induction. For GST-6×His-SGS3 and GST-6×His-RDR6, SGS3 and RDR6 were obtained from pENTR-SGS3 and pENTR-RDR6 respectively by digestion with NotI/AscI. Two nucleotides were depleted between restriction site NcoI and NotI in pAcGHLT-C (BD Biosciences) to make sure the genes ligated were in frame with GST tag. Digestion confirmed plasmid was transfected to sf9 insect cells with baculovirus.

For 35S-LUC and 35S-hpLUC, LUC was cloned into vectors pBA-DC and pBA-RNAi-DC by LR recombination.

For 3HA-RDR6, 3HA-DCL2 and 3HA-DCL4, RDR6/DCL2/DCL4 was recombined into pBA-3HA-DC to yield pBA-3HA-RDR6/DCL2/DCL4 by LR clonase. Digestion confirmed plasmids were transferred to GV3101 for transient infection in *N. bethamiana* leaves as described (Zhang, et al., 2017). Primers were listed in Table 6.

3.3.2 Cellular localization assay and Bimolecular fluorescence complementation assay of YFP (BiFC).

Large scale plasmid purification and protoplast transformation were performed as described (Ma, et al., 2018). Single positive colonies were cultured in 4 ml LB medium with 50 μg/ml of Spectinomycin at 37 °C overnight. Enlarge the culture into 500 ml TB and grow for 12h at 37 °C. Pellets were collected by centrifuge and resuspended in 80 ml Solution I (10 mM EDTA, pH 8.0). Samples were lysed in 160 ml fresh Solution II (0.1 N NaOH, 1% SDS) thoroughly for 5-10 min at room temperature followed by gently

mixed with 80 ml Solution III (2.5 M KAc, pH 5.5). After 10 min, centrifuge the samples at 4000 rpm for 15 min. The supernatant was filtered through 2-layer mirocloth into a new 500ml bottle. 200 ml isopropanol was added to each sample. After thoroughly mixed, the samples were incubated in -20 °C for 30 min. After centrifuge at 4000 rpm for 15 min, the supernatant was discarded and the pellet was dried and dissolved in 5 ml Solution I. Mix it with 2.5 ml 7.5 M LiCl thoroughly and stay for 10 min at room temperature. Centrifuge at maximum speed for 10 min. The supernatant was fetched into new 1.5 ml tubes and the same volume of isopropanol was added and mixed thoroughly for 10 min at room temperature. After centrifuge at 15000 rpm for 10 min, the pellet was kept and washed with 75% ethanol. The drought pellets from one sample were dissolved with 500 µl 10 mM EDTA containing 100 µg/ml RNase A in total and rotated at 37 °C for 1 h. Then 5 µl 20 mg/ml Proteinase K was added and rotated at 37 °C for 1 h. The samples were purified with phenol/chloroform/iso-amyl (25: 24: 1, pH 8.0) and dissolved in 500 µ water. The Leaves of 4-week-old plants of Col-0, E5-4, *five-8* and *five-8; gFVE* were used as resources of protoplast. Leaf abaxial epidermis were removed by type and the naked side faced to enzyme solution (1.25% cellulase, 0.3% macerozyme, 0.4 M mannitol, 20 mM KCl and 20 mM MES pH 5.7 was mixed well in water and incubated at 55°C for 10 min, after cool down, 10 mM $CaCl_2$, 5 mM ß-Mercaptoethanol and 0.1% BSA was added and filtered by 0.45 µm filter) and incubated in dark at room temperature for 3-4 h. Gently shake the solution every 1 hour. After the protoplasts were sufficiently isolated, an equal volume of ice-cold W5 solution (2 mM MES pH 5.7, 154 mM NaCl, 125 mM $CaCl_2$, 5 mM KCl) was added to stop reaction. The mixture was filtered with a wet 70 µm filter. Centrifuge

the flow-through at 100 g for 2 min with the minimum speed increase/decrease. The supernatant was carefully removed and the pellet was resuspended with ice cold W5 solution and tenderly rinsed and centrifuged at 100 g for 2 min. The pellet was resuspended by cold W5 solution and incubated on ice for 30 min. After a centrifuge at 100 g for 2 min, the pellet was resuspended in a proper volume of Mmg buffer (0.4 M mannitol, 15 mM $MgCl_2$, 4 mM MES pH 5.7) until the concentration of protoplasts reach $2 \times 10^{5\text{-}6}$/ml. 100 µl protoplast solution, 10-20 µg purified constructs and 120 µl PEG solution (0.2 M mannitol, (w/v) 40% PEG4000, 15 mM $MgCl_2$) were gently mixed by flipping in a 2 ml round-bottomed eppendorf tube. The mixture was cultured under light for 20-30 min and a 440 µl W5 was added and gently mixed by inverting up-side-down. After a centrifuge at 100 g for 2 min, the pellet was resuspended in 500 µl W5 solution. Eighteen hours after transfection, fluorescence signals in the protoplasts were visualized by the Leica SP8 confocal microscopy (Li, et al., 2020). Samples were excited by a 514 nm argon laser with an emission of 527 nm for YFP and 633 nm for chlorophyll autofluorescence, respectively.

3.3.3 Yeast two-hybrid (Y2H) assays

Y2H assays were performed as previously described (Wang, et al., 2018). A fresh yeast (strain AH 109) colony was inoculated to 4 ml YPDA medium and cultured at 30 °C overnight. 4 ml culture was transferred to 50 ml YPDA medium and cultured at 30 °C for 3-3.5 h until OD_{600}=0.4-0.6. The pellet was collected by a centrifuge of 700 g for 5 min and washed with autoclaved water once. 3 ml 1× TE/LiAc (10 mM Tris-HCl, 1 mM EDTA pH 7.5 and 100 mM LiAc) was added and the pellet was gently resuspended by

flipping and separated into 2 eppendorf tubes. After a centrifuge of 700 g for 3 min, the pellet was resuspended by 1200 µl 1× TE/LiAc buffer and aliquot into 100 µl/ tube. 3 µl denatured salmon sperm DNA (10 µg/µl), 600 µl 1× TE/LiAc/PEG400 buffer (10 mM Tris-HCl, 1 mM EDTA pH 7.5, 100 mM LiAc and 40% PEG4000), 2 µg pGBK plasmid, 1 µg pGAD plasmid was added to competent cells above and mixed by vortex. The mixture was cultured at 30 °C for 30 min with a mixture every 5 min. 70 µl DMSO was added to each tube and cultured at 42 °C for 15 min with a mixture every 5 min. The pellet was collected by a centrifuge of 12000 g for 30 s and resuspended with 100 µl 0.9% NaCl and spread evenly on dropout medium minus Trp and Leu (SD-TL). After 2-3 days, colonies were dropped on both dropout medium minus Trp, Leu, His and Ade.

3.3.4 Luciferase complementation imaging (LCI) assay

LCI assays were performed as previously described (Wang, et al., 2018). Agrobacteria was resuspended with 10 mM MgCl2 with 15 µM ASG and kept in dark for at least 3 h at room temperature. Cultures of different combinations were mixed equally and infiltrated to tobacco abaxial leaves with a needle-less syringe. Infiltrated tobacco was kept in dark for 24 h and then under light for 24 h. Pictures was recorded with CCD camera.

3.3.5 Immunoprecipitation (IP) and Co-IP

For Co-IP in Figure 17, 10-day-old Ler and *fve-8; P_{FVE}-FM-cFVE* seedlings were harvested and ground well in liquid nitrogen, respectively. 0.5 g powder was homogenized

in 2.5 ml IP buffer (50 mM Tris-HCl pH 7.6, 150 mM NaCl, 5 mM $MgCl_2$, 0.1% Triton X-100, 1% Glycerol, 2 mM PMSF, 5 mM DTT, 1 pellet/ 15 ml IP buffer EDTA-free proteinase inhibitor (Roche), 50 μM MG132) and mixed well for 10 min on ice. The total protein extracts were centrifuge at 15000 rpm for 15 min at 4°C twice. After total proteins were extracted, balanced anti-Flag M2 magnetic beads (Sigma-Aldrich, M8823) was added to extracts for Flag tag enrichment at 4°C for 2 h. For RNase A treatment, 0.05 mg/ml RNase A was added to IP buffer before incubation. After incubation, beads were wash four times with wash buffer (20 mM Tris-HCl pH 7.6, 100 mM NaCl, 0.05% Tween 20, 2 mM DTT, 1 pellet/ 15 ml buffer EDTA-free proteinase inhibitor (Roche)) at 4°C for 5 min. The beads were boiled in 2 × SDS protein loading buffer for 10 min before western blot. Anti-Flag antibody was used to detect IP products and anti-SGS3 antibody was used to determine the co-precipitation levels of SGS3.

For Co-IP in Figure 23, after 48 h infection, infiltrated tobacco leaves and mock leaves were harvested and crosslinked in crosslink buffer (0.4 M Sucrose, 10 mM Tris-HCl pH 8.0, 1 mM PMSF, 1 mM EDTA, 1% formaldehyde) for 10 min by vacuum infiltration. The reaction was stopped with a final concentration of 100 mM Glycine. Samples were rinsed 4 times with ice-cold water and ground well in liquid nitrogen, respectively. 0.3 g powder was homogenized in 1.1 ml IP buffer (40 mM Tris-HCl pH 7.6, 150 mM NaCl, 5 mM $MgCl_2$, 75 μM $ZnCl_2$, 0.1% Triton X-100, 0.1% Glycerol, 2 mM PMSF, 5 mM DTT, 1 pellet/ 15 ml IP buffer EDTA-free proteinase inhibitor (Roche), 15 μM MG132) for 10 min on ice. The total protein extracts were centrifuge at 15000 rpm for 15 min at 4°C twice. After total proteins were extracted, balanced anti-Flag M2

magnetic beads (Sigma-Aldrich, M8823) was added to extracts for Flag tag enrichment at 4°C for 2 h. After incubation, beads were washed four times with IP buffer at 4°C for 5 min. The beads were boiled in 2 × SDS protein loading buffer for 10 min before western blot. Anti-Flag antibody was used to detect IP products and anti-YFP antibody was used to detect co-immunoprecipitates.

3.3.6 Expression and purification of recombinant proteins

Protein expression and purification were performed as described in (Wang, et al., 2018) with modifications. 6×His-SUMO-FVE and 6×His-SUMO-FVE-8 were expressed in *E. coli* BL21 (DE3) cells. GST-6×His-SGS3, GST-6×His-RDR6 and GST-6×His-DCL4 were expressed in a baculovirus/insect cell expression system. For recombinant protein expressed in *E. coli*, transformed BL21 cells were grown in Luria Broth (LB) at 37°C until OD_{600nm} = 0.6. Then the expression was induced with 0.5 mM IPTG at 37°C for 3 hr.

For purification of FVE, the induced bacterial cells were collected and resuspended in lysis buffer (40 mM Tris-HCl buffer pH 8.0, 300 mM KCl, 2% glycerol, 1 mM β-mercaptoethanol, 1 mM PMSF, 0.1% Triton X-100). Cells were disrupted by LM20 Digital Microfluidizer Processor at 25000 psi for 3 cycles. Disrupted cells were centrifuged with 18000 rpm for 15 min at 4°C. The supernatant was filtered with a 0.45 μm filter and made up to 20 mM imidazole and 1% Triton X-100. The cleared lysate was loaded onto a HisTrap HP column (GE Healthcare, Cat#: 17-5248-02). The column was washed with 25 ml wash buffer (40 mM Tris-HCl pH 8.0, 300 mM KCl, 2% glycerol, 1

mM β-mercaptoethanol, 1 mM PMSF, 80 mM imidazole) and eluted with gradient elution buffer from 80 to 300 mM imidazole (40 mM Tris-HCl pH 8.0, 300 mM KCl, 2% glycerol, 1 mM β-mercaptoethanol, 1 mM PMSF). The peak fractions of recombinant protein were pooled and dialyzed in dialysis tubing with 10 kDa molecular weight cut-off (MWCO) stirring in dialysis buffer (20 mM Tris-HCl pH 7.5, 60 mM KCl, 2% glycerol, 2 mM β-ME, 2 mM DTT, 140 nM SUMO protease) at 4°C overnight. The uncut recombinant protein was removed by Ni-beads. The fractions were concentrated by a 30 kDa MWCO centricon (Millipore, Cat#Z71785) and loaded onto a HiLoad 16/600 Superdex 200 pg column (GE Healthcare). The gel filtration buffer contained 20 mM Tris-HCl pH 7.5, 60 mM KCl, 2 mM β-mercaptoethanol and 2 mM DTT. The peak fractions containing FVE were collected and dialyzed in dialysis tubing with 10 kDa MWCO stirring in dialysis buffer (20 mM Tris-HCl pH 7.5, 60 mM KCl, 2 mM β-ME, 2 mM DTT, 50% Glycerol) at 4°C overnight. The final dialysate was aliquoted and frozen by liquid nitrogen and stored at -80°C.

For purification of FVE-8, the induced bacterial cells were collected and resuspended in lysis buffer (40 mM Tris-HCl buffer pH 8.0, 500 mM KCl, 2% glycerol, 1 mM β-mercaptoethanol, 1 mM PMSF, 0.1% Triton X-100). Cells were disrupted by LM20 Digital Microfluidizer Processor at 25000 psi for 3 cycles. Disrupted cells were centrifuged with 18000 rpm for 15 min at 4°C. The supernatant was filtered with a 0.45 μm filter and made up to 20 mM imidazole and 1% Triton X-100. The cleared lysate was loaded onto a HisTrap HP column (GE Healthcare, Cat#: 17-5248-02). The column was washed with 25 ml wash buffer (40 mM Tris-HCl pH 8.0, 500 mM KCl, 2% glycerol, 1

mM β-mercaptoethanol, 1 mM PMSF, 80 mM imidazole) and eluted with gradient elution buffer from 80 to 300 mM imidazole (40 mM Tris-HCl pH 8.0, 500 mM KCl, 2% glycerol, 1 mM β-mercaptoethanol, 1 mM PMSF). The peak fractions of recombinant protein were pooled and dialyzed in dialysis tubing with 10 kDa MWCO stirring in dialysis buffer (20 mM Tris-HCl pH 7.5, 150 mM KCl, 2% glycerol, 2 mM β-ME, 2 mM DTT) meanwhile treated with SUMO protease at 4°C overnight. The uncut recombinant protein was removed by Ni-beads. The fractions were concentrated by a 30 kDa MWCO centricon and loaded onto a HiLoad 16/600 Superdex 200 pg column (GE Healthcare). The gel filtration buffer contained 20 mM Tris-HCl pH 7.5, 150 mM KCl, 2 mM β-mercaptoethanol and 2 mM DTT. The peak fractions containing FVE-8 were collected and dialyzed in dialysis tubing with 10 kDa MWCO stirring in dialysis buffer (20 mM Tris-HCl pH 7.5, 150 mM KCl, 2 mM β-ME, 2 mM DTT, 50% Glycerol) at 4°C overnight. The final dialysate was aliquoted and frozen by liquid nitrogen and stored at -80°C.

For purification of DRB4, the induced bacterial cells were collected and resuspended in lysis buffer (40 mM Tris-HCl buffer pH 8.0, 300 mM KCl, 2% glycerol, 1 mM β-mercaptoethanol, 1 mM PMSF, 0.1% Triton X-100). Cells were disrupted by LM20 Digital Microfluidizer Processor at 25000 psi for 3 cycles. Disrupted cells were centrifuged with 18000 rpm for 15 min at 4°C. The supernatant was filtered with a 0.45 μm filter and made up to 20 mM imidazole and 1% Triton X-100. The cleared lysate was loaded onto a HisTrap HP column (GE Healthcare, Cat#: 17-5248-02). The column was washed with 25 ml wash buffer (40 mM Tris-HCl pH 8.0, 300 mM KCl, 2% glycerol, 1 mM β-mercaptoethanol, 1 mM PMSF, 80 mM imidazole) and eluted with gradient elution

buffer from 80 to 300 mM imidazole (40 mM Tris-HCl pH 8.0, 300 mM KCl, 2% glycerol, 1 mM β-mercaptoethanol, 1 mM PMSF). The peak fractions of recombinant protein were pooled and dialyzed in dialysis tubing with 10 kDa MWCO stirring in dialysis buffer (20 mM Tris-HCl pH 7.5, 60 mM KCl, 2 mM β-ME, 2 mM DTT, 140 nM SUMO protease) at 4°C overnight. The uncut recombinant protein was removed by Ni-beads. The fractions were concentrated by a 30 kDa MWCO centricon and loaded onto a HiLoad 16/600 Superdex 200 pg column (GE Healthcare). The gel filtration buffer contained 20 mM Tris-HCl pH 7.5, 60 mM KCl, 2 mM β-mercaptoethanol and 2 mM DTT. The peak fractions containing DRB4 were collected and concentrated with 30 kDa MWCO centricon at 4°C. An equal volume of glycerol was added to and mixed with the concentrated protein. The final protein was aliquoted and frozen by liquid nitrogen and stored at -80°C.

For purification of recombinant protein in insect cells, pAcGHLT-GST-6×His vectors were transfected with BaculoGold baculovirus DNA system (BD Biosciences, Cat # 554740) into sf9 insect cells (BD Biosciences Cat# 554738; authenticated by the vendor BD Biosciences) to generate recombinant baculovirus. After two rounds of viruses were amplified, P3 virus was collected for large-scale protein expression (Wang, et al., 2018).

For GST-6×His-SGS3, the P3 virus was added to 2.5×10^6 sf9 insect cells per ml for propagation, and insect cells were collected 65 h later. Insect cells were resuspended in lysis buffer (40 mM Tris-HCl pH 8.0, 500 mM NaCl, 5% glycerol, 1 mM β-mercaptoethanol, 1 mM PMSF, 0.1% Triton X-100, 1× Proteinase inhibitor (Sigma-Aldrich)) and disrupted with by LM20 digital Microfluidizer processor at 5000 psi for 2 cycles. Disrupted cells were centrifuged at 20000 rpm for 30 min at 4°C. The supernatant

was filtered with a 0.45 μm filter and made up to 20 mM imidazole and 1% Triton X-100. The cleared lysate was loaded onto a HisTrap FF column (GE Healthcare). The column was washed with 25 ml wash buffer (40 mM Tris-HCl pH 8.0, 500 mM NaCl, 5% glycerol, 1 mM β-mercaptoethanol, 1 mM PMSF, 40 mM imidazole) and eluted with gradient elution buffer from 40 to 300 mM imidazole (40 mM Tris-HCl pH 8.0, 500 mM NaCl, 5% glycerol, 1 mM β-mercaptoethanol, 1 mM PMSF). The peak fractions of recombinant protein were pooled and dialyzed in dialysis tubing with 10 kDa MWCO stirring in dialysis buffer (40 mM Tris-HCl pH 8.0, 500 mM NaCl, 5% glycerol, 1 mM β-ME, 1 mM DTT, 1 mM PMSF) at 4°C for 4 hr. The fractions were collected and loaded onto a GSTrap HP column (GE Healthcare, Cat#: 17-528201). The column was washed with 25 ml wash buffer (40 mM Tris-HCl pH 7.5, 500 mM NaCl, 5% glycerol, 1 mM β-mercaptoethanol, 1 mM DTT) and eluted with gradient elution buffer from 0 mM to 15 mM reduced glutathione (40 mM Tris-HCl pH 8.0, 500 mM NaCl, 5% glycerol, 1 mM β-mercaptoethanol, 1 mM DTT). The peak fractions were concentrated by 50 kDa MWCO centricon (Millipore, Cat#: UFC905024) and then dialyzed in dialysis tubing with 10 kDa MWCO stirring in dialysis buffer (40 mM Tris-HCl pH 8.0, 150mM NaCl, 1 mM β-ME, 1 mM DTT, 2 mM PMSF, 50% Glycerol) at 4°C for 6 hr. The final dialysate was aliquoted and frozen by liquid nitrogen and stored at -80°C.

For GST-6×His-RDR6, the P3 virus was added to 2.5×10^6 sf9 insect cells per ml for propagation, and insect cells were collected 60 h later. Insect cells were resuspended in lysis buffer (40 mM Tris-HCl pH 8.0, 500 mM NaCl, 5% glycerol, 1 mM β-mercaptoethanol, 3 mM PMSF, 0.1% Triton X-100, 1× mg/ml Proteinase inhibitor

(Invitrogen)) and disrupted with by LM20 digital Microfluidizer processor at 5000 psi for 2 cycles. Disrupted cells were centrifuged at 20000 rpm for 30 min at 4°C. The supernatant was filtered with a 0.45 μm filter and made up to 20 mM imidazole and 1% Triton X-100. The cleared lysate was loaded onto a HisTrap FF column. The column was washed with 25 ml wash buffer (40 mM Tris-HCl pH 8.0, 500 mM NaCl, 5% glycerol, 1 mM β-mercaptoethanol, 1 mM PMSF, 40 mM imidazole) and eluted with gradient elution buffer from 40 to 300 mM imidazole (40 mM Tris-HCl pH 8.0, 500 mM NaCl, 5% glycerol, 1 mM β-mercaptoethanol, 1 mM PMSF). The peak fractions of recombinant protein were pooled and dialyzed in dialysis tubing with 10 kDa MWCO stirring in dialysis buffer (1×PBS pH 7.4, 500 mM NaCl, 2% glycerol, 1 mM β-ME, 1 mM DTT, 2 mM PMSF) at 4°C for 9 hr. The fractions were collected and loaded onto a GSTrap HP column. The column was washed with 25 ml wash buffer (1×PBS pH 7.4, 500 mM NaCl, 5% glycerol, 1 mM β-mercaptoethanol, 1 mM DTT) and eluted with gradient elution buffer from 0 mM to 15 mM reduced glutathione (1×PBS pH 7.4, 500 mM NaCl, 5% glycerol, 1 mM β-mercaptoethanol, 1 mM DTT). The peak fractions were concentrated by 50 kDa MWCO centricon and then dialyzed in dialysis tubing with 10 kDa MWCO stirring in dialysis buffer (20 mM HEPES-KOH pH 7.6, 20mM NaCl, 0.2 mM EDTA, 2 mM β-ME, 50% Glycerol) at 4°C for 6 hr. The final dialysate was aliquoted and frozen by liquid nitrogen and stored at -80°C.

3.3.7 In vitro transcription and labelling of RNA

In vitro transcription, 5' and body labeling of RNA substrates were performed as described (Zhu, et al., 2013). The substrate of ssRNA (AT1TE45390) for RdRP assay is a PCR fragment amplified from a pEGM-t-easy vector containing the T7 promoter followed by the transposon sequence as described (Ma, et al., 2018). The substrate of ssRNA for EMSA is G3A44 synthesized by T7 in vitro transcription (Zhang, et al., 2017). For the dsRNA used in EMSA and DCLs assay, two PCR fragments were amplified from LUC coding region (363-509 nt) with primers showed in Table. S1. A sense RNA strand and an antisense strand were transcribed by T7 in vitro transcriptase with [a-32P] UTP (3000 Ci/mmol) as internal labeling, respectively. Primers used are listed in Table 7.

Table 7 Primers used for in vitro T7 transcription.

For in vitro T7 transcription	**Sequence**
T7 For	TAATACGACTCACTATAG
T7-G3A47 Rev	TTTTTTTTTTTTTTTTTTTTTTTTTTTTTTTTTTTTTTTTTTTTTTCCTATAGTGAGTCGTATTA
AT1TE45390 Rev	TTGCTTGATGTTATGCTTTCAA
T7-LUC-363 For	TAATACGACTCACTATAGCAGCCTACCGTAGTGTTTGTTT
LUC-509 Rev	GATGTGACGAACGTGTACATCG
T7-LUC-509 Rev	TAATACGACTCACTATAGATGTGACGAACGTGTACATCG
LUC-363 For	GCAGCCTACCGTAGTGTTTGTTT

3.3.8 RNA-dependent RNA polymerase (RdRP) reconstitution assay

For in vitro RdRP assay, 20 µl of reaction mixtures containing 50 mM HEPES-KOH (pH 7.6), 20 mM NH_4OAc,2% (w/v) PEG4000, 16 mM $MgCl_2$, 0.1 mM EDTA, 0.1mM each of ATP, CTP and GTP, 0-50 µM UTP, and 0-0.5 µM [a-32P] UTP (3000

Ci/mmol), 1 unit/µl RNaseIn and 2 pmol of each recombinant proteins except RDR6 were mixed as indicated and pre-incubated on ice for 20 min. 10 pmol ssRNA template was added to each reaction and incubated for 30 min. 1 pmol RDR6 was added to each sample and to initiate reaction at room temperature for 20 min, respectively. The samples were digested with proteinase K for 30 min at 37°C. Samples were purified with phenol-chloroform and fractionated on 6% urea-polyacrylamide gel. The final result was visualized by radiography. The experiments were repeated three times for statistical analysis. The semi-in vitro RdRP reconstitution assay was performed as described (Curaba and Chen, 2008; Ma, et al., 2018) with modifications. 20 µl of reaction mixtures containing 50 mM HEPES-KOH (pH 7.6), 20 mM NH_4OAc,2% (w/v) PEG4000, 16 mM $MgCl_2$, 0.1 mM EDTA, 1mM each of ATP, CTP and GTP, 0.1 mM UTP, 0.5 µM [a-32P] UTP (3000 Ci/mmol), 10 pmol ssRNA template and 1 unit/µl RNaseIn and recombinant proteins were mixed and pre-incubated on ice for 30 min. Then 3 µl HA-beads containing HA-RDR6 were added to each sample and to initiate reaction at room temperature for 0.5, 1, and 1.5 h, respectively. Samples were boiled with urea loading buffer and fractionated on 6% urea-polyacrylamide gel. The final result was visualized by radiography.

3.3.9 Electrophoretic mobility shift assays (EMSA)

EMSA assay was performed as described as before with modifications (Wang, et al., 2018). Recombinant proteins were mixed in the EMSA buffer (10 mM Tris-HCl pH 7.5, 4% Glycerol, 1mM $MgCl_2$, 0.2 mM EDTA, 0.5 mM DTT). The mixture was incubated on ice for 30min before labeled RNA was added. For dsRNA EMSA, RNA was denatured

at 95°C for 3 min in (100 mM KCl, 30 mM Tris-HCl pH 7.5) and slowly cool down to room temperature. Mixtures were incubated at room temperature for 30 min. Bound complexes were resolved on a native agarose gel. The gel was incubated in fixing buffer (40% ethanol, 10% acetic acid, 5% Glycerol) for 15 min and dried at 80 °C for two hours and then visualized by radiography. The signals were quantified with Image J software. The K_d and appK_d were calculated using Prism 8 (GraphPad) software fit with a Hill slope model.

3.3.10 Ribonucleoprotein complex immunoprecipitation (RIP) RT-PCR.

For RIP, after 48 h infection, infiltrated tobacco leaves were harvested and crosslinked as described in **Co-IP**. 0.5 g powder was homogenized in 2.5 ml RIP buffer (40 mM Tris-HCl pH 7.5, 100 mM KCl, 5 mM $MgCl_2$, 0.2% Triton X-100, 0.1% Glycerol, 1 mM PMSF, 5 mM DTT, 1 pellet/ 15 ml IP buffer EDTA-free proteinase inhibitor (Roche), 15 μM MG132, 100 U/ml Rnase In, 10 U/ml TURBO DNase) prepared in RNase free water for 10 min on ice. The total protein extracts were centrifuge at 15000 rpm for 15 min at 4°C twice. After proteins were extracted, balanced anti-Flag M2 magnetic beads were added to extracts for Flag tag enrichment at 4°C for 2 h. After incubation, beads were washed twice with RIP buffer and twice with high salt buffer (40 mM Tris-HCl pH 7.5, 500 mM KCl, 5 mM $MgCl_2$, 5 mM DTT, 0.2% Triton X-100, 2% glycerol, 1 mM PMSF, 25 μM MG132, 1 pellet per 10 ml Complete EDTA-free protease inhibitor) at 4°C for 5 min, followed by one time wash with proteinase K buffer (50 mM Tris-HCl pH 7.5, 200 mM NaCl, 10 mM EDTA, 1% SDS). The beads were treated with Proteinase K (2 mg/ml)

in 150 µl Proteinase K buffer at 65 °C overnight. One share of beads was boiled in 2 × SDS protein loading buffer for 10 min before western blot. Anti-Flag antibody was used to detect IP. The other share of beads was used for RNA extraction. After TURBO DNase digestion, reverse transcription was performed as described in **RT-PCR** except primed with random primers. Primers used for PCR were listed in Table 8.

Table 8 Primers used for RIP RT-PCR.

For RIP RT-PCR	Sequence
LUC RIP For	ACTGCCTGCGTCAGATTCTCG
LUC RIP Rev	GAAGCGGTTGCAAAACGCT

3.3.11 In vitro DCL2/4 assay

HA-DCL2/4 IP assay was performed referring to a modified protocol from DCL1 immunoprecipitation (Zhu, et al., 2013). after 48 h infection, infiltrated tobacco leaves and mock leaves were harvested and ground well in liquid nitrogen, respectively. 0.5 g powder was homogenized in 2.5 ml immunoprecipitation buffer (40 mM Tris-HCl pH 7.5, 300 mM KCl, 5 mM $MgCl_2$, 0.2 mM EDTA pH 8.0, 5 mM DTT, 0.2% Triton X-100, 1 pellet/ 15 ml IP buffer EDTA-free proteinase inhibitor (Roche), 1 mM PMSF, 2% Glycerol) for 10 min on ice. After total proteins were extracted, anti-HA agarose beads (Sigma-Aldrich, A2095) was used for HA tag enrichment at 4°C for 2 h. After incubation, beads were washed four times with wash buffer (20 mM Tris-HCl pH 7.5, 1 mM DTT, 4 mM $MgCl_2$, 100 mM KCl) at 4°C for 5 min. The final beads were stored with 7 volumes of DCL storage buffer (20 mM Tris-HCl pH 7.5, 1 mM DTT, 4 mM $MgCl_2$, 20% Glycerol) and stored in -20°C before use. 1 pmol FVE, 1 pmol FVE-8 and 1 pmol SGS3 (for DCL4

assay, 1 pmol of DRB4 was also added) were added to a 20 μl reaction system respectively as needed containing 1,000 counts per minute (c.p.m) of dsRNA substrates, 20 mM Tris-HCl pH 7.5, 4 mM $MgCl_2$, 1 mM DTT, 5 mM ATP, 1 mM GTP and 1 U/μl SUPERase-In RNase Inhibitor (Thermo Fisher). The mixture above was homogenized on ice for 30 min. The assay was initiated by adding 3.5 μl HA-IP products as indicated and tumbling at 25°C at 1000 rpm in a thermomixer. The reactions were stopped by 1% SDS and 2 mg/ml proteinase K digestion at 37°C for 30 min. After phenol-chloroform purification, DCL-processed products were fractionated using 10% denaturing polyacrylamide gel and detected with a phosphor imaging plate (GE healthcare). The signals were quantified with Image J 1.52 software.

3.4 Results

3.4.1 FVE interacts with SGS3 and promotes its homodimerization

We hypothesized that FVE targets some key components in transgene-PTGS pathway. To test this, we conducted yeast two-hybrid (Y2H) screening and recovered more than a dozen candidates such as RDR2, RDR6, SGS3, DCL2, DCL3, DCL4, DRB4 and AGO1 among others (Figure 23A). Only SGS3 was recovered to show an interaction with FVE. We then reconstructed several truncated forms of SGS3 (N- terminal region, Zinc Finger domain (ZF), rice gene X and SGS3 domain (XS), and Coiled-coiled domain (CC)) and conducted Y2H assays. We found that FVE interacted with SGS3 (219 - 450 aa), which harbors ZF and XS domains (Figure 23B). These results inferred that co-

expression of FVE and SGS3 impacts yeast growth. Interestingly, positive colonies grew slowly in the four-dropout media after elongated incubation, referring the FVE and SGS3 might have interaction in vivo. Intriguingly, FVE-8, a truncated form of FVE encoding N-terminal 413 amino acid residues and missing the last two WD40 domains (FVE_{5+6}), lost its interaction with SGS3 (Figure 23A), suggested only a full-length FVE can interact with SGS3. We also noticed that FVE is monomeric, whereas FVE-8 could form a self-oligomer (Figure 23A). Furthermore, FVE-8 could not interact with FVE (Figure 23A), suggesting that the C-terminal part of FVE might harbor an auto-inhibitory domain, preventing self-interaction in a normal condition.

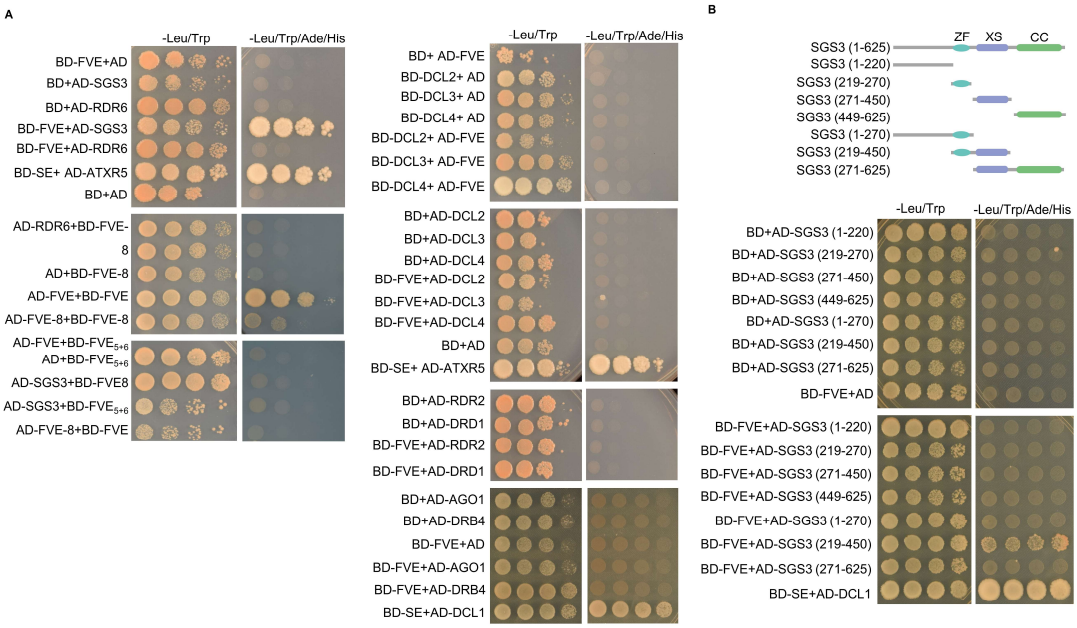

Figure 23 Y2H shows FVE interacts with SGS3.
(A) Y2H screening showed that FVE interacts with SGS3 and that FVE-8 forms homodimer. SE and ATXR5 were used as a positive control. AD and BD, GAL4 activation and DNA binding domain, respectively. At least ten independent colonies were tested for each combination and showed similar results.
(B) Y2H screening showed that SGS3 (219-450) interacts with FVE. Top panel: Schematic illustration of SGS3 variants used for Y2H; bottom panel: Y2H results of different truncated SGS3 proteins and FVE. SE and DCL1 serve as a positive control. At least ten independent colonies were tested for each interaction combination and showed similar results.

To further validate their possible interaction, we conducted immunoprecipitation (Co-IP) assay using *fve-8; P_{FVE}-FM-gFVE* transgenic lines. We immunopurified FVE complexes using an anti-Flag antibody; and readily recovered SGS3 protein in the immunoprecipitates. Importantly, the addition of RNase A did not disrupt the interaction of FVE-SGS3, indicating that their interaction is RNA-independent (Figure 24A). Molecular interaction in planta was confirmed using Luciferase-Complementation

Imaging (LCI) and molecular fluorescence complementation (BiFC) assays (Figure 24B and 24C). In our LCI, FVE displayed LUC complementation with SGS3 as did the positive control of AGO1 and CMV2b (Zhang, et al., 2006), but to a lesser extent (Figure 24B). For BiFC, we co-transfected nYFP-FVE and cYFP-SGS3 into *Arabidopsis* protoplasts with nYFP-SGS3 and cYFP-SGS3 as a positive control. Again, we observed YFP fluorescent complementation between FVE and SGS3, but not for other combinations (Figure 24C). All these results indicated that FVE can interact with SGS3 and be targeted to the cytoplasmic granules. Besides, SGS3 protein level was not affected in *fve-8* plants (Figure 24D).

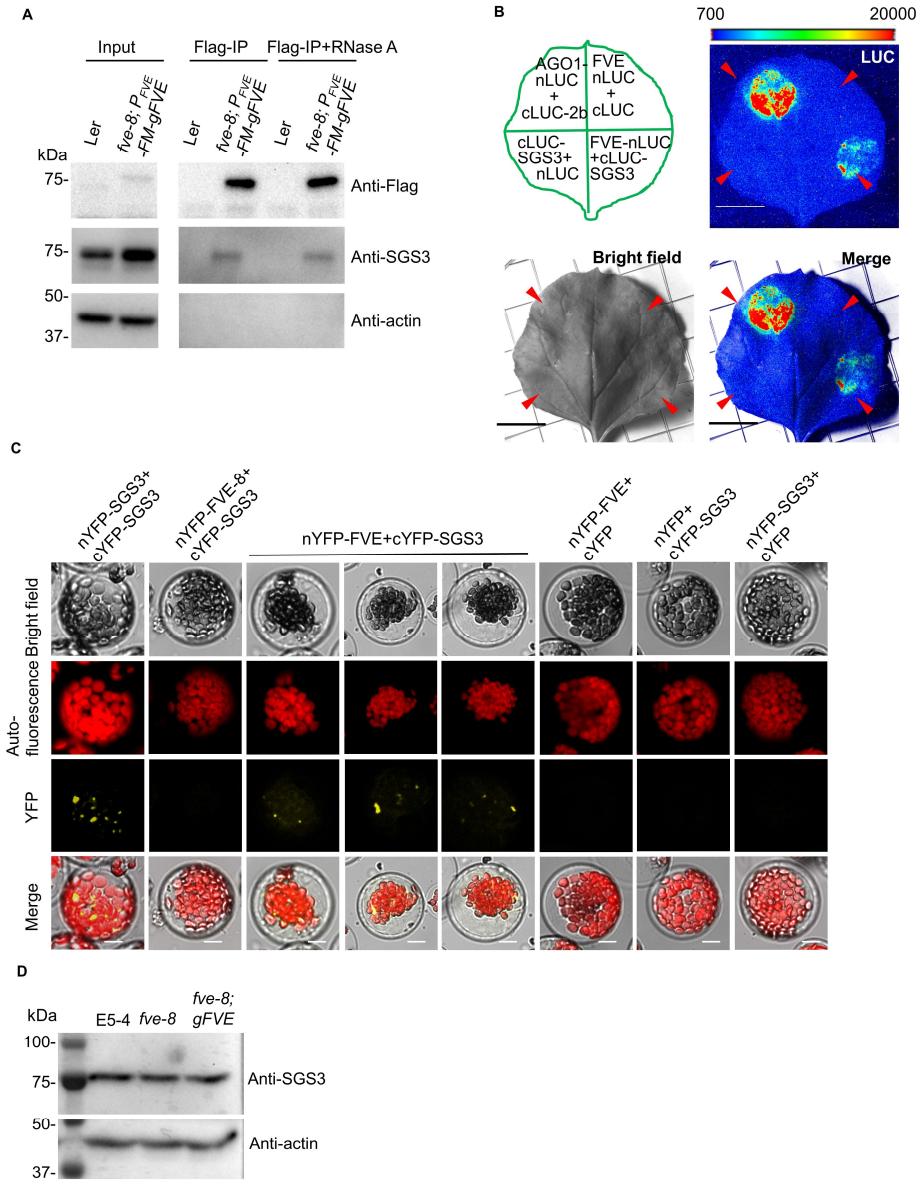

Figure 24 FVE interacts with SGS3 and this interaction occurs in cytoplasm.
(A) Co-IP validated the interaction between FVE and SGS3. IP was performed with an anti-Flag antibody with the protein extracts from ten-day-old seedlings of Ler and *fve-8; P_{FVE}-FM-gFVE*. Western blot assay was done with anti-Flag, anti-SGS3 and anti-Actin antibodies to detect the indicated proteins in input and IP products, respectively. Ler and Actin serve as negative controls. The experiment was independently repeated twice with similar results.
(B) LCI assay showed the specific FVE-SGS3 interaction in *N. benthamiana*. The infiltration scheme in the leaf shows different combinations of constructs fused to either N-terminal (nLuc) or C-terminal (cLuc) regions of luciferase. LCI complementation

(LUC), bright field, and merged photograph (Merge) are shown. The red arrows and color bar indicate the infiltration positions and the signal intensity, respectively. AGO1-nLUC and cLUC-2b served as a positive control (Zhang, et al., 2006). Red arrows indicate infiltration loci. Scale bars, 2 cm. Signals were displayed by Lightfield software.
(C) Confocal imaging assays showed the interaction between FVE and SGS3 by split-YFP. The proteins were co-expressed in protoplasts of E5-4, f*ve-8* and *fve-8; gFVE*. At least ten individual protoplasts were observed with similar results and 3 individual protoplasts were shown here. cYFP and nYFP with no proteins fused served as negative controls. nYFP-SGS3 and cYFP-SGS3 served as a positive control.
(D) Western blot assay showed that endogenous SGS3 accumulation was comparable in five-day-old seedlings of E5-4, *fve-8* and *fve-8; gFVE.* Anti-SGS3 and anti-actin antibodies were used and Actin was an internal control.

Next, we examined if *fve* mutation impacts SGS3 cellular compartmentation via confocal imaging. YFP-SGS3 driven by *35S* promoter exhibited granule-liked foci in the transfected protoplasts of E5-4, *fve-8* and *fve-8; gFVE* lines (Figure 25A), reminiscent of SGS3 foci reported before (Elmayan, et al., 2009; Kumakura, et al., 2009). The numbers of the foci per cell were comparable in those lines, referring that *fve* mutation might not change cellular localization of SGS3 (Figure 25B). However, BiFC assay for SGS3 homodimerization (Elmayan, et al., 2009) revealed that the numbers of the foci for SGS3 homodimers per protoplast were significantly reduced in E5-4 *fve-8* compared with the ones in either E5-4 or *fve-8; gFVE* (Figure 25A and 25B). These results indicated that *fve* impacts SGS3 homodimerization, and possibly SGS3-mediated function in vivo.

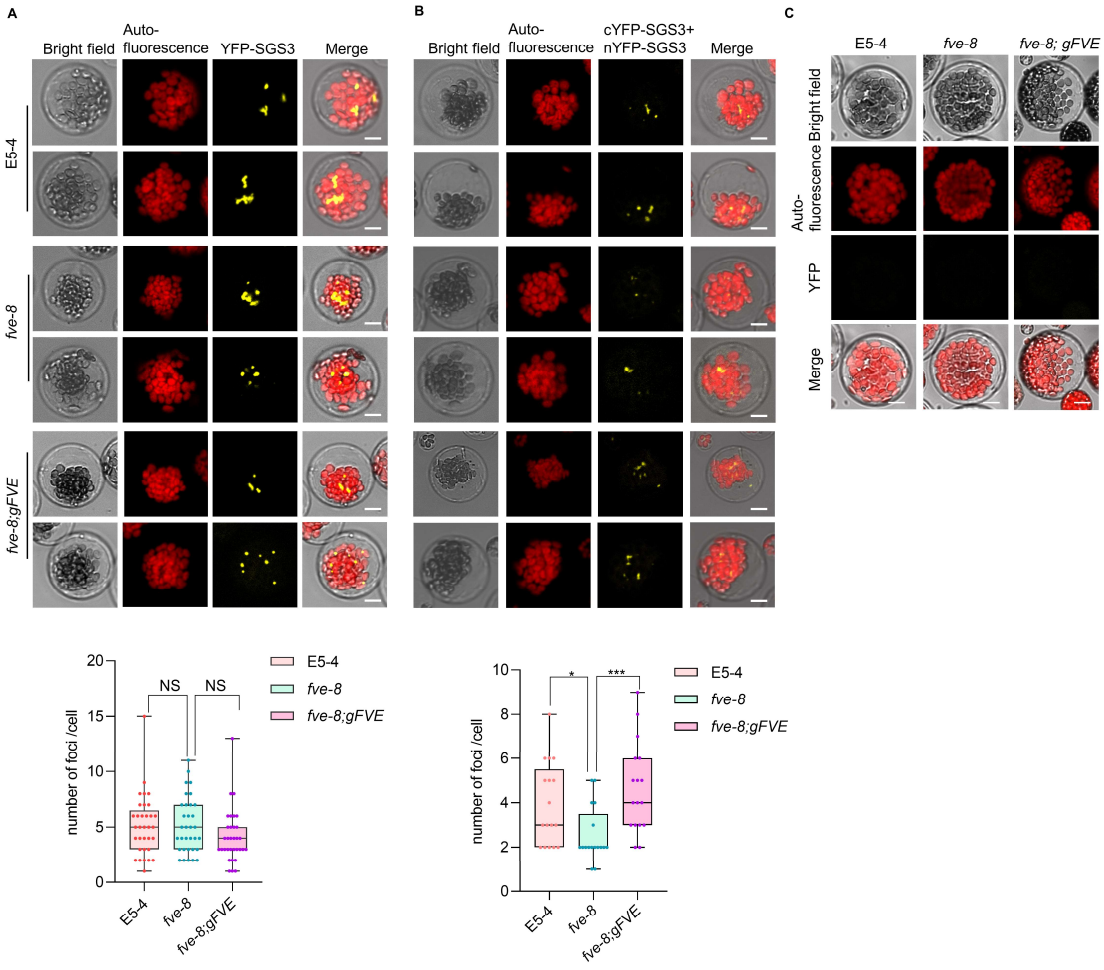

Figure 25 FVE promotes homodimerization of SGS3.

(A) Confocal imaging assays showed that FVE mutation did not alter subcellular localization of YFP-SGS3 (Top). The protein was expressed in protoplasts of E5-4, *fve-8* and *fve-8; gFVE*. Thirty-three independent protoplasts were evaluated with similar results. Box plots of YFP foci statistics (Bottom). The line in the middle of the box is plotted at the median. The whiskers are drawn from min to max percentiles. Individual data points were shown. The asterisks indicate a significant difference between samples clustered (unpaired two-tailed Student's *t*-test, **P*< 0.05; ****P*< 0.001).

(B) BiFC of YFP assays showed FVE but not FVE-8 promotes homodimerization of SGS3. The proteins were co-expressed in protoplasts of E5-4, *fve-8* and *fve-8; gFVE*. Scale bars, 10 μm. Seventeen independent protoplasts were tested with similar results. Box plot for numbers of SGS3 dimer foci. The statistics were done similarly as in (A).

(C) the un-transfected protoplasts of E5-4, *fve-8* and *fve-8; gFVE* did not exhibit background green fluorescent signal, due to the difference of light activation spectrum between GFP and YFP in the confocal microscope. Scale bars, 10 μm.

3.4.2 FVE does not affect RDR6 activity in vitro

SGS3 and RDR6 interact with each other in specific cytoplasmic granules and form SGS3/RDR6-bodies (Kumakura, et al., 2009). To investigate if FVE influences the polymerase activity of RDR6, we purified recombinant RDR6, SGS3, FVE, and FVE-8 from either *E. coli* or a baculovirus-insect cell system and established an in vitro RDR6/SGS3 reconstitution system (Figure 26A and 26B). After the reaction, the samples were digested with proteinase K and then vigorously washed by phenol and chloroform before fractionation in Urea-PAGE. Michaelis-Menten kinetics analysis showed that RDR6/SGS3 activity was not significantly affected by FVE. In contrast, FVE-8 might have some marginally inhibitory effect on RDR6/SGS3 activity in vitro (Figure 26C-26E).

We next hypothesized that the RDR6/SGS3 complex entails some endogenous cellular cofactors for optimized function. To test this, we immunoprecipitated HA-tagged RDR6 using *N.benthamiana* based on previous reports (Figure 27A) (Curaba and Chen, 2008; Ma, et al., 2018), and re-conducted the assay. This time the samples were directly denatured and fractionated in the Urea-PAGE without prior protein digestion. Again, we did not observe the enhanced effect of FVE on RDR6/SGS3 performance in vitro (Figure 27B). Unexpectedly, an unusually strong signal was detected in the reaction mixture containing FVE-8 but no other proteins. However, a closer examination of the Urea-PAGE gel revealed that the shorter RNA products disappeared in the FVE-8-containing reaction (Figure 27B). These results suggested that FVE-8 binds to RNA transcripts produced by RDR6/SGS3.

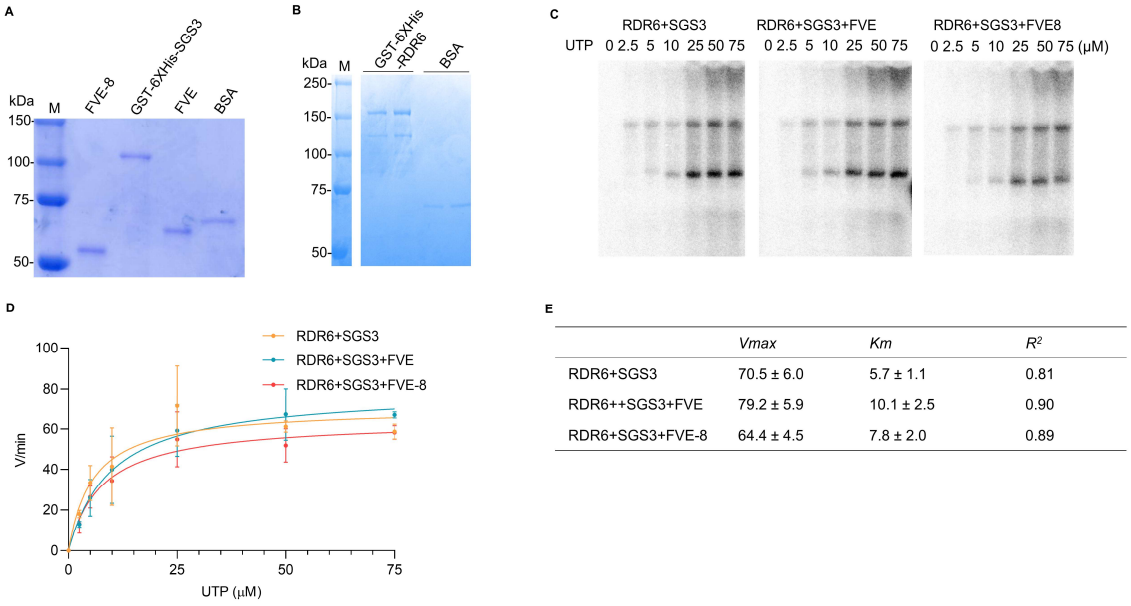

	Vmax	*Km*	R^2
RDR6+SGS3	70.5 ± 6.0	5.7 ± 1.1	0.81
RDR6++SGS3+FVE	79.2 ± 5.9	10.1 ± 2.5	0.90
RDR6+SGS3+FVE-8	64.4 ± 4.5	7.8 ± 2.0	0.89

Figure 26 In vitro reconstitution assays showed that FVE might not have significant enhancement effect on RDR6/SGS3 activity in vitro.

(A) SDS-PAGE of purified recombinant proteins FVE-8, GST-6×His-SGS3 and FVE. BSA was used as a concentration reference.

(B) SDS-PAGE of purified recombinant proteins GST-6×His-RDR6. BSA was used as a concentration reference.

(C) in vitro assays of RDR6 activity with different combinations of proteins. The reaction took place in 20 min with a range of ^{32}P-UTP dosage. At least 3 independent repeats were conducted with similar results. Signals were detected by phosphor imaging.

(D) Michaelis-Menten model of RDR6 reaction velocity calculated from (E). The velocity was calculated from image quantification of (C) with ± s.d. (n=3). Individual data points were shown.

(E) *Vmax*, *Km* and R^2 values calculated with (D).

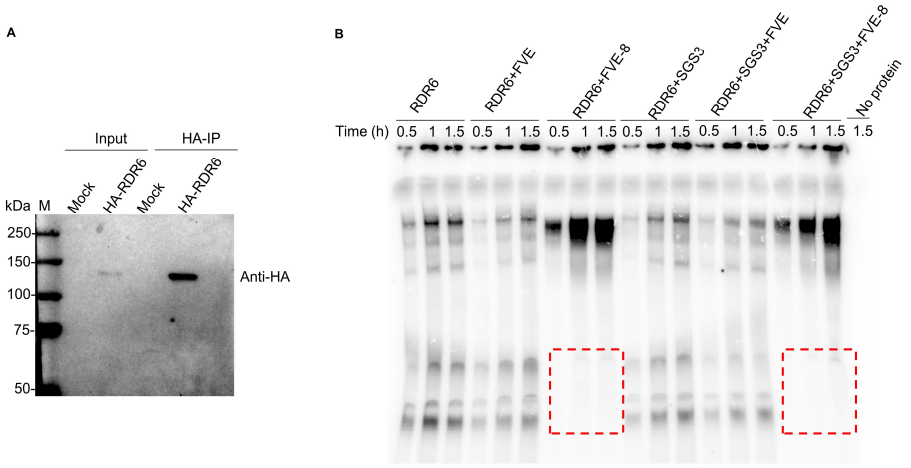

Figure 27 Semi-in vitro RDR6 activity shows a possibility of FVE-8-RNA binding activity.
(A) Western blot analysis of immunoprecipitated HA-tagged RDR6 using an anti-HA antibody. 35S-3HA-RDR6 construct was infiltrated in *N. benthamiana*. *N. benthamiana* with mock treatment served as a negative control.
(B) Semi-in vitro assays of RDR6 activity in a time course with ssRNA substrate. HA-RDR6 was incubated with and without different combinations of proteins for the indicated time points. Sample with no protein applied was negative control. Signals were detected by phosphor imaging. Note: small RNA products in the FVE-8-treated reactions otherwise in red dashed squares were shifted up compared with those in others.

3.4.3 FVE and FVE-8 bind to RNA

To further investigate if FVE and FVE-8 associated with RNA in vitro, we performed electrophoretic mobility shift assay (EMSA). EMSAs showed that FVE could bind ssRNA with an affinity with disassociation constant (K_d) =145.5 ±13.5 nM (Figure 28Aand 28B). FVE could also bind dsRNA with apparent K_d=143.5 ± 4.0 nM (Figure 28Cand 28D). Similarly, FVE-8 bound ssRNA with a moderate binding affinity (K_d =149.3 ± 76.0 nM) (Figure 28E and 28F). Different from a single-shifting band of FVE-ssRNA binding, there are two shifting bands of FVE-8-ssRNA in the EMSA assay, reminiscent of the association of dimerized HYL1 with RNA (Wang, et al., 2018).

Intriguingly, FVE-8 displayed a substantially increased binding affinity to dsRNA with an apparent dissociation constant $appK_d$= 5.3 ± 0.3 nM and h=1.997. The h value and the sigmoidal FVE-8–dsRNA binding curves suggest cooperativity between multiple nucleic acid binding sites in FVE-8 in substrate binding. This result is well in line with the fact that FVE-8 could form dimer or oligomers in vitro and in vivo. These results were unexpected as RbAp48 has not been noticed to partner with RNA before. To further validate the observation, we performed ribonucleoprotein immunoprecipitation (RIP) experiments. We co-transfected *35S-FM-FVE* with *35S-LUC* or *35S-hpLUC* constructs in *N. bentha*, respectively. The RIP result showed that *LUC* transcript was clearly recovered in the FVE immunoprecipitate, but not in the control. This result indicates that FVE indeed an RNA-binding protein in vivo (Figure 29).

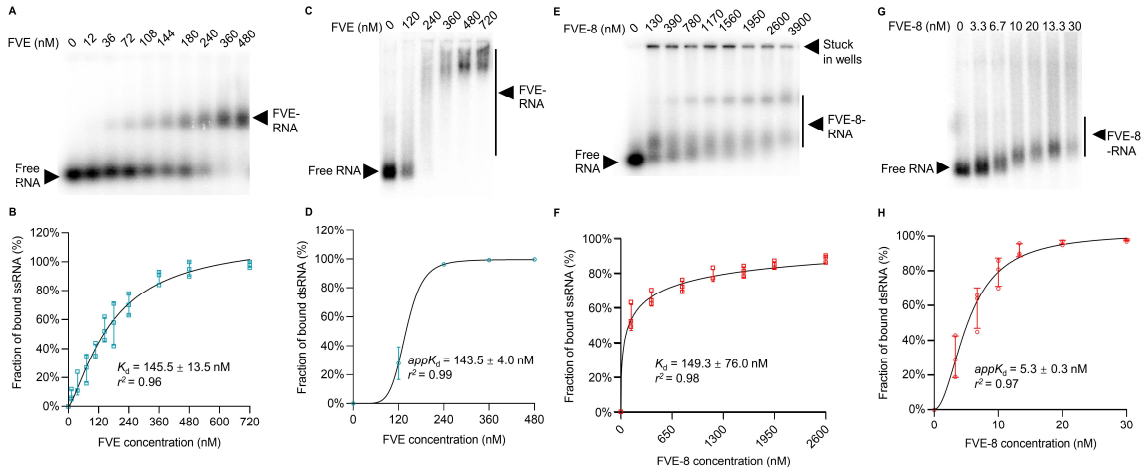

Figure 28 EMSA showed that FVE and FVE-8 display different binding affinities to ssRNA and dsRNA.

(A and C) The mobility pattern of FVE with homogenous ssRNA (A) and dsRNA (C). Protein concentrations were shown above. Arrows indicate the mobility of protein−RNA complexes or free RNA. Three independent repeats were conducted for each assay with similar results.

(B and D) The binding affinities (K_d and appK_d) were calculated from quantification of EMSA images from (A and C) and additional repeats with ± s.d. (n=3). Individual data points were shown.

(E and G) The mobility pattern of FVE-8 with homogenous ssRNA (E) and dsRNA (G). Protein concentrations were shown above. Arrows indicate the mobility of protein−RNA complexes or free RNA. Three independent repeats were conducted for each assay with similar results.

(F and H) The binding affinities (K_d and appK_d were calculated from quantification of EMSA images from (E and G) and additional repeats with ± s.d. (n=3). Individual data points were shown.

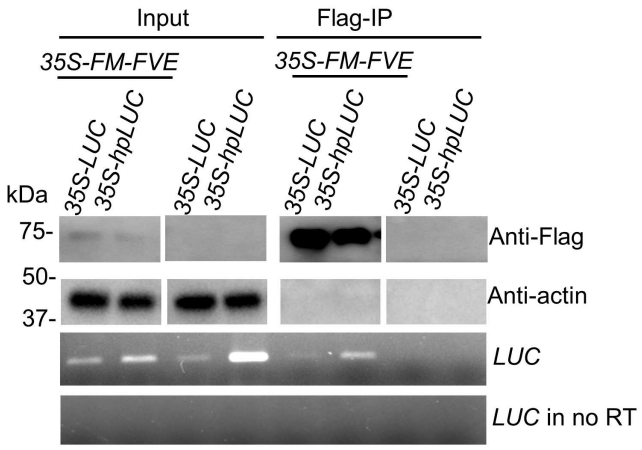

Figure 29 RIP assay showed that FVE binds RNA in vivo.
IP was performed with an anti-Flag antibody with the protein extracts from co-infiltrated *N. bentha* leaves. Western blot assay was done with anti-Flag and anti-Actin antibodies to detect the indicated proteins in input and IP products, respectively. RT was performed after TURBO DNase digestion with random primers. No RT samples were used to show no contamination from DNA.

A previous study showed that SGS3 binds dsRNA but not ssRNA (Fukunaga and Doudna, 2009). We re-visited this assay and found that SGS3 could indeed bind to dsRNA with a binding affinity of $appK_d$=30.8 ± 1.4 nM (Figure 30B and 30C). For ssRNA binding, SGS3 showed a complicated scenario, a subtle shift was observed but the bound ribonucleoprotein complexes were quickly disassociated and could not reach a complete shift (Figure 30A). In this scenario, we interpreted that SGS3 may have a low binding ability to ssRNA.

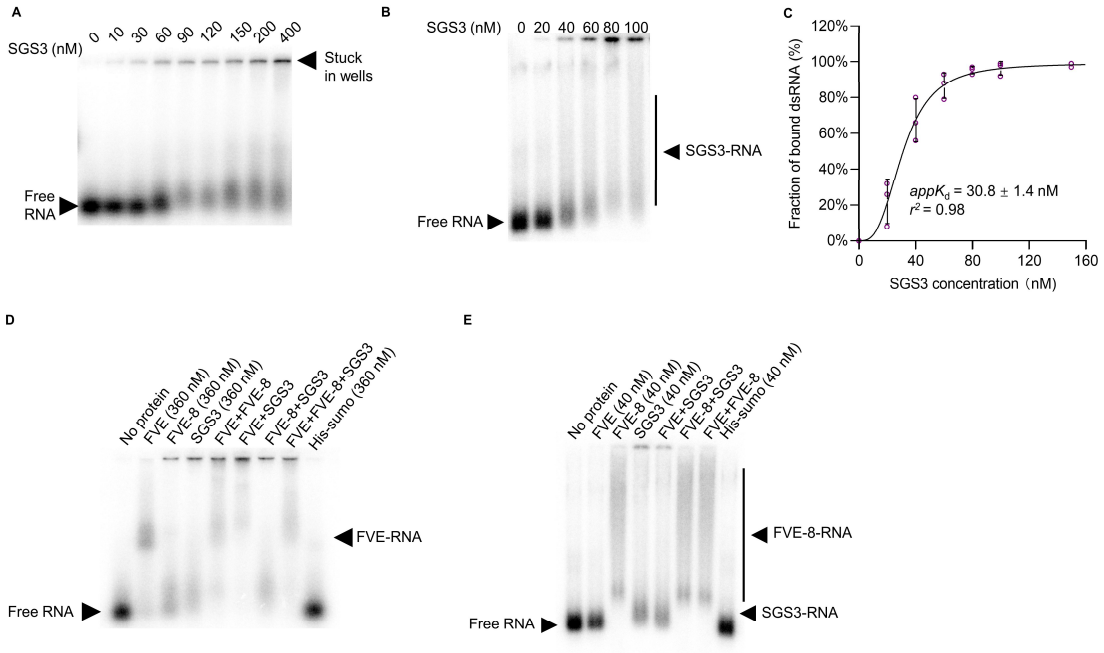

Figure 30 SGS3 binds to dsRNA but not ssRNA.
(A and B) The mobility pattern of SGS3 with homogenous ssRNA (A) and dsRNA (B). Protein concentrations were shown above. Arrows indicate the mobility of protein−RNA complexes or free RNA. Three independent repeats were conducted for each assay with similar results.
(C) The binding affinities (K_d and appK_d) were calculated from quantification of EMSA images from (B) and additional repeats with ± s.d. (n=3). Individual data points were shown.
(D and E) EMSA showed mobility patterns of different combinations of proteins-ssRNA complexes (D) and of proteins-dsRNA complexes (E). His-sumo was used as a negative control.

Given that FVE interacts with SGS3, we wondered if they could synergistically cooperate in binding to RNA. EMSA showed that co-incubation of FVE and SGS3 with ssRNA resulted in a shifting pattern different from the mobility of either FVE–ssRNA or SGS3–ssRNA complexes (Figure 30D). These results suggested that FVE-SGS3-ssRNA can form a new stable complex with a distinct electrophoretic mobility. In contrast, co-incubation of FVE-8 and SGS3 with ssRNA displayed a similar mobility-shifting pattern

to those of either SGS3-ssRNA or FVE-8-ssRNA complexes (Figure 30D). Of note, the addition of FVE-8 to FVE-ssRNA or FVE-SGS3-ssRNA complex did not alter the mobility shift patterns. These results indicated that FVE but not FVE-8, could promote SGS3-ssRNA binding with further suggestion that FVE could facilitate and strengthen SGS3 association to the transgene transcripts to produce dsRNA substrates in vivo.

For the binding to dsRNA, FVE and SGS3 appeared to be the same ribonucleoprotein complex. However, no matter which protein was co-incubated with FVE-8, the shifting pattern of the mobility was always identical to that of FVE-8-dsRNA alone, clearly due to its predominately strong affinity to dsRNA compared with other proteins (Figure 30E). Although the differential RNA-binding patterns by a combination of proteins above do not seem to impact dsRNA synthesis in the RDR6/SGS3 assays in vitro, they likely affect their function in vivo and also downstream step of siRNA synthesis.

3.4.4 FVE promotes while FVE-8 impedes DCL2/4 activity in vitro

The dsRNA products by RDR6/SGS3 are next routed to DRB4/DCL2/4 complexes for further metabolic processing. DRB4 serves as an auxiliary factor of DCL4 (Fukudome and Fukuhara, 2017), similar to HYL1 with DCL1 in processing miRNAs (Zhu, et al., 2013; Wang, et al., 2018). Given that FVE can interact with DRB2, we next hypothesized that FVE might interact with DRB4, a homolog of DRB2 (Clavel, et al., 2015), to regulate DRB4/DCL2/4 activity. Although Y2H assay did not show their interaction (Figure 23A), both FVE and FVE-8 showed interaction with DRB4 in the LCI assay (Figure 31A). The interaction between FVE and DRB4 was further confirmed by

the Co-IP assay with protein extracts from transfected *N. benthamiana* leaves (Figure 31B) (Li, et al., 2020). These results suggested that the FVE/SGS3/dsRNA ribonucleoprotein complex could be channeled to DRB4/DCL2/4 machinery through FVE/DRB4 interaction. This result is well in line with the previously reported partial co-localization of SGS3 with DCL4 complexes (Pontes, et al., 2013).

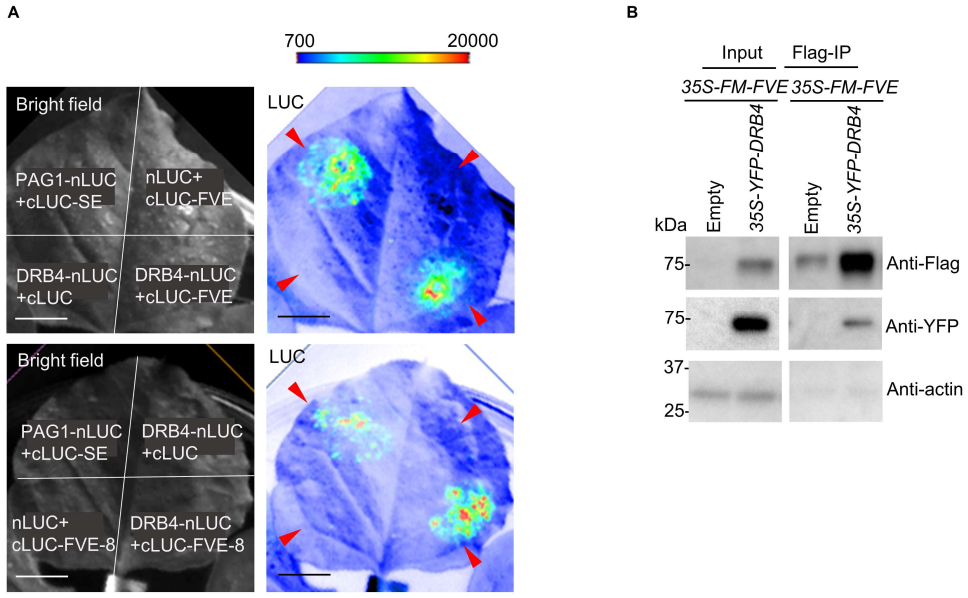

Figure 31 FVE interacts with DRB4.
(A) Luciferase complementary imaging (LCI) assay showed that FVE (top) and FVE-8 (bottom) interact with DRB4 in *N. benthamiana*. The infiltration scheme in the leaf shows different combinations of constructs fused to either N-terminal (nLUC) or C-terminal (cLUC) regions of luciferase. Bright field and LCI complementation (LUC) images are shown. PAG1-nLUC and cLUC-SE serve as a positive control (Li, et al., 2020). The red arrows and color bar indicate the infiltration positions and the signal intensity, respectively. At least 3 individual leaves were observed with similar results.
(B) Co-IP validated the interaction between FVE and DRB4. IP was performed with an anti-Flag antibody with the protein extracts from co-infiltrated *N. benthamiana* leaves. Western blot assay was done with anti-Flag, anti-YFP and anti-Actin antibodies to detect the indicated proteins in input and IP products, respectively.

Interestingly, we extended the Y2H and LCI assays for SGS3 and DRB4 and observed their interaction in vivo (Figure 32Aand 32B). These results suggested that the FVE/SGS3/dsRNA ribonucleoprotein complex could be channeled to DRB4/DCL2/4 machinery through FVE/SGS3/DRB4 interaction. This result is well in line with the previously reported partial co-localization of SGS3 with DCL4 complexes (Pontes, et al., 2013).

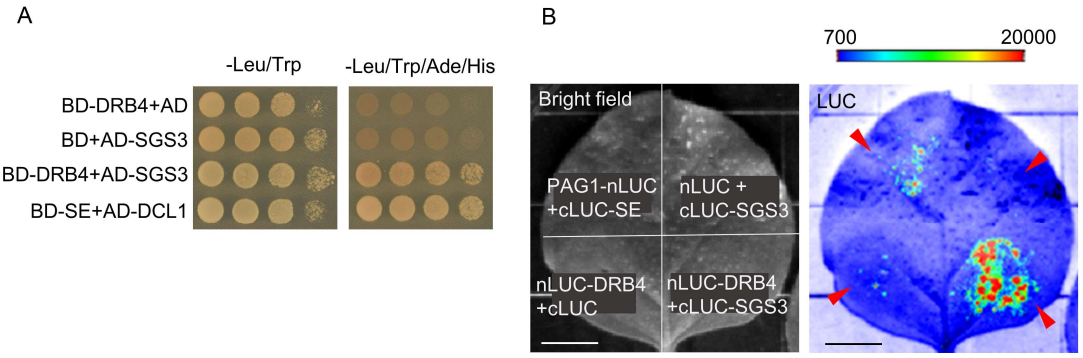

Figure 32 DRB4 interacts with SGS3.
(A) Y2H screening showed that DRB4 interacts with SGS3. SE and DCL1 were used as a positive control. AD and BD, GAL4 activation and DNA binding domain, respectively. At least ten independent colonies were tested for each combination and showed similar results.
(B) LCI assay showed that SGS3 interacts with DRB4 in *N. bentha.* The infiltration scheme in the leaf shows different combinations of constructs fused to either N-terminal (nLUC) or C-terminal (cLUC) regions of luciferase. Bright field and LCI complementation (LUC) images are shown. PAG1-nLUC and cLUC-SE serve as a positive control (Li, et al., 2020). The red arrows and color bar indicate the infiltration positions and the signal intensity, respectively. At least 3 individual leaves were observed with similar results.

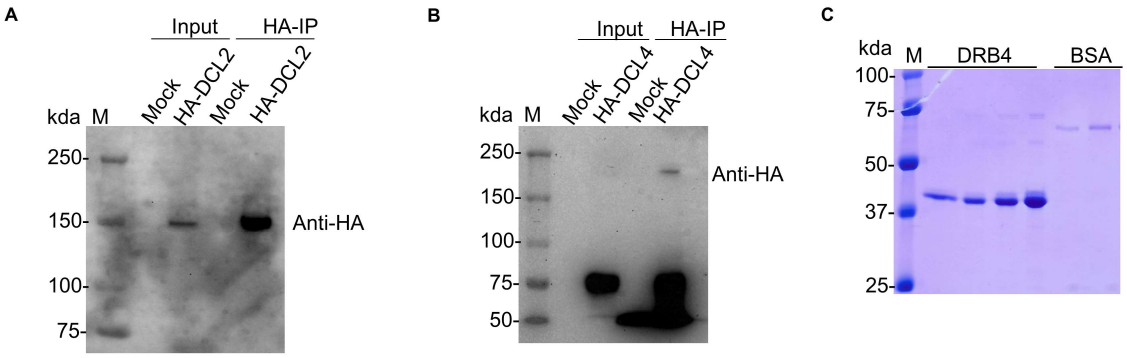

Figure 33 HA-IP of HA-DCL2/4 and purification of DRB4.
(A and B) Western blot analyses of immunoprecipitated HA-tagged DCL2 (A) and HA-tagged DCL4 (B) using an anti-HA antibody. *35S-3HA-DCL2* and *35S-3HA-DCL4* construct were infiltrated in *N. benthamiana*, respectively. *N. benthamiana* with mock treatment served as a negative control.
(C) SDS-PAGE of purified recombinant protein DRB4. BSA was used as a concentration reference.

We finally investigated the impact of FVE and FVE-8 on DRB4/DCL2/4 activity. 3HA-DCL2 and 3HA-DCL4 IP products were immunoprecipitated from *N. benthamiana* leaves that were transfected with corresponding constructs, respectively (Figure 33Aand 33B). DRB4 was purified from transgenic *E. coli* (Figure 33C). We performed in vitro DCL2/4 assays incubated with dsRNA substrates with different combinations of FVE or FVE-8. HA-IP products immunoprecipitated from mock-treated *N. benthamiana* leaves exhibited no DCL activity (Figure 34A and 34B). Interestingly, the incubation with FVE notably and consistently enhanced the DCL2 and DCL4 activity, compared with incubation with IP products only, while the incubation with FVE-8 remarkably quenched the activities of DCLs (Figure 34A-33D). Our results suggested that FVE could directly fine-tune DCL4 activity likely through interaction with its partner DRB4, whereas FVE-

8 hijacked dsRNA despite its interaction with DRB4. Thus, the decrease of *LUC* and *GUS* transgenic siRNAs should result from the compromised DRB4/DCL2/4 activity in *fve-8*. The result also explained that the reduction of transgenic siRNAs in *fve-cas9-hpCHS* mutants should attribute to the compromised DRB4/DCL2/4 activity in the absence of FVE.

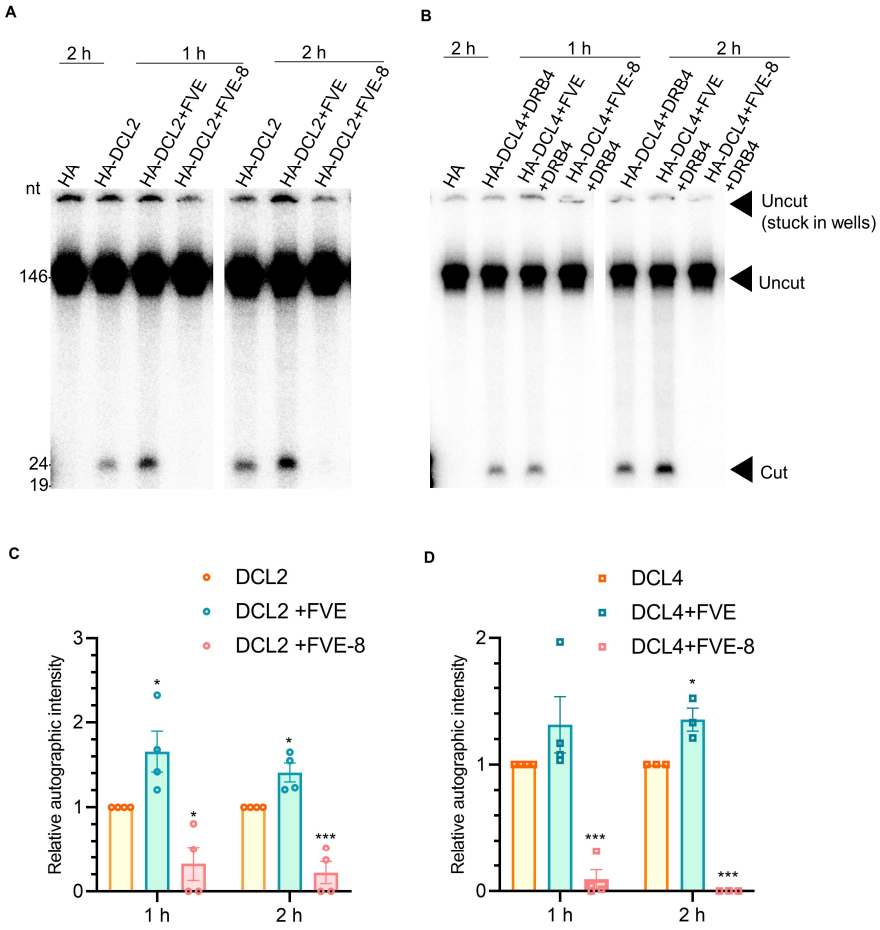

Figure 34 In vitro reconstitution assay showed that FVE promotes whereas FVE-8 inhibits activities of DCL2/4-DRB4 complexes.

(A and B) DCL2 (A) and DCL4 (B) dicing activity with and without FVE/FVE-8 at indicated time points. Radioisotope ^{32}P-labelled dsRNA was incubated with HA-DCL2 and -DCL4 immunoprecipitated from *N. benthamiana* and purified recombinant DRB4 protein from *E. coli.* The immunoprecipates from the mock-treated *N. benthamiana* was used as the negative control. RNAs recovered from the reaction mix were fractionated on 12% denaturing gels. The positions of intact substrates, processed products, and RNA markers are shown. Signals were detected by phosphor imaging. At least 3 independent repeats were conducted with similar results.

(C and D) Statistics of image quantitation of DCL2 (C) and DCL4 (D) activity in (A) and (B). The relative autographic intensities were presented as the mean of 4 or 3 replicates ± sem (unpaired two-tailed Student's *t*-test, **P*< 0.05; ****P*< 0.001). Individual data points were shown.

3.5 Discussion

In Chapter II, we discovered FVE, a very classical epigenetic component, as a new player in the PTGS pathway. Here, we proposed that FVE coordinates with SGS3 and DCL4/DRB4 function to promote the biogenesis of transgene-derived siRNAs (Figure 35). Several pieces of evidence support our notion: First, loss-of-function of *FVE* compromised siRNAs from transgenic transcripts from several independent reporter lines. Second, FVE protein is well accumulated in cytoplasm, although it was previously thought to be exclusively in nucleus; moreover, cytoplasmic FVE could fully rescue the defect of *fve-8* in RNA silencing, indicating that the workplace for this function is indeed in cytoplasm where PTGS typically takes place. Third, FVE directly interacts with SGS3 and promotes its homodimerization, which is the prerequisite for SGS3 function in PTGS (Elmayan, et al., 2009) (Figure 23-Figure 25). Fourth, FVE binds ssRNA substrate, whereas SGS3 barely (Figure 28-Figure 30). In this scenario, FVE might bind to ssRNA while associating with SGS3, which in turn recruits RDR6 for dsRNA synthesis in vivo, although this function was unnecessary in vitro. On the other hand, FVE-8 still binds to ssRNA but fails to interact with SGS3 to promote its dimerization, leading to inefficient launching of SGS3-RDR6 to ssRNA substrate in vivo (Figure 28). Fifth, given that FVE interacts with DRB4, dsRNA, once generated, could be channeled from FVE/SGS3 into DRB4/DCL4 complexes for further processing to produce siRNAs. Finally, FVE protein itself could directly promote activity of DCL4/DRB4 to produce siRNAs. However, FVE-8 forms a homodimer and is granted a neo function to bind dsRNA (Figure 23A and Figure 28G). Because FVE-8 binds dsRNA with a significantly higher affinity relative to SGS3, the

protein could compete with SGS3 and hijack the dsRNA product and prevent the downstream processing by DRB4/DCL2/4 complex (Figure 34C and Figure 27D). Thus, FVE directly coordinates two consecutive processes of transgene silencing and promotes siRNA production through interaction with SGS3 and DRB4 and its RNA-binding ability.

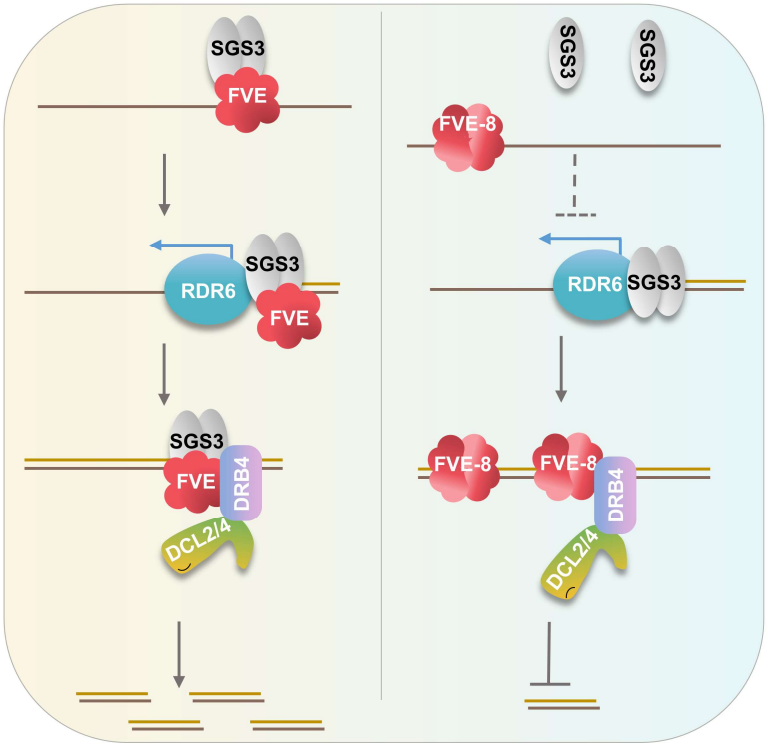

Figure 35 Proposed model for the impact of FVE and FVE-8 on transgene silencing.
FVE promotes SGS3 dimerization and launching SGS3 on ssRNA substrate, which in turn recruits RDR6 activity to produce dsRNA in vivo. Once dsRNA is generated, FVE/SGS3/dsRNA is translocated to DCL4/DRB4 complexes for siRNA biogenesis. On the other hand, FVE-8 does not interact with SGS3 and inefficiently promotes RDR6/SGS3 association with ssRNA substrates. Furthermore, FVE promotes DCL4/DRB4 activity while FVE-8 sequesters dsRNA to prevent DCL4/DRB4 function in producing siRNAs.

How does FVE evolve a new function in PTGS? One reason is that FVE harbors six tandem repeated WD40 domains. WD40 domains are widely involved in protein-protein interaction and serve as a glue or a scaffold for the assembly of large protein complexes (Stirnimann, et al., 2010; Xu and Min, 2011). The presence of a six-WD40-domain allows FVE to partner with different targets or to shuffle between macromolecular complexes to fulfill various functions. Here, we also discovered two new features of FVE as a WD40-domain protein: First, wild-type FVE protein does not typically form oligomer so that it could create a platform or scaffold for other partners. However, the truncated variants like FVE-8 are self-adhesive; correspondingly, the FVE-8 homo-dimerization could block the interaction interface, and subsequently the assembly of macromolecular complexes for proper functions. Thus, the integrity of WD40 domains is critical for FVE biological roles. Second, WD40-domain is one of the most abundant and conserved domains in eukaryotes (Stirnimann, et al., 2010; Xu and Min, 2011). Emerging evidence show that mammalian WD40-domain proteins have been reported to specifically bind to Sm site [$A(U)_{4-6}G$] and $m^7G_{ppp}G$ cap of pre-snRNAs (Jin, et al., 2016; Xu, et al., 2016). Also, it has been predicted but not tested that RbAp48, the mammalian homolog of FVE, may also have the potential to bind to RNA (Bellucci, et al., 2011). Here we found that FVE bind to RNA in a sequence-independent manner. Moreover, FVE can bind to both ss and dsRNA substrates. This discovery would largely expand the spectrum of potential functions for WD40 domain-enriched proteins. Thus, the evolution of FVE to bind RNA would allow the protein directly to modulate the functions of ribonucleoprotein complexes from SGS3/RDR6 to DRB4/DCL4. In human pluripotent stem cells, the localization of

PRC2 complex on chromatins requires RNA binding to regulate stem cell differentiation (Long, et al., 2020). Since FVE is involved in PRC2 in plants, the RNA-binding ability may also facilitate the localization of PRC2 on chromatins in plants.

SGS3 also has some unique features, allowing it to be easily targeted by FVE. SGS3 harbors coiled-coiled (CC) domain that is essential for protein-protein interaction and homodimerization, and XS domain that is critical for RNA-binding activity (Zhang and Trudeau, 2008; Fukunaga and Doudna, 2009). SGS3 also contains an N-terminal highly disordered region with Prion-like character (Figure 36) (Oates, et al., 2012; Lancaster, et al., 2014). These features refer that SGS3 would have different partners and function through various ribonucleoprotein complexes. Here, FVE promotes SGS3 dimerization which is essential for the formation of cytoplasmic granule-like foci, called siRNA bodies (Elmayan, et al., 2009). Since SGS3 and DCL4 complexes are partially co-localized (Pontes, et al., 2013), SGS3 could translocate FVE, or vice versa, to the siRNA bodies to modulate the downstream siRNA production. Of note, SGS3 has been recently reported to contribute to translocating some proteasome subunit RPT2a into proximity of the siRNA-bodies to repress RNA quality control and to promote PTGS (Kim, et al., 2019). That said, it would be predicted that SGS3/FVE might be able to translocate additional but yet unidentified targets to si-RNA bodies for fine-tuning PTGS activities.

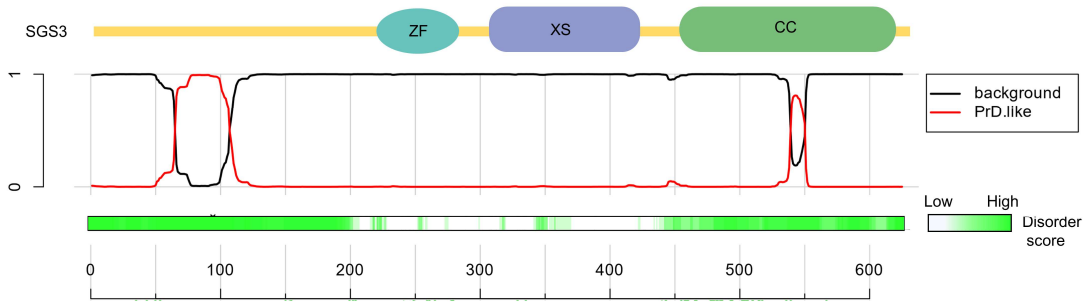

Figure 36 Schematic domains of SGS3.
Top: protein schematic structure of SGS3. ZF, zinc finger domain. XS, rice gene X and SGS3 domain. CC, coiled-coiled domain. Bottom: PrLDs (prion-like domains) and disorder score predicted by Prion-like Amino Acid Composition (PLAAC; http://plaac.wi.mit.edu/) and D^2P^2 algorithms (http://d2p2.pro/about/predictors/), respectively.

As a well-known epigenetic element, FVE has evolved to secure a new role in PTGS. This feature allows FVE to shuttle between nucleus and cytoplasm to suppress gene expression at both TGS and PTGS levels. The fact that the very same protein has multiple functions in TGS and PTGS is reminiscent of several other well-known genes. Chromatin remodeling factor 2 (CHR2), best known to remodel chromatin structures to regulate gene transcription can also interact with SE to remodel pri-miRNAs and suppress miRNA production (Wang, et al., 2018). On the other hand, SE not only regulates RNA processing but also participates in epigenetic silencing of transposable elements (TE) and protein-coding genes (Ma, et al., 2018; Speth, et al., 2018). However, different from CHR2 and SE which likely act in different but co-transcriptional processes, FVE's functions are spatiotemporally separated. This feature might allow FVE to regulate a broad spectrum of targets.

Many components are shared in sRNA biogenesis for endogenous RNA and foreign transcripts in PTGS. Here, SGS3 and DCL2/4 also contribute to the production of ta-siRNAs. It appears that FVE has more impacts on transgene silencing than endogenous RNA silencing. This scenario is also reminiscent of some reported genes such as *FCA/FPA*, *JMJ14* and *RPT2a* that appear only to affect transgene siRNA production, but not affect the abundance of endogenous sRNAs (Baurle, et al., 2007; Searle, et al., 2010; Kim, et al., 2019). One plausible explanation is that expression of transgenes, but not endogenous loci, might often lead to production of aberrant transcripts that reach the threshold of RNA quality control machinery. The abundant transgene transcripts could be easily caught by RNA binding proteins like FVE. Of course, there might be many other unknown fundamental mechanisms that would be revealed in the field.

Here we have provided clear evidence that FVE targets the SGS3-DCL4/DRB4 metabolism channel to promote PTGS. Given this scenario, it might be tempting to hypothesize that these FVE partners might also directly influence SGS3/DCL4/DRB4 function. In addition, FVE and its mammalian homologs like RbAp48 are well conserved through the eukaryotes, whether mammalian FVE plays a similar role in RNA biology would be another exciting question in the future.

CHAPTER IV

OTHER ARS MUTANTS RECOVED FROM THIS SYSTEM

4.1 Summary

Apart from *fve-8*, there are other *ars* mutants recovered from the same system. Here I would like to introduce 2 *ars* mutants briefly. They all showed increased LUC signal but were not continued. I would like to talk about these mutants briefly including the discovery and different fates of them. Also, I described the problem we faced and potential solution.

4.2 Introduction

In Chapter II and Chapter III, we presented a comprehensive study on FVE and its allele *fve-8*/*ars1-1*. Apart from *ars1-1*, I recovered hundreds of *ars* mutants. Due to different kinds of reasons, some of them were given up and some of them were continued. Here, I displayed 2 examples: *ars2-1* and *ars3-1*. All of them showed increased LUC signal in mutants compared to E5-4. NGS were performed to them. Unfortunately, *ars2-1* was unable to be mapped to the interval region calculated from NGS data. On the other hand, *ars3-1* in the later generations did not showed uniform LUC signal.

4.3 Materials and Methods

4.3.1 Vector construction and transgenic plants

Vector construction is similar to *2.3.1* by homolog recombination method. The primers used in this chapter is listed in Table 9. Transgenic plants were obtained with same method described in 2.3.1.

Table 9 Primers used in 4.3.1.

For constructs	**Sequence**
At2g26610-full-Inf-F Sac1	TGTATGATAATTCGAGCTGAGCTCGGATTCGCGGTATCGCTATAG
At2g26610-full-Inf-R Asc1	AGAAAGCTGGGTCGGGGCGCGCCTCAACATTGTCTAAATTAGTTCG ACAG
At2g26610-f1-Inf-R	TTATCATAGACCTCGAAAGATATATTAGGATGGAG
At2g26610-f2-Inf-F	TCTTTCGAGGTCTATGATAAAAACTGGAACCTTC
At2g26610-f2-Inf-R	ACCATTTTTCTCAAATCCTGTAGATGATGG
At2g26610-f3-Inf-F	CAGGATTTGAGAAAAATGGTTCTATGGTAAGTC

4.3.2 Plant materials and growth conditions

Plant materials and growth conditions are consistent with that in *2.3.2*.

4.3.3 EMS mutagenesis, mutant screen and Luciferase Assays

Mutant screen and Luciferase assays are consistent with that in *2.3.3*.

4.3.4 RNA blot and small RNA blot

RNA blot and small RNA blot are consistent with that in *2.3.6*.

4.4 Results

A mutant *ars2-1*, displayed an enhanced LUC luminescent signal compared with that of E5-4 (Figure 37A) but the LUC was not as strong as that in *fve-8*. The mutant showed a smaller size of biomass and a late-flowering phenotype (Figure 37B and 37C). Further RNA blot assay showed that *LUC* expression level was more than 2-fold in *ars2-1* mutant compared with that in E5-4 (Figure 37D). *ars2-1* was outcrossed with Col-0 to generate F2 mapping populations. We first performed rough genetic mapping and then NGS sequencing. Unfortunately, the linkage region calculated from NGS analysis showed a high recombination ratio (31%-50%) from fine mapping results (Figure 38), which made it difficult to select candidate genes.

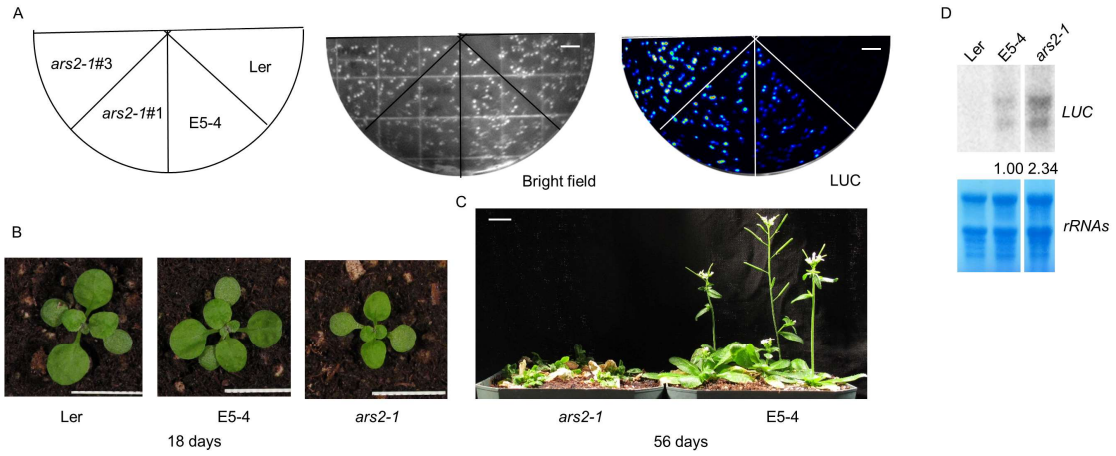

Figure 37 Isolation of *ars2-1* through the forward genetic screening.
(A) Mutation in *FVE* caused increased LUC luminescence. 5-day seedlings of E5-4, *ars2-1* and *Ler* were photographed in bright field (top panel) and under CCD camera for LUC signal. The signals were displayed by Winview32 software. Scale bar, 1 cm.
(B) 18-day-old seedlings of Ler, E5-4 and *ars2-1*. Scale bar, 1 cm.
(C) 56-day-old plants of Ler, E5-4 and *ars2-1*. Scale bar, 1 cm.
(D) Northern blot showed that *LUC* transcripts accumulated in *ars2-1* compared with E5-4. rRNAs serve as an internal control.

A

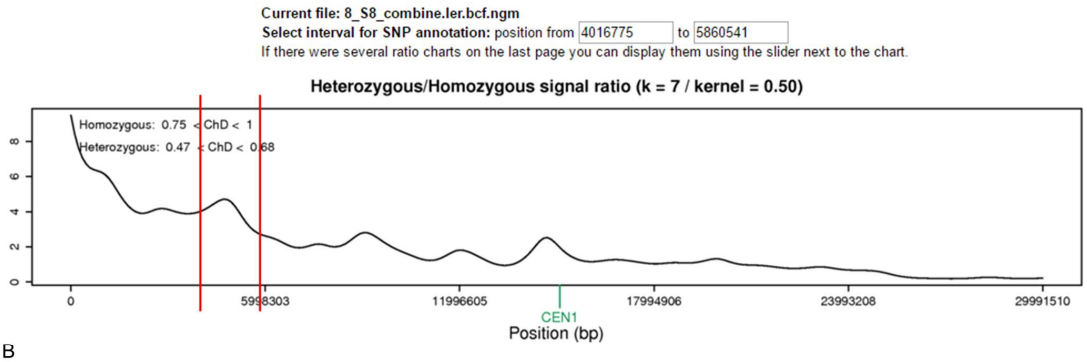

B

Marker name	chr1.533-534	chr1. 529-530	chr1.8660844
Location	3025000	3570000	8660944
Recombination ratio	31%	44%	50%

Figure 38 NGS mapping result is not repeatable by rough mapping.
(A) NGS mapping results showing a peak between 4 Mb to 5.9 Mb.
(B) Rough mapping shows a high recombination ratio in a large physical region containing the region from NGS results.

Another mutant *ars3-1* also displayed an enhanced LUC luminescent signal compared with that of E5-4 (Figure 39A) and the signal was not as strong as that in *fve-8*, either. *ars3-1* showed a smaller size and an early-flowering phenotype (Figure 39B and C). We failed to get a convincing RNA blot result of *LUC* transcripts level.

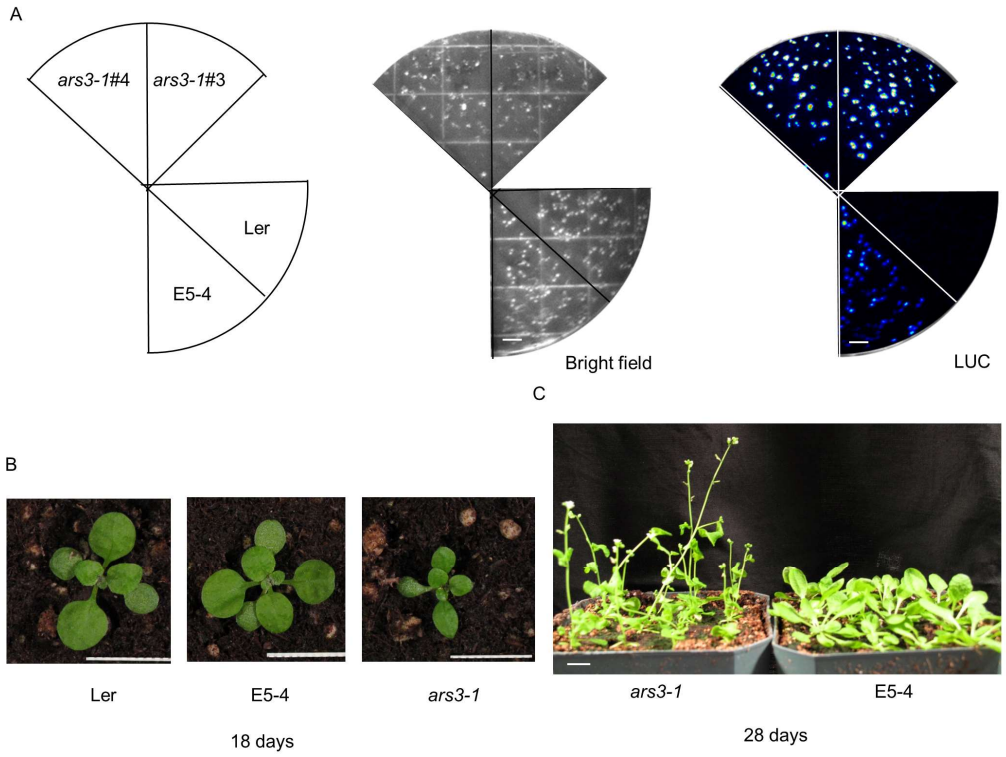

Figure 39 Isolation of *ars3-1* through the forward genetic screening.
(A) Mutation in *FVE* caused increased LUC luminescence. 5-day seedlings of E5-4, *ars2-1* and *Ler* were photographed in bright field (top panel) and under CCD camera for LUC signal. The signals were displayed by Winview32 software. Scale bar, 1 cm.
(B) 18-day-old seedlings of Ler, E5-4 and *ars3-1*. Scale bar, 1 cm.
(C) 28-day-old plants of Ler, E5-4 and *ars3-1*. Scale bar, 1 cm.

ars3-1 was outcrossed with Col-0 to generate F2 population for and NGS. Sequencing result was analyzed by both ShoreMap and NGM analysis (Figure 40). Based on the analyses, several candidate genes were predicted, after ruling out the genes that were generally recovered from all sequence results, TEs and genes with non-effect mutations, we had one candidate gene At2g26610 with an AA change of Serine to Leucine. We performed complementation experiment to *ars3-1* but the complementary lines failed to rescue LUC signal (Figure 41A). We then later backcrossed *ars3-1* with E5-

4 and get *ars3-1 BC1F2* plants. We used *ars3-1 BC1F2* performed the complementation experiment again and then found the wildtype At2g26610 can rescue the LUC phenotype (Figure 41B). Unfortunately, later generation of *ars3-1* started to show heterogenous LUC signal, which made it difficult to measure *LUC* expression level.

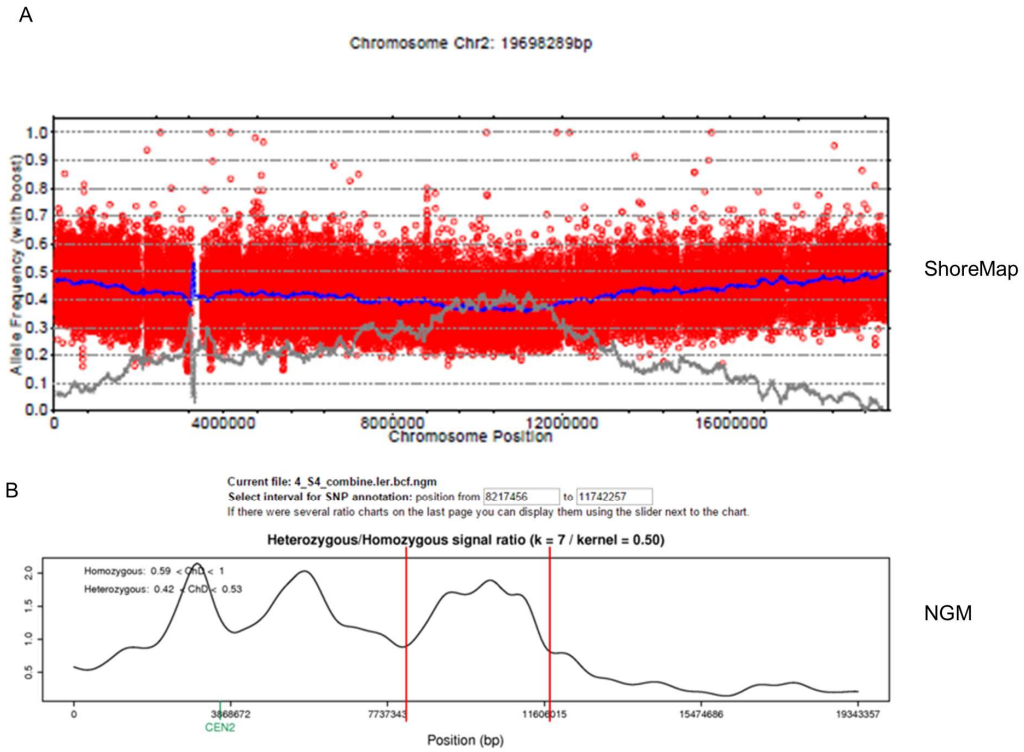

Figure 40 NGS mapping result analyzed by two software.
(A) NGS analyzed by ShoreMap. Red dots indicate allele frequency estimated from individual markers. The blue line means the average allele frequency. The brown line shows the boost-values.
(B) NGS analyzed by NGM. The region between red lines shows the mapping interval.

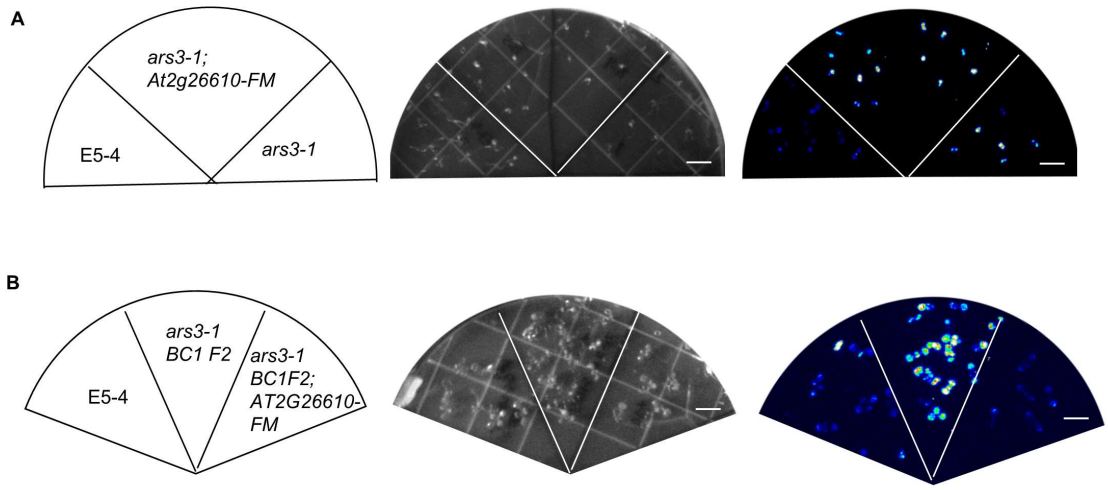

Figure 41 Complementation experiments of *ars3-1*.
(A) Complementation assay of LUC luminescence. Five-day seedlings of E5-4, *ars3-1* and transformants of At2G26610 expressed in *ars1-1* were photographed in bright field (middle) and under CCD camera for LUC signal (right).
(B) Complementation assay of LUC luminescence. Five-day seedlings of E5-4, *ars3-1 BC1F2* and transformants of At2G26610 expressed in *ars3-1 BC1F2* were photographed in bright field (middle) and under CCD camera for LUC signal (right).
The signals were displayed by Winview32 software. Scale bar, 1 cm.

4.5 Discussion

Even though hundreds of *ars* mutants were recovered from the screening system, not all of them were viable projects. Some of them did not show a stable LUC signal from the very beginning. Some of them failed to generate valuable F2 for mapping. Here, we showed two *ars* mutants that await for further investigation. *ars2-1* showed a moderate LUC signal. But the mapping intervals conflicted between fine mapping and NGS result. This might due to the fact that F2 population was not precisely chosen. LUC signal can have a certain degree of variations between different individuals, which made F2 population harder to be chosen. *ars3-1* showed unstable LUC signals in later generations

due to a complicated genetic background. This makes it a challenge to measure LUC expression and other following experiments. Later we can determine LUC signal in the corresponding T-DNA insertion mutant background. If LUC is stably increased in Salk_line background, then we can use T-DNA insertion mutant to replace *ars3-1* for further experiments.

CHAPTER V

CONCLUSIONS AND FUTURE WORK

Although the main biochemical themes for RNA silencing have been extensively studied and auxiliary factors that impact the processes have been identified (Stepien, et al., 2017; Song, et al., 2019), RNA silencing remains to be fully understood. My research has been focused on FVE, a new component involved in PTGS. In this dissertation, I used a forward genetic screening system to identify a new allele of *fve* (*fve-8*) that is compromised in ta-siRNA and transgene-PTGS pathway. Loss-of-function of *fve* mutants had reduced siRNA production from sense and hairpin transgenes. FVE is localized in both nucleus and cytoplasm but cytoplasmic portion of FVE could fully rescue *fve* defect in PTGS (Chapter II). We found that FVE but not its truncated mutant, FVE-8, could interact with SGS3 and promote its homodimerization. Unexpectedly, FVE binds ssRNAs and dsRNAs with moderate affinity while FVE-8 has a significantly increased binding affinity to dsRNA, and these features impact SGS3/RNA association and routing to DRB4/DCL2/4 complexes. In turn, FVE promotes whereas FVE-8 suppresses DRB4/DCL2/4 activity in generating siRNAs in vitro. We concluded that FVE synchronizes SGS3-DRB4-DCL2/4 channel to promote siRNA production whereas FVE-8 hijacks dsRNA substrates to prevent their downstream processing (Chapter III). Thus, this study reveals an uncanonical role of the epigenetic element FVE in transgene-PTGS and sheds light on a new regulatory layer in RNA silencing. In this chapter, conclusions from the study and potential future works are described.

The first question is, as a protein containing an NLS signal, how does FVE perform a role in cytoplasm? How does the protein shuttle between nucleus and cytoplasm? Since SGS3 is well known to be localized in cytoplasm but also detectable in nucleus (Pontes, et al., 2013), and also since we found that the localization of SGS3 was not altered by *fve* (Figure 24A), it is possible that SGS3 may affect the subcellular localization of FVE. To answer this question, we can design experiments to see if FVE distribution is altered with or without SGS3 in vivo. Furthermore, SGS3 itself shows poor binding affinity with ssRNAs while FVE shows a moderate binding ability to ssRNAs, which might be required to guide RNAs to shuttle from nucleus to cytoplasm. To verify this hypothesis, we can detect the FVE-bound RNAs in nucleus and cytoplasm fractions.

How dose FVE and SGS3 coordinately promote transgene silencing? In this study, a model was raised based on both in vivo and in vitro results. More details await more genetic evidence. Transgene expression levels might be altered more in *fve-8 sgs3-1* double mutant compared with single mutants.

A second question is, since the interaction between FVE and SGS3 was captured in cytoplasm, does this interaction also occur in nucleus? As a well-known transcription factor, FVE promotes the deposit of negative modification marks to chromatins. Does FVE recruit SGS3 to chromatin loci? Do FVE and SGS3 coordinately determine transgene transcripts in nucleus? To solve these questions, a ChIP RT-PCR is suggested to test if the occupancy of FVE on transgenic loci is affected in *sgs3* mutant background and a ChIP RT-PCR to test if SGS3 can also be enriched at the same loci and if the enrichment is affected in *fve* or FVE_{NES} background.

FVE interacts with XS domain of SGS3, an RNA-binding domain. DRB4 also contains two RBDs. Furthermore, HYL1 form a homodimer, like SGS3. It is reasonable to ask that if DRB4 forms a homodimer, too. If so, does FVE also affect its homodimerization? Moreover, how does FVE-8 play an opposite role? How does FVE promote DCL4/DRB4 activity at an atomic level awaits future crystal and cyro-EM analysis.

Recent our Y2H screening suggested that FVE also interacts with CHR2 and SE. Since CHR2 can bind with both DNA and RNA and SE is involved in regulating transcription, and furthermore, now we know FVE also binds with both DNA and RNA, we may propose a question: do these proteins have overlapping in some pathway such as regulating transcription? To answer this question, we may take full advantage of the published high-throughput sequencing data such as RNA seq data of mutants and ChIP-seq data of CHR2 and SE and compare any overlapping of them with differently expressed genes in *fve* mutant or FM-FVE ChIP data.

REFERENCES

S F Abou-Elwafa, B Buttner, T Chia, et al. (2011). "Conservation and divergence of autonomous pathway genes in the flowering regulatory network of Beta vulgaris." J Exp Bot **62**(10): 3359-3374.

X Adenot, T Elmayan, D Lauressergues, et al. (2006). "DRB4-dependent TAS3 trans-acting siRNAs control leaf morphology through AGO7." Current Biology **16**(9): 927-932.

E Allen, Z Xie, A M Gustafson, et al. (2005). "microRNA-directed phasing during trans-acting siRNA biogenesis in plants." Cell **121**(2): 207-221.

H F Allen, P A Wade and T G Kutateladze (2013). "The NuRD architecture." Cellular and molecular life sciences **70**(19): 3513-3524.

W Aufsatz, M F Mette, J van der Winden, et al. (2002). "HDA6, a putative histone deacetylase needed to enhance DNA methylation induced by double‐stranded RNA." The EMBO journal **21**(24): 6832-6841.

I Ausin, C Alonso-Blanco, J A Jarillo, et al. (2004). "Regulation of flowering time by FVE, a retinoblastoma-associated protein." Nat Genet **36**(2): 162-166.

D P Bartel (2018). "Metazoan micrornas." Cell **173**(1): 20-51.

M Barton (2010). "Twenty years on: the inner workings of the shoot apical meristem, a developmental dynamo." Developmental biology **341**(1): 95-113.

A Bateman (2002). "The SGS3 protein involved in PTGS finds a family." BMC bioinformatics **3**: 21.

I Baurle and C Dean (2008). "Differential interactions of the autonomous pathway RRM proteins and chromatin regulators in the silencing of Arabidopsis targets." PLoS One **3**(7): e2733.

I Baurle, L Smith, D C Baulcombe, et al. (2007). "Widespread role for the flowering-time regulators FCA and FPA in RNA-mediated chromatin silencing." Science **318**(5847): 109-112.

M Bellucci, F Agostini, M Masin, et al. (2011). "Predicting protein associations with long noncoding RNAs." Nature methods **8**(6): 444-445.

D Bielewicz, M Kalak, M Kalyna, et al. (2013). "Introns of plant pri‐miRNAs enhance miRNA biogenesis." EMBO reports **14**(7): 622-628.

T Blevins, F Pontvianne, R Cocklin, et al. (2014). "A two-step process for epigenetic inheritance in Arabidopsis." Molecular cell **54**(1): 30-42.

A Boland, F Tritschler, S Heimstadt, et al. (2010). "Crystal structure and ligand binding of the MID domain of a eukaryotic Argonaute protein." EMBO Rep **11**(7): 522-527.

N G Bologna, R Iselin, L A Abriata, et al. (2018). "Nucleo-cytosolic Shuttling of ARGONAUTE1 Prompts a Revised Model of the Plant MicroRNA Pathway." Mol Cell **69**(4): 709-719 e705.

F Borges and R A Martienssen (2015). "The expanding world of small RNAs in plants." Nat Rev Mol Cell Biol **16**(12): 727-741.

O Borsani, J Zhu, P E Verslues, et al. (2005). "Endogenous siRNAs derived from a pair of natural cis-antisense transcripts regulate salt tolerance in Arabidopsis." Cell **123**(7): 1279-1291.

N Bouché, D Lauressergues, V Gasciolli, et al. (2006). "An antagonistic function for Arabidopsis DCL2 in development and a new function for DCL4 in generating viral siRNAs." The EMBO journal **25**(14): 3347-3356.

M Brameier, A Krings and R M MacCallum (2007). "NucPred—predicting nuclear localization of proteins." Bioinformatics **23**(9): 1159-1160.

P Brodersen, L Sakvarelidze-Achard, M Bruun-Rasmussen, et al. (2008). "Widespread translational inhibition by plant miRNAs and siRNAs." Science **320**(5880): 1185-1190.

C A Brosnan, N Mitter, M Christie, et al. (2007). "Nuclear gene silencing directs reception of long-distance mRNA silencing in Arabidopsis." Proc Natl Acad Sci U S A **104**(37): 14741-14746.

X Cao, W Aufsatz, D Zilberman, et al. (2003). "Role of the DRM and CMT3 methyltransferases in RNA-directed DNA methylation." Current Biology **13**(24): 2212-2217.

C Castillo-Gonzalez, X Liu, C Huang, et al. (2015). "Geminivirus-encoded TrAP suppressor inhibits the histone methyltransferase SUVH4/KYP to counter host defense." Elife **4**: e06671.

S Chang and C S Pikaard (2005). "Transcript profiling in Arabidopsis reveals complex responses to global inhibition of DNA methylation and histone deacetylation." Journal of Biological Chemistry **280**(1): 796-804.

T Chantarachot and J Bailey-Serres (2018). "Polysomes, Stress Granules, and Processing Bodies: A Dynamic Triumvirate Controlling Cytoplasmic mRNA Fate and Function." Plant Physiol **176**(1): 254-269.

S Cheloufi, C O Dos Santos, M M Chong, et al. (2010). "A dicer-independent miRNA biogenesis pathway that requires Ago catalysis." Nature **465**(7298): 584-589.

H M Chen, L T Chen, K Patel, et al. (2010). "22-Nucleotide RNAs trigger secondary siRNA biogenesis in plants." Proc Natl Acad Sci U S A **107**(34): 15269-15274.

X Cheng and A Wang (2017). "The Potyvirus Silencing Suppressor Protein VPg Mediates Degradation of SGS3 via Ubiquitination and Autophagy Pathways." J Virol **91**(1).

M Christie, L J Croft and B J Carroll (2011). "Intron splicing suppresses RNA silencing in Arabidopsis." Plant J **68**(1): 159-167.

M Clavel, T Pelissier, J Descombin, et al. (2015). "Parallel action of AtDRB2 and RdDM in the control of transposable element expression." BMC Plant Biol **15**: 70.

J Cui, C You and X Chen (2017). "The evolution of microRNAs in plants." Curr Opin Plant Biol **35**: 61-67.

Y Cui, X Fang and Y Qi (2016). "TRANSPORTIN1 Promotes the Association of MicroRNA with ARGONAUTE1 in Arabidopsis." Plant Cell **28**(10): 2576-2585.

J T Cuperus, A Carbonell, N Fahlgren, et al. (2010). "Unique functionality of 22-nt miRNAs in triggering RDR6-dependent siRNA biogenesis from target transcripts in Arabidopsis." Nat Struct Mol Biol **17**(8): 997-1003.

J Curaba and X Chen (2008). "Biochemical activities of Arabidopsis RNA-dependent RNA polymerase 6." J Biol Chem **283**(6): 3059-3066.

S J Curtin, J M Watson, N A Smith, et al. (2008). "The roles of plant dsRNA-binding proteins in RNAi-like pathways." FEBS letters **582**(18): 2753-2760.

Y Dai, W Li and L An (2016). "NMD mechanism and the functions of Upf proteins in plant." Plant Cell Reports **35**(1): 5-15.

T Dalmay, A Hamilton, S Rudd, et al. (2000). "An RNA-dependent RNA polymerase gene in Arabidopsis is required for posttranscriptional gene silencing mediated by a transgene but not by a virus." Cell **101**(5): 543-553.

A Deleris, J Gallego-Bartolome, J Bao, et al. (2006). "Hierarchical action and inhibition of plant Dicer-like proteins in antiviral defense." Science **313**(5783): 68-71.

M Dotto, M S Gómez, M S Soto, et al. (2018). "UV‐B radiation delays flowering time through changes in the PRC2 complex activity and miR156 levels in Arabidopsis thaliana." Plant, cell & environment **41**(6): 1394-1406.

J Du, L M Johnson, S E Jacobsen, et al. (2015). "DNA methylation pathways and their crosstalk with histone methylation." Nat Rev Mol Cell Biol **16**(9): 519-532.

A L Eamens, N A Smith, S J Curtin, et al. (2009). "The Arabidopsis thaliana double-stranded RNA binding protein DRB1 directs guide strand selection from microRNA duplexes." RNA **15**(12): 2219-2235.

A L Eamens, K Wook Kim and P M Waterhouse (2012). "DRB2, DRB3 and DRB5 function in a non-canonical microRNA pathway in Arabidopsis thaliana." Plant Signaling & Behavior **7**(10): 1224-1229.

T Elmayan, X Adenot, L Gissot, et al. (2009). "A neomorphic sgs3 allele stabilizing miRNA cleavage products reveals that SGS3 acts as a homodimer." FEBS J **276**(3): 835-844.

Y Endo, H O Iwakawa and Y Tomari (2013). "Arabidopsis ARGONAUTE7 selects miR390 through multiple checkpoints during RISC assembly." EMBO Rep **14**(7): 652-658.

X Fang, Y Cui, Y Li, et al. (2015). "Transcription and processing of primary microRNAs are coupled by Elongator complex in Arabidopsis." Nat Plants **1**: 15075.

X Fang and Y Qi (2016). "RNAi in Plants: An Argonaute-Centered View." Plant Cell **28**(2): 272-285.

Q Fei, R Xia and B C Meyers (2013). "Phased, secondary, small interfering RNAs in posttranscriptional regulatory networks." Plant Cell **25**(7): 2400-2415.

A Fire, D Albertson, S W Harrison, et al. (1991). "Production of antisense RNA leads to effective and specific inhibition of gene expression in C. elegans muscle." Development **113**(2): 503-514.

A Fire, S Xu, M K Montgomery, et al. (1998). "Potent and specific genetic interference by double-stranded RNA in Caenorhabditis elegans." Nature **391**(6669): 806-811.

F Frank, N Sonenberg and B Nagar (2010). "Structural basis for 5'-nucleotide base-specific recognition of guide RNA by human AGO2." Nature **465**(7299): 818-822.

A Fukudome and T Fukuhara (2017). "Plant dicer-like proteins: double-stranded RNA-cleaving enzymes for small RNA biogenesis." J Plant Res **130**(1): 33-44.

A Fukudome, A Kanaya, M Egami, et al. (2011). "Specific requirement of DRB4, a dsRNA-binding protein, for the in vitro dsRNA-cleaving activity of Arabidopsis Dicer-like 4." RNA **17**(4): 750-760.

R Fukunaga and J A Doudna (2009). "dsRNA with 5′ overhangs contributes to endogenous and antiviral RNA silencing pathways in plants." The EMBO journal **28**(5): 545-555.

F Y Gaffar and A Koch (2019). "Catch Me If You Can! RNA Silencing-Based Improvement of Antiviral Plant Immunity." Viruses **11**(7): 673.

Z Gao, H-L Liu, L Daxinger, et al. (2010). "An RNA polymerase II-and AGO4-associated protein acts in RNA-directed DNA methylation." Nature **465**(7294): 106-109.

V Gasciolli, A C Mallory, D P Bartel, et al. (2005). "Partially redundant functions of Arabidopsis DICER-like enzymes and a role for DCL4 in producing trans-acting siRNAs." Current Biology **15**(16): 1494-1500.

E Glick, A Zrachya, Y Levy, et al. (2008). "Interaction with host SGS3 is required for suppression of RNA silencing by tomato yellow leaf curl virus V2 protein." Proc Natl Acad Sci U S A **105**(1): 157-161.

R J Golden, B Chen, T Li, et al. (2017). "An Argonaute phosphorylation cycle promotes microRNA-mediated silencing." Nature **542**(7640): 197-202.

B D Gregory, R C O'Malley, R Lister, et al. (2008). "A link between RNA metabolism and silencing affecting Arabidopsis development." Developmental cell **14**(6): 854-866.

X Gu, D Jiang, W Yang, et al. (2011). "Arabidopsis homologs of retinoblastoma-associated protein 46/48 associate with a histone deacetylase to act redundantly in chromatin silencing." PLoS Genet **7**(11): e1002366.

S Guo and K J Kemphues (1995). "par-1, a gene required for establishing polarity in C. elegans embryos, encodes a putative Ser/Thr kinase that is asymmetrically distributed." Cell **81**(4): 611-620.

I Gy, V Gasciolli, D Lauressergues, et al. (2007). "Arabidopsis FIERY1, XRN2, and XRN3 are endogenous RNA silencing suppressors." The Plant Cell **19**(11): 3451-3461.

A J Hamilton and D C Baulcombe (1999). "A species of small antisense RNA in posttranscriptional gene silencing in plants." Science **286**(5441): 950-952.

R Harmoko, W I D Fanata, J Y Yoo, et al. (2013). "RNA-dependent RNA polymerase 6 is required for efficient hpRNA-induced gene silencing in plants." Molecules and Cells **35**(3): 202-209.

E R Havecker, L M Wallbridge, T J Hardcastle, et al. (2010). "The Arabidopsis RNA-directed DNA methylation argonautes functionally diverge based on their expression and interaction with target loci." Plant Cell **22**(2): 321-334.

A Hiraguri, R Itoh, N Kondo, et al. (2005). "Specific interactions between Dicer-like proteins and HYL1/DRB- family dsRNA-binding proteins in Arabidopsis thaliana." Plant Molecular Biology **57**(2): 173-188.

D Holoch and D Moazed (2015). "RNA-mediated epigenetic regulation of gene expression." Nature reviews. Genetics **16**(2): 71.

D Holoch and D Moazed (2015). "RNA-mediated epigenetic regulation of gene expression." Nat Rev Genet **16**(2): 71-84.

M D Howell, N Fahlgren, E J Chapman, et al. (2007). "Genome-wide analysis of the RNA-DEPENDENT RNA POLYMERASE6/DICER-LIKE4 pathway in Arabidopsis reveals dependency on miRNA-and tasiRNA-directed targeting." The Plant Cell **19**(3): 926-942.

G Hutvagner and M J Simard (2008). "Argonaute proteins: key players in RNA silencing." Nat Rev Mol Cell Biol **9**(1): 22-32.

V Jauvion, M Rivard, N Bouteiller, et al. (2012). "RDR2 partially antagonizes the production of RDR6-dependent siRNA in sense transgene-mediated PTGS." PLoS One **7**(1): e29785.

W Jin, J Wang, C-P Liu, et al. (2020). "Structural basis for pri-miRNA recognition by Drosha." Molecular cell.

W Jin, Y Wang, C-P Liu, et al. (2016). "Structural basis for snRNA recognition by the double-WD40 repeat domain of Gemin5." Genes & Development **30**(21): 2391-2403.

J H Jung, J H Park, S Lee, et al. (2013). "The cold signaling attenuator HIGH EXPRESSION OF OSMOTICALLY RESPONSIVE GENE1 activates FLOWERING LOCUS C transcription via chromatin remodeling under short-term cold stress in Arabidopsis." Plant Cell **25**(11): 4378-4390.

A L Kenzior and W R Folk (1998). "AtMSI4 and RbAp48 WD‐40 repeat proteins bind metal ions 1." FEBS letters **440**(3): 425-429.

A Khvorova, A Reynolds and S D Jayasena (2003). "Functional siRNAs and miRNAs exhibit strand bias." Cell **115**(2): 209-216.

H J Kim, Y Hyun, J Y Park, et al. (2004). "A genetic link between cold responses and flowering time through FVE in Arabidopsis thaliana." Nat Genet **36**(2): 167-171.

M H Kim, J Jeon, S Lee, et al. (2019). "Proteasome subunit RPT2a promotes PTGS through repressing RNA quality control in Arabidopsis." Nat Plants **5**(12): 1273-1282.

S Kim, J-Y Yang, J Xu, et al. (2008). "Two cap-binding proteins CBP20 and CBP80 are involved in processing primary MicroRNAs." Plant and cell physiology **49**(11): 1634-1644.

H Koiwa, A W Barb, L Xiong, et al. (2002). "C-terminal domain phosphatase-like family members (AtCPLs) differentially regulate Arabidopsis thaliana abiotic stress signaling, growth, and development." Proceedings of the National Academy of Sciences **99**(16): 10893-10898.

R Komiya (2017). "Biogenesis of diverse plant phasiRNAs involves an miRNA-trigger and Dicer-processing." Journal of plant research **130**(1): 17-23.

M Koornneef, C J Hanhart and J H van der Veen (1991). "A genetic and physiological analysis of late flowering mutants in Arabidopsis thaliana." Mol Gen Genet **229**(1): 57-66.

S Kosmidis, A Polyzos, L Harvey, et al. (2018). "RbAp48 protein is a critical component of GPR158/OCN signaling and ameliorates age-related memory loss." Cell reports **25**(4): 959-973. e956.

N Kumakura, A Takeda, Y Fujioka, et al. (2009). "SGS3 and RDR6 interact and colocalize in cytoplasmic SGS3/RDR6-bodies." FEBS Lett **583**(8): 1261-1266.

Y Kurihara, Y Takashi and Y Watanabe (2006). "The interaction between DCL1 and HYL1 is important for efficient and precise processing of pri-miRNA in plant microRNA biogenesis." RNA **12**(2): 206-212.

P B Kwak and Y Tomari (2012). "The N domain of Argonaute drives duplex unwinding during RISC assembly." Nat Struct Mol Biol **19**(2): 145-151.

A K Lancaster, A Nutter-Upham, S Lindquist, et al. (2014). "PLAAC: a web and command-line application to identify proteins with prion-like amino acid composition." Bioinformatics **30**(17): 2501-2502.

S Laubinger, T Sachsenberg, G Zeller, et al. (2008). "Dual roles of the nuclear cap-binding complex and SERRATE in pre-mRNA splicing and microRNA processing in Arabidopsis thaliana." Proceedings of the National Academy of Sciences **105**(25): 8795-8800.

S Laubinger, G Zeller, S R Henz, et al. (2010). "Global effects of the small RNA biogenesis machinery on the Arabidopsis thaliana transcriptome." Proc Natl Acad Sci U S A **107**(41): 17466-17473.

J A Law and S E Jacobsen (2010). "Establishing, maintaining and modifying DNA methylation patterns in plants and animals." Nature Reviews Genetics **11**(3): 204-220.

D Li, A M S Palanca, S Y Won, et al. (2017). "The MBD7 complex promotes expression of methylated transgenes without significantly altering their methylation status." Elife **6**.

H Li, J Ruan and R Durbin (2008). "Mapping short DNA sequencing reads and calling variants using mapping quality scores." Genome research **18**(11): 1851-1858.

S Li, K Liu, B Zhou, et al. (2018). "MAC3A and MAC3B, two core subunits of the MOS4-associated complex, positively influence miRNA biogenesis." The Plant Cell **30**(2): 481-494.

S Li, L Liu, X Zhuang, et al. (2013). "MicroRNAs inhibit the translation of target mRNAs on the endoplasmic reticulum in Arabidopsis." Cell **153**(3): 562-574.

Y Li, D Sun, Z Ma, et al. (2020). "Degradation of SERRATE via ubiquitin-independent 20S proteasome to survey RNA metabolism." Nature Plants: 1-13.

Z Li, S Wang, J Cheng, et al. (2016). "Intron Lariat RNA Inhibits MicroRNA Biogenesis by Sequestering the Dicing Complex in Arabidopsis." PLoS Genet **12**(11): e1006422.

X-h Liang, Joshua G Nichols, C-W Hsu, et al. (2019). "mRNA levels can be reduced by antisense oligonucleotides via no-go decay pathway." Nucleic Acids Research **47**(13): 6900-6916.

C Liu, M J Axtell and N V Fedoroff (2012). "The helicase and RNaseIIIa domains of Arabidopsis Dicer-Like1 modulate catalytic parameters during microRNA biogenesis." Plant Physiol **159**(2): 748-758.

L Liu and X Chen (2016). "RNA Quality Control as a Key to Suppressing RNA Silencing of Endogenous Genes in Plants." Mol Plant **9**(6): 826-836.

Y Long, T Hwang, A R Gooding, et al. (2020). "RNA is essential for PRC2 chromatin occupancy and function in human pluripotent stem cells." Nature Genetics: 1-8.

A Loyola and G Almouzni (2004). "Histone chaperones, a supporting role in the limelight." Biochimica et Biophysica Acta (BBA)-Gene Structure and Expression **1677**(1): 3-11.

M Luo, R Tai, C W Yu, et al. (2015). "Regulation of flowering time by the histone deacetylase HDA5 in Arabidopsis." Plant J **82**(6): 925-936.

Z Ma, C Castillo-Gonzalez, Z Wang, et al. (2018). "Arabidopsis Serrate Coordinates Histone Methyltransferases ATXR5/6 and RNA Processing Factor RDR6 to Regulate Transposon Expression." Dev Cell **45**(6): 769-784 e766.

Z Ma and X Zhang (2018). "Actions of plant Argonautes: predictable or unpredictable?" Current Opinion in Plant Biology **45**: 59-67.

P A Manavella, J Hagmann, F Ott, et al. (2012). "Fast-forward genetics identifies plant CPL phosphatases as regulators of miRNA processing factor HYL1." Cell **151**(4): 859-870.

A Marí-Ordóñez, A Marchais, M Etcheverry, et al. (2013). "Reconstructing de novo silencing of an active plant retrotransposon." Nature Genetics **45**(9): 1029-1039.

A E Martinez de Alba, E Elvira-Matelot and H Vaucheret (2013). "Gene silencing in plants: a diversity of pathways." Biochim Biophys Acta **1829**(12): 1300-1308.

A E Martinez de Alba, A B Moreno, M Gabriel, et al. (2015). "In plants, decapping prevents RDR6-dependent production of small interfering RNAs from endogenous mRNAs." Nucleic Acids Res **43**(5): 2902-2913.

O Mathieu, J Reinders, M Čaikovski, et al. (2007). "Transgenerational stability of the Arabidopsis epigenome is coordinated by CG methylation." Cell **130**(5): 851-862.

M Matzke, T Kanno, L Daxinger, et al. (2009). "RNA-mediated chromatin-based silencing in plants." Current opinion in cell biology **21**(3): 367-376.

M A Matzke, T Kanno and A J Matzke (2015). "RNA-directed DNA methylation: the evolution of a complex epigenetic pathway in flowering plants." Annual review of plant biology **66**: 243-267.

M A Matzke and R A Mosher (2014). "RNA-directed DNA methylation: an epigenetic pathway of increasing complexity." Nat Rev Genet **15**(6): 394-408.

A D McCue, K Panda, S Nuthikattu, et al. (2015). "ARGONAUTE 6 bridges transposable element m RNA ‐ derived si RNA s to the establishment of DNA methylation." The EMBO journal **34**(1): 20-35.

C W Melnyk, A Molnar and D C Baulcombe (2011). "Intercellular and systemic movement of RNA silencing signals." EMBO J **30**(17): 3553-3563.

S Mi, T Cai, Y Hu, et al. (2008). "Sorting of small RNAs into Arabidopsis argonaute complexes is directed by the 5' terminal nucleotide." Cell **133**(1): 116-127.

S Mlotshwa, G J Pruss, A Peragine, et al. (2008). "DICER-LIKE2 Plays a Primary Role in Transitive Silencing of Transgenes in Arabidopsis." PLoS One **3**(3): e1755.

T Montavon, Y Kwon, A Zimmermann, et al. (2017). "A specific dsRNA-binding protein complex selectively sequesters endogenous inverted-repeat siRNA precursors and inhibits their processing." Nucleic Acids Res **45**(3): 1330-1344.

T A Montgomery, M D Howell, J T Cuperus, et al. (2008). "Specificity of ARGONAUTE7-miR390 interaction and dual functionality in TAS3 trans-acting siRNA formation." Cell **133**(1): 128-141.

P Morel, C Tréhin, S Breuil-Broyer, et al. (2008). "Altering FVE/MSI4 results in a substantial increase of biomass in Arabidopsis—the functional analysis of an ontogenesis accelerator." Molecular Breeding **23**(2): 239-257.

A B Moreno, A E Martinez de Alba, F Bardou, et al. (2013). "Cytoplasmic and nuclear quality control and turnover of single-stranded RNA modulate post-transcriptional gene silencing in plants." Nucleic Acids Res **41**(8): 4699-4708.

R A Mosher, C W Melnyk, K A Kelly, et al. (2009). "Uniparental expression of PolIV-dependent siRNAs in developing endosperm of Arabidopsis." Nature **460**(7252): 283-286.

P Mourrain, C Beclin, T Elmayan, et al. (2000). "Arabidopsis SGS2 and SGS3 genes are required for posttranscriptional gene silencing and natural virus resistance." Cell **101**(5): 533-542.

J Müller, C M Hart, N J Francis, et al. (2002). "Histone methyltransferase activity of a Drosophila Polycomb group repressor complex." Cell **111**(2): 197-208.

C Napoli, C Lemieux and R Jorgensen (1990). "Introduction of a chimeric chalcone synthase gene into petunia results in reversible co-suppression of homologous genes in trans." The Plant Cell **2**(4): 279-289.

E Nicolas, V Morales, L Magnaghi-Jaulin, et al. (2000). "RbAp48 belongs to the histone deacetylase complex that associates with the retinoblastoma protein." Journal of Biological Chemistry **275**(13): 9797-9804.

S Nuthikattu, A D McCue, K Panda, et al. (2013). "The initiation of epigenetic silencing of active transposable elements is triggered by RDR6 and 21-22 nucleotide small interfering RNAs." Plant Physiology **162**(1): 116-131.

M E Oates, P Romero, T Ishida, et al. (2012). "D2P2: database of disordered protein predictions." Nucleic Acids Research **41**(D1): D508-D516.

V Olmedo-Monfil, N Durán-Figueroa, M Arteaga-Vázquez, et al. (2010). "Control of female gamete formation by a small RNA pathway in Arabidopsis." Nature **464**(7288): 628-632.

J S Parent, N Bouteiller, T Elmayan, et al. (2015). "Respective contributions of Arabidopsis DCL 2 and DCL 4 to RNA silencing." The Plant Journal **81**(2): 223-232.

J S Parent, V Jauvion, N Bouche, et al. (2015). "Post-transcriptional gene silencing triggered by sense transgenes involves uncapped antisense RNA and differs from silencing intentionally triggered by antisense transgenes." Nucleic Acids Res **43**(17): 8464-8475.

J E Park, I Heo, Y Tian, et al. (2011). "Dicer recognizes the 5' end of RNA for efficient and accurate processing." Nature **475**(7355): 201-205.

A C Partin, K Zhang, B-C Jeong, et al. (2020). "Cryo-EM Structures of Human Drosha and DGCR8 in Complex with Primary MicroRNA." Molecular cell.

E Pavlopoulos, S Jones, S Kosmidis, et al. (2013). "Molecular mechanism for age-related memory loss: the histone-binding protein RbAp48." Science translational medicine **5**(200): 200ra115-200ra115.

M Pazhouhandeh, J Molinier, A Berr, et al. (2011). "MSI4/FVE interacts with CUL4-DDB1 and a PRC2-like complex to control epigenetic regulation of flowering time in Arabidopsis." Proc Natl Acad Sci U S A **108**(8): 3430-3435.

M Pazhouhandeh, J Molinier, A Berr, et al. (2011). "MSI4/FVE interacts with CUL4–DDB1 and a PRC2-like complex to control epigenetic regulation of flowering time in Arabidopsis." Proceedings of the National Academy of Sciences **108**(8): 3430-3435.

T Pélissier, M Clavel, C Chaparro, et al. (2011). "Double-stranded RNA binding proteins DRB2 and DRB4 have an antagonistic impact on polymerase IV-dependent siRNA levels in Arabidopsis." RNA **17**(8): 1502-1510.

A Peragine, M Yoshikawa, G Wu, et al. (2004). "SGS3 and SGS2/SDE1/RDR6 are required for juvenile development and the production of trans-acting siRNAs in Arabidopsis." Genes Dev **18**(19): 2368-2379.

C S Pikaard and O M Scheid (2014). "Epigenetic regulation in plants." Cold Spring Harbor perspectives in biology **6**(12): a019315.

O Pontes, A Vitins, T S Ream, et al. (2013). "Intersection of small RNA pathways in Arabidopsis thaliana sub-nuclear domains." PLoS One **8**(6): e65652.

D Pontier, C Picart, F Roudier, et al. (2012). "NERD, a plant-specific GW protein, defines an additional RNAi-dependent chromatin-based pathway in Arabidopsis." Mol Cell **48**(1): 121-132.

M M Pooggin (2017). "RNAi-mediated resistance to viruses: a critical assessment of methodologies." Curr Opin Virol **26**: 28-35.

N Pumplin, A Sarazin, P E Jullien, et al. (2016). "DNA Methylation Influences the Expression of DICER-LIKE4 Isoforms, Which Encode Proteins of Alternative Localization and Function." Plant Cell **28**(11): 2786-2804.

F J Quintero, B Garciadeblas and A Rodríguez-Navarro (1996). "The SAL1 gene of Arabidopsis, encoding an enzyme with 3'(2'), 5'-bisphosphate nucleotidase and inositol polyphosphate 1-phosphatase activities, increases salt tolerance in yeast." The Plant Cell **8**(3): 529-537.

A S Reddy, Y Marquez, M Kalyna, et al. (2013). "Complexity of the alternative splicing landscape in plants." The Plant Cell **25**(10): 3657-3683.

G Ren, M Xie, S Zhang, et al. (2014). "Methylation protects microRNAs from an AGO1-associated activity that uridylates 5′ RNA fragments generated by AGO1 cleavage." Proceedings of the National Academy of Sciences **111**(17): 6365-6370.

F V Rivas, N H Tolia, J J Song, et al. (2005). "Purified Argonaute2 and an siRNA form recombinant human RISC." Nat Struct Mol Biol **12**(4): 340-349.

K Rogers and X Chen (2013). "Biogenesis, turnover, and mode of action of plant microRNAs." Plant Cell **25**(7): 2383-2399.

N T Schirle and I J MacRae (2012). "The crystal structure of human Argonaute2." Science **336**(6084): 1037-1040.

K Schneeberger, S Ossowski, C Lanz, et al. (2009). "SHOREmap: simultaneous mapping and mutation identification by deep sequencing." Nat Methods **6**(8): 550-551.

I R Searle, O Pontes, C W Melnyk, et al. (2010). "JMJ14, a JmjC domain protein, is required for RNA silencing and cell-to-cell movement of an RNA silencing signal in Arabidopsis." Genes & Development **24**(10): 986-991.

C L Simms, L L Yan and H S Zaher (2017). "Ribosome collision is critical for quality control during no-go decay." Molecular cell **68**(2): 361-373. e365.

J-J Song, S K Smith, G J Hannon, et al. (2004). "Crystal structure of Argonaute and its implications for RISC slicer activity." Science **305**(5689): 1434-1437.

X Song, Y Li, X Cao, et al. (2019). "MicroRNAs and their regulatory roles in plant–environment interactions." Annual Review of Plant Biology **70**: 489-525.

F F Souret, J P Kastenmayer and P J Green (2004). "AtXRN4 degrades mRNA in Arabidopsis and its substrates include selected miRNA targets." Molecular cell **15**(2): 173-183.

C Speth, E X Szabo, C Martinho, et al. (2018). "Arabidopsis RNA processing factor SERRATE regulates the transcription of intronless genes." Elife **7**: e37078.

A Stepien, K Knop, J Dolata, et al. (2017). "Posttranscriptional coordination of splicing and miRNA biogenesis in plants." Wiley Interdiscip Rev RNA **8**(3).

C U Stirnimann, E Petsalaki, R B Russell, et al. (2010). "WD40 proteins propel cellular networks." Trends in biochemical sciences **35**(10): 565-574.

H Stroud, M V Greenberg, S Feng, et al. (2013). "Comprehensive analysis of silencing mutants reveals complex regulation of the Arabidopsis methylome." Cell **152**(1-2): 352-364.

Y Sunagawa, M Funamoto, K Shimizu, et al. (2019). "P4998 Novel GATA4 binding proteins, RbAp48/46, regulate cardiomyocyte hypertrophy with depending on the phosphorylate State of GATA4." European Heart Journal **40**(Supplement_1): ehz746. 0176.

H I Suzuki, R A Young and P A Sharp (2017). "Super-Enhancer-Mediated RNA Processing Revealed by Integrative MicroRNA Network Analysis." Cell **168**(6): 1000-1014 e1015.

I Szádeczky-Kardoss, T Csorba, A Auber, et al. (2018). "The nonstop decay and the RNA silencing systems operate cooperatively in plants." Nucleic Acids Research **46**(9): 4632-4648.

K A Tatosyan, I G Ustyantsev and D A Kramerov (2020). "RNA Degradation in Eukaryotic Cells." Molecular Biology **54**(4): 485-502.

M Tijsterman, R F Ketting and R H Plasterk (2002). "The genetics of RNA silencing." Annu Rev Genet **36**: 489-519.

Y Tomari, T Du and P D Zamore (2007). "Sorting of Drosophila small silencing RNAs." Cell **130**(2): 299-308.

Y Tomari, C Matranga, B Haley, et al. (2004). "A protein sensor for siRNA asymmetry." Science **306**(5700): 1377-1380.

M R Tucker, T Okada, Y Hu, et al. (2012). "Somatic small RNA pathways promote the mitotic events of megagametogenesis during female reproductive development in Arabidopsis." Development **139**(8): 1399-1404.

H Vaucheret (2008). "Plant ARGONAUTES." Trends Plant Sci **13**(7): 350-358.

H Vaucheret (2008). "Plant argonautes." Trends in Plant Science **13**(7): 350-358.

F Vazquez, H Vaucheret, R Rajagopalan, et al. (2004). "Endogenous trans-acting siRNAs regulate the accumulation of Arabidopsis mRNAs." Mol Cell **16**(1): 69-79.

H Wang, X Zhang, J Liu, et al. (2011). "Deep sequencing of small RNAs specifically associated with Arabidopsis AGO1 and AGO4 uncovers new AGO functions." Plant J **67**(2): 292-304.

H L Wang and J A Chekanova (2016). "Small RNAs: essential regulators of gene expression and defenses against environmental stresses in plants." Wiley Interdiscip Rev RNA **7**(3): 356-381.

J Wang, J Mei and G Ren (2019). "Plant microRNAs: biogenesis, homeostasis, and degradation." Frontiers in plant science **10**: 360.

L Wang, X Song, L Gu, et al. (2013). "NOT2 proteins promote polymerase II-dependent transcription and interact with multiple MicroRNA biogenesis factors in Arabidopsis." Plant Cell **25**(2): 715-727.

W Wang, R Ye, Y Xin, et al. (2011). "An importin beta protein negatively regulates MicroRNA activity in Arabidopsis." Plant Cell **23**(10): 3565-3576.

W Wang, R Ye, Y Xin, et al. (2011). "An importin β protein negatively regulates microRNA activity in Arabidopsis." The Plant Cell **23**(10): 3565-3576.

Z Wang, Z Ma, C Castillo-González, et al. (2018). "SWI2/SNF2 ATPase CHR2 remodels pri-miRNAs via Serrate to impede miRNA production." Nature **557**(7706): 516-521.

W Wei, Z Ba, M Gao, et al. (2012). "A role for small RNAs in DNA double-strand break repair." Cell **149**(1): 101-112.

S V Wesley, C A Helliwell, N A Smith, et al. (2001). "Construct design for efficient, effective and high‐throughput gene silencing in plants." The Plant Journal **27**(6): 581-590.

L Williams and G Grafi (2000). "The retinoblastoma protein–a bridge to heterochromatin." Trends in plant science **5**(6): 239-240.

S Y Won, S Li, B Zheng, et al. (2012). "Development of a luciferase-based reporter of transcriptional gene silencing that enables bidirectional mutant screening in Arabidopsis thaliana." Silence **3**(1): 6.

H Wu, B Li, H O Iwakawa, et al. (2020). "Plant 22-nt siRNAs mediate translational repression and stress adaptation." Nature **581**(7806): 89-93.

L Wu, L Mao and Y Qi (2012). "Roles of dicer-like and argonaute proteins in TAS-derived small interfering RNA-triggered DNA methylation." Plant Physiology **160**(2): 990-999.

Y Y Wu, B H Hou, W C Lee, et al. (2017). "DCL2‐and RDR6‐dependent transitive silencing of SMXL4 and SMXL5 in Arabidopsis dcl4 mutants causes defective phloem transport and carbohydrate over‐accumulation." The Plant Journal **90**(6): 1064-1078.

M Xie, G Ren, P Costa-Nunes, et al. (2012). "A subgroup of SGS3-like proteins act redundantly in RNA-directed DNA methylation." Nucleic Acids Res **40**(10): 4422-4431.

Z Xie, L K Johansen, A M Gustafson, et al. (2004). "Genetic and Functional Diversification of Small RNA Pathways in Plants." PLOS Biology **2**(5): e104.

C Xu, H Ishikawa, K Izumikawa, et al. (2016). "Structural insights into Gemin5-guided selection of pre-snRNAs for snRNP assembly." Genes & Development **30**(21): 2376-2390.

C Xu and J Min (2011). "Structure and function of WD40 domain proteins." Protein Cell **2**(3): 202-214.

Y Xu, Y Wang, H Stroud, et al. (2013). "A matrix protein silences transposons and repeats through interaction with retinoblastoma-associated proteins." Curr Biol **23**(4): 345-350.

S W Yang, H Y Chen, J Yang, et al. (2010). "Structure of Arabidopsis HYPONASTIC LEAVES1 and its molecular implications for miRNA processing." Structure **18**(5): 594-605.

R Ye, W Wang, T Iki, et al. (2012). "Cytoplasmic assembly and selective nuclear import of Arabidopsis Argonaute4/siRNA complexes." Molecular cell **46**(6): 859-870.

M Yoshikawa, T Iki, Y Tsutsui, et al. (2013). "3' fragment of miR173-programmed RISC-cleaved RNA is protected from degradation in a complex with RISC and SGS3." Proc Natl Acad Sci U S A **110**(10): 4117-4122.

M Yoshikawa, A Peragine, M Y Park, et al. (2005). "A pathway for the biogenesis of trans-acting siRNAs in Arabidopsis." Genes Dev **19**(18): 2164-2175.

B Yu, Z Yang, J Li, et al. (2005). "Methylation as a crucial step in plant microRNA biogenesis." Science **307**(5711): 932-935.

C W Yu, K Y Chang and K Wu (2016). "Genome-Wide Analysis of Gene Regulatory Networks of the FVE-HDA6-FLD Complex in Arabidopsis." Front Plant Sci **7**: 555.

B Zhang, C You, Y Zhang, et al. (2020). "Linking key steps of microRNA biogenesis by TREX-2 and the nuclear pore complex in Arabidopsis." Nature Plants **6**(8): 957-969.

D Zhang and V L Trudeau (2008). "The XS domain of a plant specific SGS3 protein adopts a unique RNA recognition motif (RRM) fold." Cell Cycle **7**(14): 2268-2270.

H Zhang, R Xia, B C Meyers, et al. (2015). "Evolution, functions, and mysteries of plant ARGONAUTE proteins." Curr Opin Plant Biol **27**: 84-90.

S Zhang, M Xie, G Ren, et al. (2013). "CDC5, a DNA binding protein, positively regulates posttranscriptional processing and/or transcription of primary microRNA transcripts." Proc Natl Acad Sci U S A **110**(43): 17588-17593.

X Zhang and H Guo (2017). "mRNA decay in plants: both quantity and quality matter." Curr Opin Plant Biol **35**: 138-144.

X Zhang, R Henriques, S-S Lin, et al. (2006). "Agrobacterium-mediated transformation of Arabidopsis thaliana using the floral dip method." Nature protocols **1**(2): 641.

X Zhang, Y-R Yuan, Y Pei, et al. (2006). "Cucumber mosaic virus-encoded 2b suppressor inhibits Arabidopsis Argonaute1 cleavage activity to counter plant defense." Genes & Development **20**(23): 3255-3268.

X Zhang, H Zhao, S Gao, et al. (2011). "Arabidopsis Argonaute 2 regulates innate immunity via miRNA393(*)-mediated silencing of a Golgi-localized SNARE gene, MEMB12." Mol Cell **42**(3): 356-366.

Z Zhang, X Guo, C Ge, et al. (2017). "KETCH1 imports HYL1 to nucleus for miRNA biogenesis in Arabidopsis." Proc Natl Acad Sci U S A **114**(15): 4011-4016.

Z Zhang, F Hu, M W Sung, et al. (2017). "RISC-interacting clearing 3'-5'exoribonucleases (RICEs) degrade uridylated cleavage fragments to maintain functional RISC in Arabidopsis thaliana." Elife **6**: e24466.

Z Zhang, A Jones, H Y Joo, et al. (2013). "USP49 deubiquitinates histone H2B and regulates cotranscriptional pre-mRNA splicing." Genes Dev **27**(14): 1581-1595.

Z Zhang, X Liu, X Guo, et al. (2016). "Arabidopsis AGO3 predominantly recruits 24-nt small RNAs to regulate epigenetic silencing." Nat Plants **2**(5): 16049.

Y Zhou, M Honda, H Zhu, et al. (2015). "Spatiotemporal sequestration of miR165/166 by Arabidopsis Argonaute10 promotes shoot apical meristem maintenance." Cell Rep **10**(11): 1819-1827.

H Zhu, F Hu, R Wang, et al. (2011). "Arabidopsis Argonaute10 specifically sequesters miR166/165 to regulate shoot apical meristem development." Cell **145**(2): 242-256.

H Zhu, Y Zhou, C Castillo-Gonzalez, et al. (2013). "Bidirectional processing of pri-miRNAs with branched terminal loops by Arabidopsis Dicer-like1." Nat Struct Mol Biol **20**(9): 1106-1115.